# A thermal model of the spot welding process

**Please check the document version of this publication:**

• A submitted manuscript is the version of the article upon submission and before peer-review. There can be important differences between the submitted version and the official published version of record. People interested in the research are advised to contact the author for the final version of the publication, or visit the DOI to the publisher's website.
• The final author version and the galley proof are versions of the publication after peer review.
• The final published version features the final layout of the paper including the volume, issue and page numbers.

Link to publication

# A THERMAL MODEL OF THE
# SPOT WELDING PROCESS



APA.J. HULST

# A THERMAL MODEL OF THE SPOT WELDING PROCESS

A.P.A.J. HULST

# A THERMAL MODEL OF THE SPOT WELDING PROCESS

**PROEFSCHRIFT**

DOOR

## ALOYSIUS PETRUS ALBERTUS JOHANNES HULST

GEBOREN TE UTRECHT

Dit proefschrift is goedgekeurd door de promotor

PROF. DR. P. C. VEENSTRA

aan mijn moeder

aan Dorothé

**CONTENTS**

List of Symbols

The symbols used are defined in the section, figure or equation referred
to between brackets.

$A_r$    area of element perpendicular to r-axis (fig.2.5);      –

   area of apparent contact surface (4.3.1)            $m^2$

$A_z$    area of element perpendicular to z-axis (fig.2.5)       –

$a$    = $\lambda/c$, thermal diffusivity of workpiece metal;      $m^2.s^{-1}$

   radius of microscopic contact spot               m

$b$    = $\pi \sqrt{(\lambda\theta_m/\rho)}/4$                        $A.m^{-1}$

$C$    electric analogue of heat capacity (fig.2.6)            F

$C_o$    unit capacitor (2.2.3)                      = $10^{-6}$F

$c$    volumetric specific heat of workpiece metal          $J.m^{-3}.deg^{-1}$

$c$, $c_1$, $c_2$   various constants

$c_E$    volumetric specific heat of electrode metal          $J.m^{-3}.deg^{-1}$

$D_E$    electrode tip diameter (fig.1.1)                  m

$D_m$    hole diameter (fig.5.2)                      m

$D_N$    weld nugget diameter (fig.1.1)                  m

$d$    electrode displacement (fig.3.5)                m

$d_i$    indentation of electrode into workpiece (fig.3.5)      m

$d_{max}$   maximum electrode displacement (fig.3.5)          m

$d_s$    sheet separation (fig.6.1)                    m

$F$    electrode force (fig.1.1)                    N

$F_s$    tensile shear force (3.3.2)                    N

$f$    = $R_o'/R_o$, in general (eq.(4.5))                  –

$f'$    = $R_o'/R_o$, with artificial current constriction (eq.(5.15))   –

$G$    unit step function (eq.(2.18))                  –

$g$    heat production function (eq.(4.37))              –

10

| | | |
|---|---|---|
| $H_v$ | Vickers hardness | $\mathrm{N.m^{-2}}$ |
| $h$ | distance from electrode face to coolant channel (fig.1.1) | $\mathrm{m}$ |
| $I$ | electric analogue of heat production (fig.2.6) | $\mathrm{A}$ |
| $i, i_{rms}$ | r.m.s. value of welding current (fig.1.1) | $\mathrm{A}$ |
| $i_p$ | peak value of welding current (4.3.2) | $\mathrm{A}$ |
| $J$ | $= 4i/\pi D_E^2$, current density in general | $\mathrm{A.m^{-2}}$ |
| | $= 4i/\pi D_m^2$, with artifical current constriction (5.2.2) | |
| $k$ | $= \alpha(i/i_p)\sqrt{2Q_{\theta m}}$ | $-$ |
| $k_1$ | $= k/Q_D$ | $-$ |
| $k_2$ | $= kg/Q_D$ | $-$ |
| $L$ | Lorentz' constant | $\approx 2.4\times10^{-8}\ \mathrm{V^2.deg^{-2}}$ |
| $m, n$ | array variables denoting axial and radial position of a model element respectively (fig.2.4); various exponents and constants | $-$ |
| $Q_c$ | $= c_E/c$ | $-$ |
| $Q_D$ | $= D_E/s$ in general; | $-$ |
| | $= D_m/s$ with artificial current constriction (eq.(5.11)) | $-$ |
| $Q_F$ | $= 4F/\pi D_E^2 H_V$ | $-$ |
| $Q_h$ | $= h/D_E$ | $-$ |
| $Q_r$ | $= r/s$ | $-$ |
| $Q_t$ | $= at/s^2$ | $-$ |
| $Q_{t'}$ | $= at'/s^2$ | $-$ |
| $Q_v$ | $= \sqrt{Q_\theta}/Q_D^2$ | $-$ |
| $Q_z$ | $= z/s$ | $-$ |
| $Q_\theta$ | $= \lambda\theta/\rho J^2 s^2$, dimensionless weld temperature, generally in the point B($z = 0$, $r = D_E/2$) | $-$ |
| $Q_{\theta c}$ | calculated value of $Q_\theta$ from model measurements (4.3.3) | |
| $Q_{\theta m}$ | measured value of $Q_\theta$ from experimental verification, value of $Q_\theta$ for $\theta = \theta_m$ (4.3.2) | $-$ |

| | | |
|---|---|---|
| $Q_\lambda$ | $= \lambda_E/\lambda$ | — |
| $Q_\rho$ | $= \rho_E/\rho$ | — |
| $q$ | $= Q_{\theta m}/Q_{\theta c}$ | — |
| $R$ | total resistance of the workpieces | $\Omega$ |
| $R_c$ | constriction resistance (4.3.1) | $\Omega$ |
| $R_k$ | contact resistance (4.3.1) | $\Omega$ |
| $R_r$ | electric analogue of thermal resistance in radial direction (fig.2.6) | $\Omega$ |
| $R_s$ | supply resistance (fig.2.6) | $\Omega$ |
| $R_z$ | electric analogue of thermal resistance in axial direction (fig.2.6) | $\Omega$ |
| $R_o$ | $= 8\rho s/\pi D_E^2$, assumed body resistance in the model in general; | $\Omega$ |
| | $= 8\rho s/\pi D_m^2$, with artificial current constriction (5.2.2); | $\Omega$ |
| | unit resistor (2.2.3) $= 10^6$ | $\Omega$ |
| $R_o'$ | actual body resistance (4.2) | $\Omega$ |
| $r$ | radial coordinate | m |
| $s$ | sheet thickness (fig.1.1) | m |
| $t$ | time coordinate | s |
| $t'$ | welding time, determined by means of the electrode displacement curve (fig.3.5) | s |
| $t_h$ | heating time | s |
| $t_m$ | analogue time (2.2.3) | s |
| $t_s$ | time at which splashing occurs (fig.3.6) | s |
| $U$ | electric analogue of temperature (fig.2.6); | V |
| | $= iR$, total voltage across the workpieces (3.3.2); | V |
| | $= iR_k$, contact voltage (4.3.2) | V |
| $U_s$ | $= IR_s$, supply voltage in the analogue model (fig.2.6) | V |
| $V$ | volume of model element | — |
| $w$ | width of workpiece specimen | m |

12

$w_L$    overlap length of workpiecespecimens (fig.1.1)    m

$Y_t$    $= t_m R_o C_o$    –

$Y_U$    $= U/U_s$    –

$z$    axial coordinate    m


$\alpha$    $= (\rho\lambda)'/\rho\lambda$, multiplying factor    –

$\beta$    a constant (eq.(4.27))    $s^{-1}$

$\Delta$    $= d_{max}/s$    –

$\delta$    dimensionless electrode displacement rate (eq.(6.11))    –

$\varepsilon$    dimension of model element (fig.2.4)    –

$\zeta$    a constant (eq.(4.41))    –

$\theta$    supertemperature;    deg

        weld temperature, generally in the point $B(z = 0,\ r = D_E/2)$    deg

$\theta_e$    equilibrium temperature of the weld (eq.(4.28))    deg

$\theta_m$    melting temperature of workpiece metal    deg

$\lambda$    thermal conductivity of workpiece metal    $W.m^{-1}.deg^{-1}$

$\lambda_E$    thermal conductivity of electrode metal    $W.m^{-1}.deg^{-1}$

$\mu$    coefficient of linear thermal expansion    $deg^{-1}$

$\xi$    a constant (eq.(4.8))    –

$\rho$    electric resistivity of workpiece metal    $\Omega.m$

$\rho_E$    electric resistivity of electrode metal    $\Omega.m$

$\sigma_M$    ultimate tensile strength of workpiece metal    $N.m^{-2}$

$\sigma_s$    a constant (eq.(6.3))    $N.m^{-2}$

$\tau_s$    a constant (eq.(6.4))    $N.m^{-2}$

$\phi$    total heat production in the weld (eq.(4.40));    J

        angular coordinate    –

$\phi_k$    heat production owing to the contact resistance (eq.(4.26))    J

$\phi_o$    heat production owing to the body resistance assumed

        in the model (eq.(4.2))    J

$\phi_o'$   heat production owing to the actual body resistance (4.2)   J

Notes.

(1) All temperature values used are supertemperatures with respect to
    the ambience.

(2) The subscripts 1 and 2 generally denote symbols related to the upper
    sheet and upper electrode or lower sheet and lower electrode
    respectively, as shown in fig. 1.1.

14

# Chapter 1. INTRODUCTION

## 1.1. General Background

Resistance welding embraces that branch of the welding art in which
the welding heat in the parts to be joined is generated by the
resistance of these parts to the passage of an electric current. It
differs from other welding methods in that no extraneous materials
are added, and mechanical pressure is applied to forge weld the
heated parts together [1].

Spot welding is undoubtedly the most widely used type of resistance
welding. The process mainly consists of clamping two or more pieces
of sheet metal between two welding electrodes of relatively good
electrical and thermal conductivity and passing an electric current
of sufficient force and duration through the pieces to cause them
to weld together. The type of joint made in this way is called
lap-joint, which means that the welded parts overlap each other
over a distance of a few times the weld diameter.

The fused zone generally has the form of a nugget, for which reason
it is referred to as the weld nugget. Its dimensions and metallurgi-
cal structure are of major importance for the strength and the
quality of the joint made.

Fig. 1.1 shows an arrangement of the spot welding electrodes and of
the position of the workpieces which can be regarded as typical for
this kind of welding process. As can be seen, the electrodes have
three important functions, viz. to supply the welding force to the
workpieces, to guide the electric current through the pieces to be
welded, and to carry off the heat generated near the electrode-
workpiece contact surface so as to prevent fusion from occurring in
this area. As a result of the passage of a current pulse of well-
defined shape, magnitude and duration, melting and fusion is caused
in the area that is most suited on the basis of the geometric and
thermal data, i.e. at the interworkpiece contact plane. A
subsequent short forging period allows the nugget to cool down
under pressure in order to obtain a good coherence between the
welded parts and to prevent porosity as might be caused by
shrinkage.
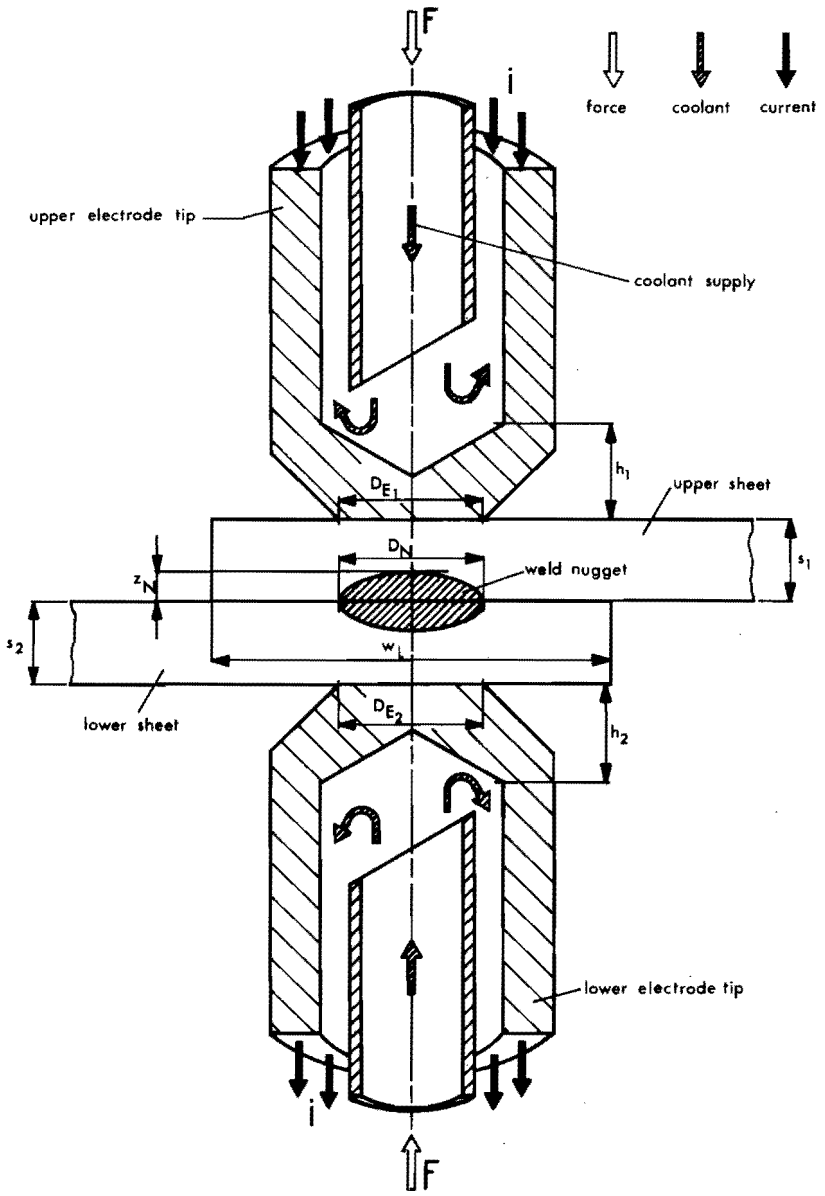
Fig. 1.1. Typical Arrangement of Spot Welding Electrode Tips and
Workpieces

Out of the extensive quantity of available literature the following sources may be recommended for general information.

| On | ref. |
|---|---|
| fundamentals | $[1,4,5,6,7]$, |
| machines and welding controls | $[4,5,7,8,9,11,12]$, |
| electrodes | $[1,4]$, |
| power requirements | $[1,4,5,11,12]$, |
| industrial machine settings | $[1,2,4]$, |
| standards | $[4,10]$, |
| applications | $[3,8,9,11,12]$. |

1.2. Definition of the Problem

Until some years ago spot welding was chiefly applied for mass-produced articles and for purposes where strength and reliability are not imperative. However, during the last fifteen years the tendency has increased to use the process also in cases where high demands are made with respect to the static and dynamic strength of the joint as well as to the quality of its external appearance. As examples of this kind of applications may be mentioned railway car production [13,14], critical joints in motor-car coach work [11(KRIMIANIS),9,16], aircraft construction [12(FIALA),19], aircraft jet engines [12(SCHLOSSER),17,18] and launch vehicles [12(ROHRMANN)].

For these applications it becomes urgent to gain a better understanding of the fundamentals of the process. This understanding has to be not only qualitative but quantitative as well, because of the need to choose optimum machine settings and especially to design adequate devices for the control of weld quality. As a consequence of the very short duration of the welding process such a control has to act automatically, governed by one or more process variables.

Another demand for an automatic control is brought about by the use of resistance welding techniques for the manufacture of miniature and subminiature products like semi-conductors [20] and for the

17

assembly of electronic components [21]. Here, the extreme small
dimensions of the workpieces make automation almost inevitable.
It is the fundamental idea of this work that spot welding primarily
can be considered as a thermal process. Factors determining the
quality of the weld such as the metallurgical structure of the weld
nugget and its surroundings, mechanical deformations resulting from
thermal expansion or electrode impression as well as the size of the
weld itself can be regarded as consequences of the thermal cycle.
Therefore, the first work to be done is to determine the tempera-
tures during spot welding, dependent on both time and space
coordinates. However, the problem here is the impossibility of
measuring temperatures in an area of a few square millimeters where
gradients in the order of $10^6$ deg.m$^{-1}$ and time derivatives of some
$10^5$ deg.s$^{-1}$ exist without disturbing the electric current or heat
flux fields.
The only conclusions regarding temperature distributions at the end
of the heating cycle can be drawn from the dimensions of the weld
nugget and, to a much lower degree of accuracy, from the metallur-
gical structure of the weld and the heat-affected zone [22].
Generally, a well-distinguishable boundary exists between the areas
that have been liquefied or not. At this boundary, temperature has
just reached the melting point of the metal concerned. This goes
for the circumference of the weld nugget in the workpiece interface
as well.
The main subject of these investigations will be to theoretically
determine temperatures in spot welding and to try to verify the
computations by means of the above-mentioned considerations. For a
thourough analysis close attention has to be given to welding
parameters, material properties and weld geometry.
A further object will be to consider the possibilities of quality
control and adaptive control on basis of this analysis.


1.3. Limitations

Some restrictions have to be made as to the scope of this work in
order to limit the number of experiments to a reasonable quantity.

The construction of a satisfactory mathematical and physical model is considered to be of more importance than the investigation of all possible geometrical arrangements or the various designs of workpieces and electrodes. Consequently, only a system consisting of two workpieces of equal dimensions and materials and of two equal electrodes is considered in the first place. The workpieces consist of two sheets, the length and width of which are irrelevant in as far as minimum dimensions as defined in section 2.2.2 are taken into account. An extension of this set-up will be given in section 5.1. A generally applied electrode shape, viz. the truncated cone is used.

The metallurgical structure of the weld is greatly affected by the post-weld cooling rate. It is not only important for medium and high carbon steels or for precipitation hardening alloys, but it also influences the solidification structure of any metal. Grain dimensions, residual stresses and weld ductility are to a high degree defined by the cooling cycle. To improve weld quality, an additional post weld heat treatment is frequently carried out in the welding machine.

Cooling rate, therefore, is to be considered of great importance throughout the weld material. It is easily determined with the aid of the analogue described in chapter 2. However, since no method is known to verify the curves and because of the requirement of limiting the extent of experimental results, no cooling curves are presented in this work.

19

## Chapter 2. THE ANALOGUE MODEL

### 2.1. Review of the Problem

### 2.1.1. Introduction

As indicated in chapter 1 the object of the mathematical model will
be to evaluate the temperatures during spot welding, dependent on
welding parameters, material properties and weld geometry. The most
important welding parameters are welding current i, welding time t
and electrode force F. Those are the variables regulated on the
welding machine by the operator. Significant material properties
are of thermal or electrical nature, viz. volumetric specific heat
c, thermal conductivity $\lambda$ and electric resistivity $\rho$ of both work-
piece and electrode materials. Weld geometry comprises, as a matter
of fact, all dimensions of workpieces and electrodes, but workpiece
thickness s, electrode face diameter $D_E$ and the distance h between
electrode face and coolant channel are of special importance.
The temperature distribution resulting from heat generation and
conduction in a solid is governed by Fourier's law

$$c \frac{\partial \theta}{\partial t} = \nabla.(\lambda \nabla \theta) + \rho J^2 \tag{2.1}$$

Since the mean value of the current density J is determined by i
and $D_E$ this differential equation contains most of the above-
mentioned variables, while the others appear in the boundary
conditions. The main exception is the electrode force F which
influences the values of the contact resistances occurring at the
material interfaces, resulting in an additional heat development in
those areas.
The solution of temperatures from equation (2.1) dependent on place
and time for the spot weld case offers great mathematical
difficulties even if no allowance is made for the role of the
contact resistance. A fundamental increase of these difficulties
lies in the fact that the thermal and electrical properties c, $\lambda$
and $\rho$ are temperature-dependent, thus giving a non-linear character
to the equation.

The work done by several investigators either to solve equation
(2.1) in a more or less simplified form or to approach the problem
from an empirical point of view will be considered briefly in the
next sections.

## 2.1.2. Empirical Methods

At the present time, determination of the machine settings
required to obtain an adequate weld on a given spot welder is
purely empirical. Common practices recommended by welding manuals
are used as a guidance, but the experience of the welding engineer
is required if high-quality welds are imperative. Of course, these
recommended practices originate from numerous experimental results
in their turn.
A few investigators have tried to generalize these results by
using products of some of the welding variables and by studying
their mutual relations. These products may be of an empirical
nature themselves [23] or they may be derived from equation (2.1)
and its boundary conditions [24]. In both cases some criterion is
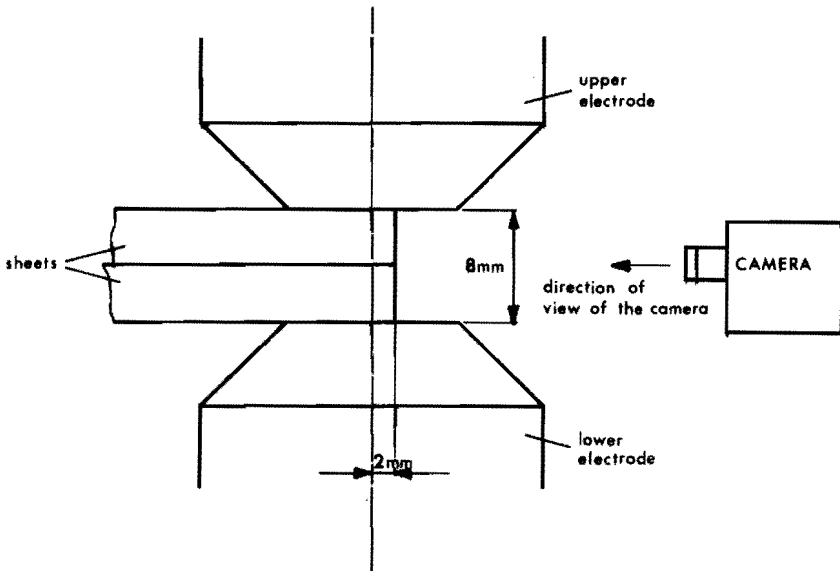required to define a weld of sufficient quality.



Fig. 2.1. Arrangement for Measuring Temperatures during Spot Welding
as described in [25]

A newly developed experimental method to evaluate the temperatures
during spot welding is described in reference [25]. Here, the weld
is made with the electrodes partly situated over the edge of the
sheets, as shown in fig. 2.1. The weld is intersected, as it were,
before welding, thus enabling the investigators to record the weld
formation on a high speed colour film and to evaluate temperatures
afterwards by colour comparison. Although with high energy produc-
tion rates the maximum temperature level is limited as a result of
the tendency of the molten metal to be pushed away in the direction
of the camera or to cover less heated parts of the weld, the method
seems to offer a useful possibility to determine welding tempera-
tures or to study weld formation.

### 2.1.3. Analytical Methods

Owing to the complexity of the problem no solution can be obtained
in the form of an explicit function of the relevant parameters
satisfying equation (2.1) as well as the initial and boundary
conditions. However, several investigators have tried to simplify
the problem in order to permit the derivation of an analytical
solution. The advantages of such a procedure are obvious. The
solution can be given in a very compact form; it is valid for the
complete range of the variables involved and no expensive and
laborious expedients are necessary. Finally, an explicit function
offers the possibility to easily differentiate with respect to time
in order to determine the values of heating or cooling rates. On
the other hand, the problem solved differs substantially from the
real situation.
The main characteristic of such solutions is the neglect of elec-
tric contact resistance, of electrode properties and of heat
production distribution. Simplifications regarding heat transfer to
either the surrounding sheet or the electrodes commonly are made,
in order to reduce the number of space coordinates.
This results in a one-dimensional solution given by references
[26] and [27]. The welding heat is supposed to be generated at the
workpiece interface only and to flow in the direction of the
electrode face, the temperature of which equals that of the
ambience. The analysis is applied to the welding of foil gauges
where a one-dimensional heat flow seems to be a fair approximation

indeed because of the very high electrode diameter to sheet thickness ratios employed there.

Two-dimensional radial heat flow resulting from a line source along the z-axis is assumed in [28]. This solution might represent the opposite case, i.e. a very small electrode diameter compared with sheet thickness.

Three-dimensional solutions depart from either a point source in an infinite solid [29] or from a weld nugget of uniform temperature during the whole welding cycle [6]. The first completely disregards the presence of electrodes with high thermal conductivity, while the second uses a single coefficient of surface heat transfer to account for the amount of heat flowing to the surrounding sheet as well as to the electrodes.

Generally, the analytic solutions are useful for a limited range of applications, but they fail to give a coherent description of the thermal aspects of the spot welding process.

2.1.4. Numerical Solutions

Numerical methods must be used to avoid the simplifications required for an analytical approach. With the aid of relation (2.1) difference equations can be established applicable to small elements of the welding work. These elements are defined by space increments. In a three-dimensional set-up the number of elements and thus the number of equations will soon be of such an extent that the employment of a digital or analogue computer becomes indispensable. Since the treatment of the problem on an analogue computer would require at least one integrator for every volume element, the possibilities of this method are limited. In most cases, the storage capacity of a digital computer offers greater facilities for more extensive systems.

The first numerical solution established with the aid of a digital computer was given by GREENWOOD [30]. Here, heat generation distribution throughout the workpiece body and actual weld geometry were taken into account. The cooling effect of the electrodes was included by means of a coefficient of surface heat transfer for the workpiece-electrode interface. The dependence of material properties on temperature and the contact resistances were ignored. The

reason for these neglects was the lack of information about these
phenomena particularly on the breakdown of contact resistance
during the welding cycle. For the same reason the diameter of the
interworkpiece contact area was assumed to have the same dimension
as the electrode tip diameter.

One important conclusion can be drawn from this work with regard to
the shape of the well nugget in dependence on weld time. Fig. 2.2
shows that for a very short weld time – which means high heat
production rate – a ring-shaped welding zone develops, while
maximum temperatures of the electrode face occur at its edge. Medium
energy input, resulting in a longer weld time yields a cylinder-
shaped nugget, whereas at low energy production rate the well-known
ellipsoidal nugget form arises and the maximum temperatures of the
electrode face occur at its centre.

Experimental verifications of these computations were carried out
by several authors [22, 25, 31]. Generally, a fair agreement is
observed between theory and experiments especially during the later
stages of heat build-up. In the beginning of the heating cycle,
however,the contact resistances at the electrodes and at the work-
piece interface tend to increase the calculated temperature values.
According to [22] further discrepancies between calculated and
observed temperatures may have been caused by the influence of
temperature on material properties.

Another numerical calculation [32] shows the possibility of
accounting for contact resistances, variable material properties
and shape of the welding current pulse in the one-dimensional case
of welding laminated bars of comparitively small cross-section
axially to each other.


## 2.1.5. Simulation by means of an Analogue

An attractive method of evaluating the temperatures during spot
welding is the use of the analogy of the process in question with
any other phenomenon subjected to the same differential equation
and boundary conditions. This approach of the problem is not merely
empirical, since the physical laws which control the process under
review as well as the analogue model have to be known in detail.
It is noted that this approach is distinctly different from the use
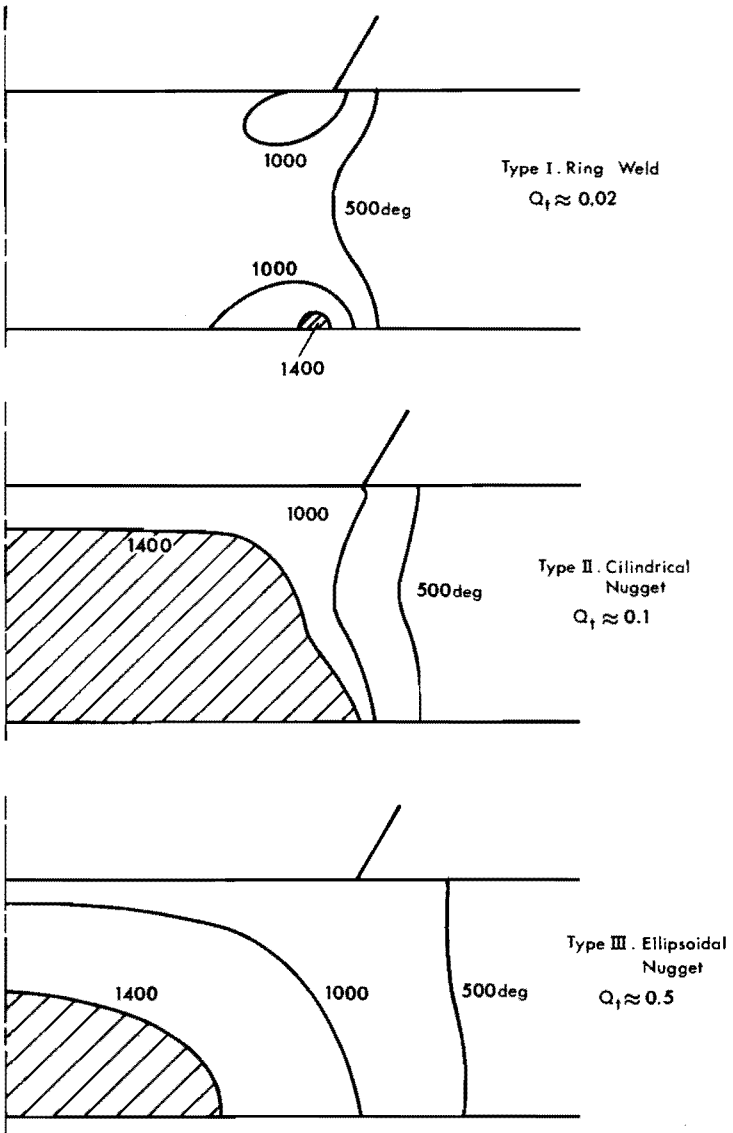of an analogue computer.

24

Fig. 2.2. Different Shapes of Weld Nuggets in dependence on Heating Time, as described in [25]

Temperature values are given for reference only

The most obvious analogue would be the spot welding process itself.
The geometric dimensions should then be enlarged to values in the
order of ten to hundred times the usual sizes and also the time
scale requires sufficient extending in order to permit the
measurement of the thermal and electrical potentials. To confine
the magnitude of the welding current to reasonable values the
electric and thermal conductivities should be diminished by a same
factor of ten to hundred. A baked carbon [36] with electric
resistivity of about $10^{-4}\Omega.m$ and thermal conductivity of 2
$W.m^{-1}.deg^{-1}$ might prove to be useful for the purpose.

However, the analogy most widely used is to relate transient heat
transfer to the flow of electric currents through a network of
resistors and capacitors representing thermal resistance and heat
capacity respectively. Though in a simple form, GENGENBACH [12]
used a one-dimensional performance of this Beuken model [33] to
determine spot weld temperatures, particularly for the case of
series welding.

A more realistic analogue was developed by RIEGER and RUGE [34].
The performance is fundamentally three-dimensional although the
existence of axial symmetry in fact reduces the number of space
coordinates to two. The RC-network employed resembles very much the
model described in this thesis, but the use of it is restricted to
the determination of the final temperatures in spot welding 1 mm
copper and aluminium sheets.

The absence of a simple method to simulate temperature-dependent
material properties may be regarded as a disadvantage of the
passive RC analogue compared with a digital computer, although
several possibilities arise with the use of active electronic
elements [35].

2.1.6. The Role of the Contact Resistance

The contact resistance is an extra resistance between two points
on either side of a contact surface, additional to the ordinary
body resistance. This additional resistance is due to the imper-
fection of the contact between the two members, produced by the
irregularities of the surfaces that cause them to contact each
other only at a number of small spots. Furthermore, the influence

of thin oxide layers or films may reduce the electric conductivity of these spots. If alien substances such as grease or dirt are present the resistance increases to values much higher than the total body resistance of the contact members [6, 36].

In spot welding such contact resistances exist between the work-pieces as well as between workpieces and electrodes. However, they have a dynamic character. When the electric current starts to flow the contact spots are rapidly heated to high temperatures [36] so that they tend to grow in dimension and in number as a result of the weakening of the metal. The total resistance thus decreases rapidly. Several investigators observed the contact resistance to break down to zero value during the first half cycle when alter-nating welding current was used [6, 37, 38].

Nevertheless [22] observes a notable effect of contact resistance on the temperature distribution in spot welding mild steel. For aluminium the value of the initial contact resistance greatly affects the quality of the weld made. Reduction of this resistance to a minimum value will in this case enhance weld consistency, weld nugget shape and electrode tip life [37, 44].

[39], on the other hand, shows that in welding highly resistive metals with only a small tendency towards the forming of oxide films, such as nimonic 80, 18/8 stainless steel and titanium alloys, the heat production is only slightly influenced by the presence of contact resistances. It is demonstrated that when heating a single sheet of these materials or when welding two sheets with unequal thickness (3:1 ratio) the nugget always forms in the middle of the total thickness.

In conclusion, the influence of contact resistance on the welding process is commonly considered to increase if

(a) the sheet thickness decreases,
(b) the electrode force decreases,
(c) the thickness of the oxide film increases,
(d) the resistivity of the oxide increases in proportion to body resistivity and
(e) the weld time decreases.

For the obtainance of high-quality welds it is a general practice to minimize surface resistance by mechanical or chemical cleaning methods [1, 10]. From the foregoing it appears to be impossible to

27

predict the value of contact resistance with universal validity.
For both reasons this resistance will be disregarded in the first
instance; the resultant deviations will be considered in section
4.3.

Apart from the electric contact resistance there is also a thermal
contact resistance in the same planes. Its influence on the welding
process, however, is far less pronounced. At the workpiece inter-
face it does not play a role at all because of the absence of
thermal flow on account of symmetry. At the electrode face its
value is relatively small compared with its electric equivalent;
this is due to the fact that oxides and air gaps do not act as
insulators for heat flow as they do for electric current [41]. Its
influence is therefore disregarded.


2.1.7. The Use of Dimensionless Parameters


The use of dimensionless parameters offers important advantages in
experimental work in which a great number of variables is concerned.
According to [40] the number of dimensionless parameters equals the
number of variables minus the number of fundamental dimensions
involved. In this way the thirteen significant variables
- including temperature - ( see section 2.1.1) can be reduced to
eight dimensionless parameters, being products of those variables.
The five fundamental dimensions are length, mass, time, electric
current and temperature.

The quantity of experiments required to verify a theoretical
calculation is therefore reduced substantially, since this quantity
tends to increase with the n-th power of the number of parameters
to be considered, n representing the number of levels on which
each parameter is varied. If the results of calculations or experi-
ments are not given in the form of analytic formulas but in graphs
or tables, this representation is simplified and diminished in size
as well.

To evaluate the relevant dimensionless products the differential
equation (2.1) and its boundary conditions have to be considered.
In the case of constancy of coefficients and axial symmetry the
equation can be written

28

$$c \frac{\partial \theta}{\partial t} = \lambda \left( \frac{\partial^2 \theta}{\partial z^2} + \frac{\partial^2 \theta}{\partial r^2} + \frac{1}{r} \frac{\partial \theta}{\partial r} \right) + \rho J^2 \qquad (2.2)$$

Dimensionless variables can now be introduced

$$Q_z = \frac{z}{s} ; \qquad Q_r = \frac{r}{s} \qquad (2.3)$$

$$Q_\theta = \frac{\theta}{\theta_{ch}} ; \qquad Q_t = \frac{t}{t_{ch}} \qquad (2.4)$$

where $\theta_{ch}$ and $t_{ch}$ denote characteristic values still to be defined for temperature and time respectively. By introducing the products $Q_1$ and $Q_2$ equation (2.2) can be rewritten

$$\frac{\partial Q_\theta}{\partial Q_t} = Q_1 \left( \frac{\partial^2 Q_\theta}{\partial Q_z^2} + \frac{\partial^2 Q_\theta}{\partial Q_r^2} + \frac{1}{Q_r} \frac{\partial Q_\theta}{\partial Q_r} \right) + Q_2$$

with $Q_1 = \dfrac{\lambda t_{ch}}{s^2 c} = \dfrac{a t_{ch}}{s^2}$

and $Q_2 = \dfrac{\rho J^2 t_{ch}}{c \theta_{ch}}$ .

If $t_{ch}$ and $\theta_{ch}$ are chosen to satisfy $Q_1 = Q_2 = 1$ it follows

$$t_{ch} = \frac{s^2}{a} \qquad \text{and} \qquad \theta_{ch} = \frac{\rho J^2 s^2}{\lambda} \qquad (2.5)$$

and hence

$$\frac{\partial Q_\theta}{\partial Q_t} = \frac{\partial^2 Q_\theta}{\partial Q_z^2} + \frac{\partial^2 Q_\theta}{\partial Q_r^2} + \frac{1}{Q_r} \frac{\partial Q_\theta}{\partial Q_r} + 1 \qquad (2.6)$$

where $\qquad Q_\theta = \dfrac{\lambda \theta}{\rho J^2 s^2} \qquad \text{and} \qquad Q_t = \dfrac{at}{s^2} \qquad (2.7)$

29

The other six products result from boundary conditions, electrode properties and weld geometry

$$Q_c = \frac{c_E}{c} \; ; \qquad Q_\lambda = \frac{\lambda_E}{\lambda} \; ; \qquad Q_\rho = \frac{\rho_E}{\rho} \; ;$$

$$Q_F = \frac{4F}{\pi D_E^2 H_V} \; ; \qquad Q_D = \frac{D_E}{s} \; ; \qquad Q_h = \frac{h}{D_E} \qquad (2.8)$$

## 2.2. The Mathematical Model

### 2.2.1. Choice of the Computation Method

In order to obtain a coherent physical model of spot welding suitable as a basis for workshop practice, some degree of the mathematically achievable accuracy has to be relinquished in favor of easier interpretation by the employer. This does not only mean that variables with relatively little influence on the results are omitted. It also indicates that a variable of which the influence can be quantitatively expressed by multiplying the results by a known factor may be excluded from the model in the initial stages, This will be shown to be more or less applicable to

(a) temperature-dependent material properties,
(b) latent heat of fusion, and
(c) the influence of the contact resistance.

As a matter of fact, the described model is based on the assumption of a simplified current distribution. It will be shown by the experimental results that the introduction of an adequate multiplicator sufficiently accounts for the deviations caused by this simplification.
As already pointed out, various investigators have developed methods to determine spatial temperature distributions during the welding of specified materials and geometries, using the above assumptions. For technical applications, however, the need for

30

general information regarding temperature-time relations is
considered of primary importance in order to facilitate the setting
of welding variables when a given strength or dimension of the
weld is desired. Therefore, the determination of the interrelation
of temperature and time for a few important areas of the weld will
be emphasised in the present work.

It may be concluded from the foregoing review of computation
methods that only a numerical approach or the application of an
analogue will yield acceptable results. The advantages of a
digital computer over an analogue model, viz. its higher accuracy
and its disposition to solve a non-linear form of equation (2.1),
are not relevant if the accuracy is already affected by the intro-
duction of necessary simplifications and if the equation is
linearized by means of the statements (a) and (b). In this
situation the analogue has pronounced advantages. The results are
more easily perceptible as they can immediately be read from an
oscillograph and necessary changes in the computation programme are
less laborious [35]. For these reasons the RC analogue is chosen to
determine temperatures in spot welding, especially as functions of
time. Besides, the use of dimensionless variables is considered to
be of great convenience.


2.2.2. Assumptions, Initial and Boundary Conditions

The mathematical model comprises a combination of specifications,
appropriate physical laws, boundary conditions with respect to
space and time and assumptions. It is assumed to describe the
process quantitatively with an accuracy sufficient for practical
applications.

If a coordinate system is chosen with its origin in the centre of
the weld, the positive z-axis coinciding with the electrode axis
and the r-axis lying in the interworkpiece contact plane, obviously
axial symmetry exists. If, in accordance with section 1.3, the
dimensions of the electrodes and those of the sheets are equal,
plane symmetry exists with regard to the plane $z = 0$ as well. This
implies that no heat can flow across this plane, hence only the
system consisting of one sheet and one electrode has to be
considered.

Since [30] demonstrates that heat loss by radiation or convection from the free surface of the sheets is negligible compared with the total heat production, these surfaces are supposed to be insulated. A uniform temperature is assumed to be present in the workpiece-electrode contact plane. No serious deviation from the real situation is introduced by this assumption [22, 25]. As a result, the heat flow to the electrode can be considered to be one-dimensional. This greatly simplifies the study of variable electrode dimensions and properties.

The effect of the latent heat of fusion on the temperature development of the weld cannot easily be predicted quantitatively. Of course, the time in which the centre of the weld reaches the melting point is not influenced by latent heat. The same applies to the region $r < 0.3D_E$ in the plane $z = 0$, since local temperature gradients are comparatively small before melting initiates. During the growth of the melting area the surrounding region will no longer receive heat from the centre, since there the gradients reduce to zero. Consequently the temperatures in the surrounding region increase at a slower rate. To some extent this effect is compensated by the higher energy production rate due to the increase of electrical resistivity with temperature.

As indicated earlier the latent heat of fusion as well as the influence of temperature on physical properties will be neglected mathematically. Their effects are accounted for by means of empirical values of the variables $\rho$, c and $\lambda$ as to be defined in chapter 3.

In accordance with section 2.1.6 the thermal contact resistances are neglected, the electrical contact resistances being considered in chapter 4.

Minor simplifications regard the coolant temperature, which is assumed to be equal to the ambient temperature, the electrode shape (see fig. 2.3) and the shape of the welded sheets, which are supposed to be circular and to have a diameter of 100.s. Our experiments indicate that this shape has no influence at all on the results as long as a minimum diameter of $5D_E$ is maintained. Finally, an approximate method is used to account for the non-uniform distribution of electric current and, consequently, of heat generation in the workpiece. This method consists in comparing the real body resistance of the sheets between the electrodes with the
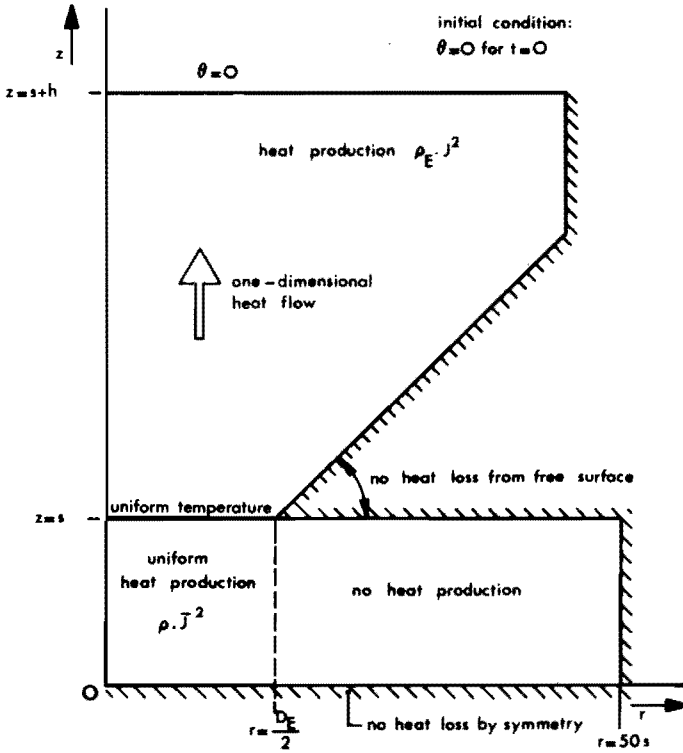
Fig. 2.3. Cross-section of the Mathematically Relevant Part of the Weld.
Main Assumptions and Boundary Conditions

resistance of a cylinder of diameter $D_E$ and height $2s$. The total
quantity of heat developed in this cylinder is adjusted by means of
the resistance ratio thus found.

In doing so, the assumed distribution of the heat generation in
the analogue model is substantially simplified, viz.

$$\rho J^2 = \frac{16\rho i^2}{\pi^2 D_E^{\,4}} = \rho \bar{J}^2 \qquad \text{for} \qquad r \leq \frac{D_E}{2} \left.\vphantom{\begin{array}{c}a\\b\\c\\d\end{array}}\right\}$$

$$\rho J^2 = 0 \qquad \text{for} \qquad r > \frac{D_E}{2}$$

(2.9)

33

In section 4.2 the required adjustment will be shown to depend on $Q_D$ only.

Fig. 2.3 shows a cross-section of the mathematically relevant part of the weld geometry, in which the main assumptions and boundary conditions are demonstrated.

## 2.2.3. Description of the Analogue Model

At this point, the object of the analogue model can be defined more closely. The aim is to solve equation (2.6) along with the assumptions, initial and boundary conditions mentioned in the foregoing section. As a first step this differential equation will be linearised with respect to the space derivatives. For this purpose the sheet is thought of as divided in ring-shaped elements having a cross-section $\epsilon^2$ as shown in fig. 2.4. The volume of an element $[m,n]$ depends on n only

$$V[m,n] = \tfrac{1}{2}(2n - 1)\phi\epsilon^3 \qquad (2.10)$$

Its surfaces perpendicular to the $Q_z$-axis are

$$A_z[m-1,n] = A_z[m,n] = \tfrac{1}{2}(2n - 1)\phi\epsilon^2 \qquad (2.11)$$

and perpendicular to the $Q_r$-axis

$$A_r(Q_r) = \phi Q_r \epsilon \qquad (2.12)$$

as illustrated in fig. 2.5.

Subsequent integration of the terms of equation (2.6) over the volume element $[m,n]$, assuming that the potential $Q_\theta$ does not vary within the element, yields for the first term

34
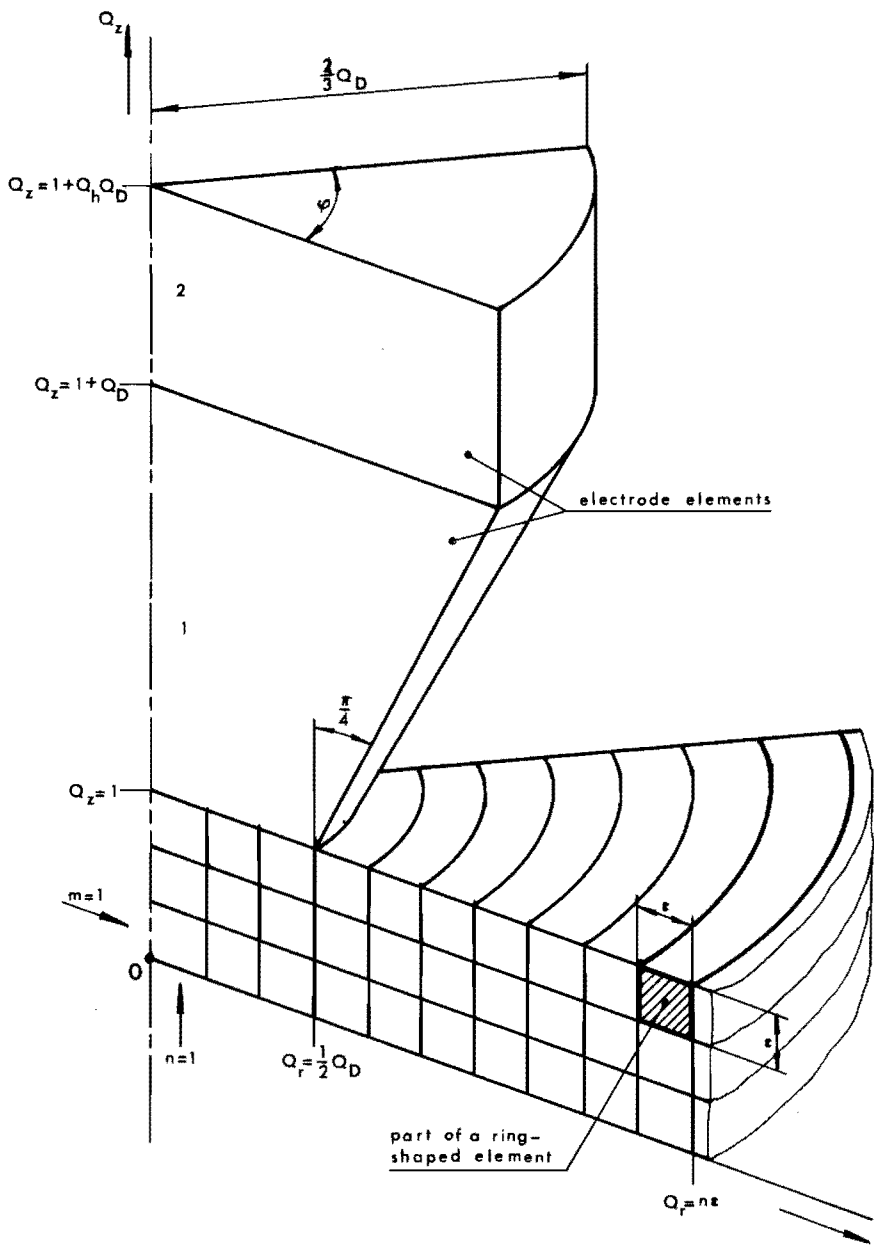
Fig. 2.4. Division of the Workpiece and the Electrode in
Volume Elements, drawn for the case $Q_D = 2$
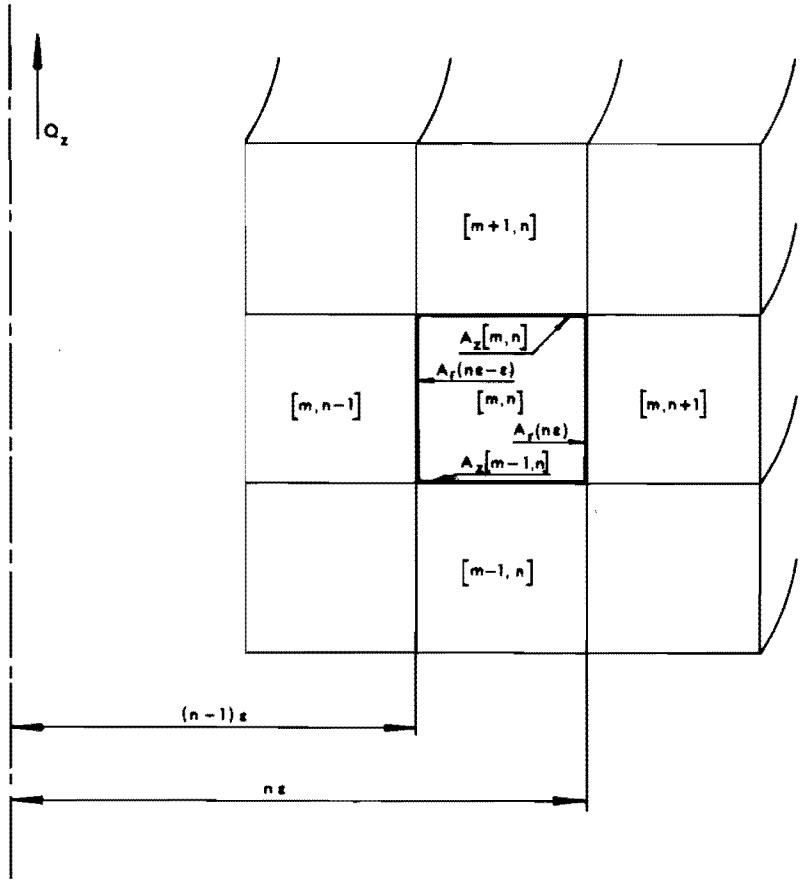
Fig. 2.5. Position of the Element $[m,n]$ amid its neighbouring Elements.
Nomenclature of the bounding surfaces

$$\iiint\limits_{V[m,n]} \frac{\partial Q_\theta}{\partial Q_t} [m,n] dV = \frac{\partial Q_\theta}{\partial Q_t} [m,n] \cdot \tfrac{1}{2}(2n - 1)\phi\varepsilon^3 \qquad (2.13)$$

To the second term Gauss' theorem is applied

$$\iiint\limits_{V[m,n]} \{\frac{\partial^2 Q_\theta}{\partial Q_z^2} + \frac{\partial^2 Q_\theta}{\partial Q_r^2} + \frac{1}{Q_r} \frac{\partial Q_\theta}{\partial Q_r}\} \, dV =$$

$$= \iint\limits_{A_z} \frac{\partial Q_\theta}{\partial Q_z} \, d A_z + \iint\limits_{A_r} \frac{\partial Q_\theta}{\partial Q_r} \, d A_r =$$

$$= \{ \frac{\partial Q_\theta}{\partial Q_z}[m,n] - \frac{\partial Q_\theta}{\partial Q_z}[m-1,n] \} . \tfrac{1}{2}(2n - 1)\phi\epsilon^2 +$$

$$+ \{ \frac{\partial Q_\theta}{\partial \log Q_r}[m,n] - \frac{\partial Q_\theta}{\partial \log Q_r}[m,n-1] \} . \phi\epsilon \qquad (2.14)$$

This term is linearised by means of

$$\frac{\partial Q_\theta}{\partial Q_z}[m,n] = \frac{1}{\epsilon}(Q_\theta[m+1,n] - Q_\theta[m,n]) \qquad (2.15)$$

and

$$\frac{\partial Q_\theta}{\partial \log Q_r}[m,n] = \frac{Q_\theta[m,n+1] - Q_\theta[m,n]}{\log (n+\tfrac{1}{2}) - \log (n-\tfrac{1}{2})} \qquad (2.16)$$

According to equation (2.9) the third term becomes

$$\iiint\limits_{V[m,n]} G(Q_r) dV = \tfrac{1}{2}(2n - 1)\phi\epsilon^3 G(Q_r) \qquad (2.17)$$

where 
$$\left. \begin{array}{l} G(Q_r) = 1 \quad \text{for} \quad Q_r \leq \dfrac{Q_D}{2} \\[4em] G(Q_r) = 0 \quad \text{for} \quad Q_r > \dfrac{Q_D}{2} \end{array} \right\} \qquad (2.18)$$

Eventually, equation (2.6) transforms into [1])

$$(2n - 1) \frac{\partial Q_\theta}{\partial \Omega_t}[m,n] = \varepsilon^{-2}(2n - 1)(Q_\theta[m+1,n] - Q_\theta[m,n]) +$$

$$+ \varepsilon^{-2}(2n - 1)(Q_\theta[m-1,n] - Q_\theta[m,n]) +$$

$$+ 2\varepsilon^{-2}\log^{-1}(\frac{2n + 1}{2n - 1})(Q_\theta[m,n+1] - Q_\theta[m,n]) +$$

$$+ 2\varepsilon^{-2}\log^{-1}(\frac{2n - 1}{2n - 3})(Q_\theta[m,n-1] - Q_\theta[m,n]) +$$

$$+ (2n - 1) \, G(Q_r) \tag{2.19}$$

It is observed that the angular coordinate $\phi$ disappears from the formula.

Next, the nodal point $[m,n]$ of the RC-network of fig. 2.6 is considered. The application of Kirchhoff's first law to this point yields

$$C[m,n] \frac{dU}{dt_m} [m,n] = \frac{1}{R_z[m,n]} (U[m+1,n] - U[m,n]) +$$

$$+ \frac{1}{R_z[m-1,n]} (U[m-1,n] - U[m,n]) +$$

$$+ \frac{1}{R_r[m,n]} (U[m,n+1] - U[m,n]) +$$

$$+ \frac{1}{R_r[m,n-1]} (U[m,n-1] - U[m,n]) +$$

$$+ I[m,n] \tag{2.20}$$

38
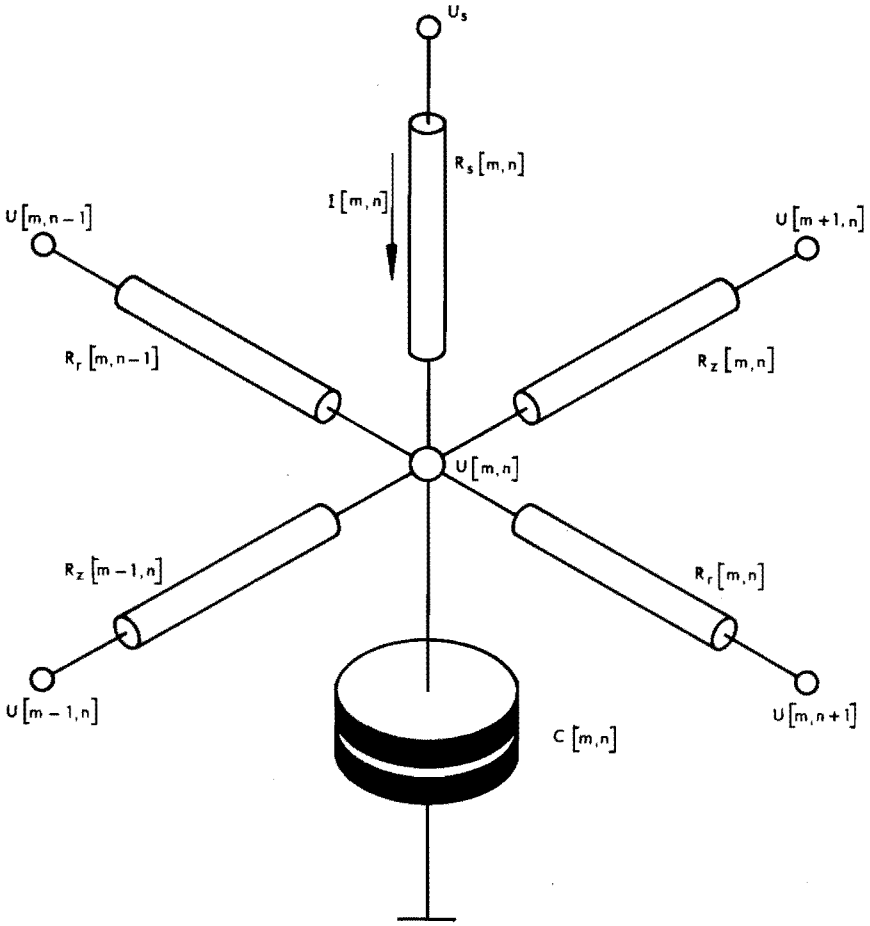
Fig. 2.6. Analogue Network Element $[m,n]$

If $U[m,n] \ll U_s$ then for $I[m,n]$ can be written

$$I[m,n] = \frac{U_s}{R_s[m,n]} \qquad (2.21)$$

By introducing the basic resistor $R_o$ and capacitor $C_o$ as arbitrary units and by defining the dimensionless products

$$Y_U[m,n] = \frac{U[m,n]}{U_s} \qquad \text{and} \qquad Y_t = \frac{t_m}{R_o C_o} \qquad (2.22)$$

equation (2.20) can be written

$$\frac{C[m,n]}{C_o} \frac{dY_U}{dY_t}[m,n] = \frac{R_o}{R_z[m,n]} (Y_U[m+1,n] - Y_U[m,n]) +$$

$$+ \frac{R_o}{R_z[m-1,n]} (Y_U[m-1,n] - Y_U[m,n]) +$$

$$+ \frac{R_o}{R_r[m,n]} (Y_U[m,n+1] - Y_U[m,n]) +$$

$$+ \frac{R_o}{R_r[m,n-1]} (Y_U[m,n-1] - Y_U[m,n]) +$$

$$+ \frac{R_o}{R_s[m,n]} \qquad (2.23)$$

Comparison of the equations (2.19) and (2.23) shows that both relations are homologue if

$$\frac{C[m,n]}{C_o} = 2n - 1 \qquad (2.24)$$

$$\frac{R_z[m,n]}{R_o} = \frac{10^{-2}}{2n - 1} \qquad (2.25)$$

40

$$\frac{R_r[m,n]}{R_o} = \frac{10^{-2}}{2} \log \left(\frac{2n + 1}{2n - 1}\right) \qquad (2.26)$$

$$\frac{R_s[m,n]}{R_o} = \frac{1}{2n - 1} \cdot \frac{1}{G(\theta_r)} \qquad (2.27)$$

$$Q_\theta = 10^2 \varepsilon^2 Y_U \qquad (2.28)$$

$$Q_t = 10^2 \varepsilon^2 Y_t \qquad (2.29)$$

where $C_o$ and $R_o$ may still be given any value. The factor $10^2$ is added in order to obtain that

$$R_s[m,n] = 10^2 \cdot R_z[m,n]$$

which ensures the validity of relation (2.21).

An electric network representing the geometric arrangement of fig. 2.4 can now be designed. The set-up of the complete analogue is shown in fig. 2.7. The inner part of the sheet is divided in forty-five elements arranged in three rows of fifteen elements. The corresponding nodal points represent the centres of the volume elements. From the number of rows it follows that $\varepsilon = \frac{1}{3}$. The outer part of the sheet is divided in coarser elements 16, 17 and 18, the centres of which lie at distances of $19.3\varepsilon$, $43.0\varepsilon$ and $102.7\varepsilon$ from the symmetry axis respectively. The electrode is divided in only two elements, 1 and 2.

The value of $Q_D$ is varied by connecting the electrode network to the required number of nodal points of the fourth row of the workpiece network, by applying the supply voltage $U_s$ to the appropriate points and by adjusting the values of the electrode network components. These values are determined in dependence on the electrode dimensions, expressed in multiples of $\varepsilon$, and the variables $Q_c$, $Q_\lambda$ and $Q_\rho$ by dealing with the differential equation
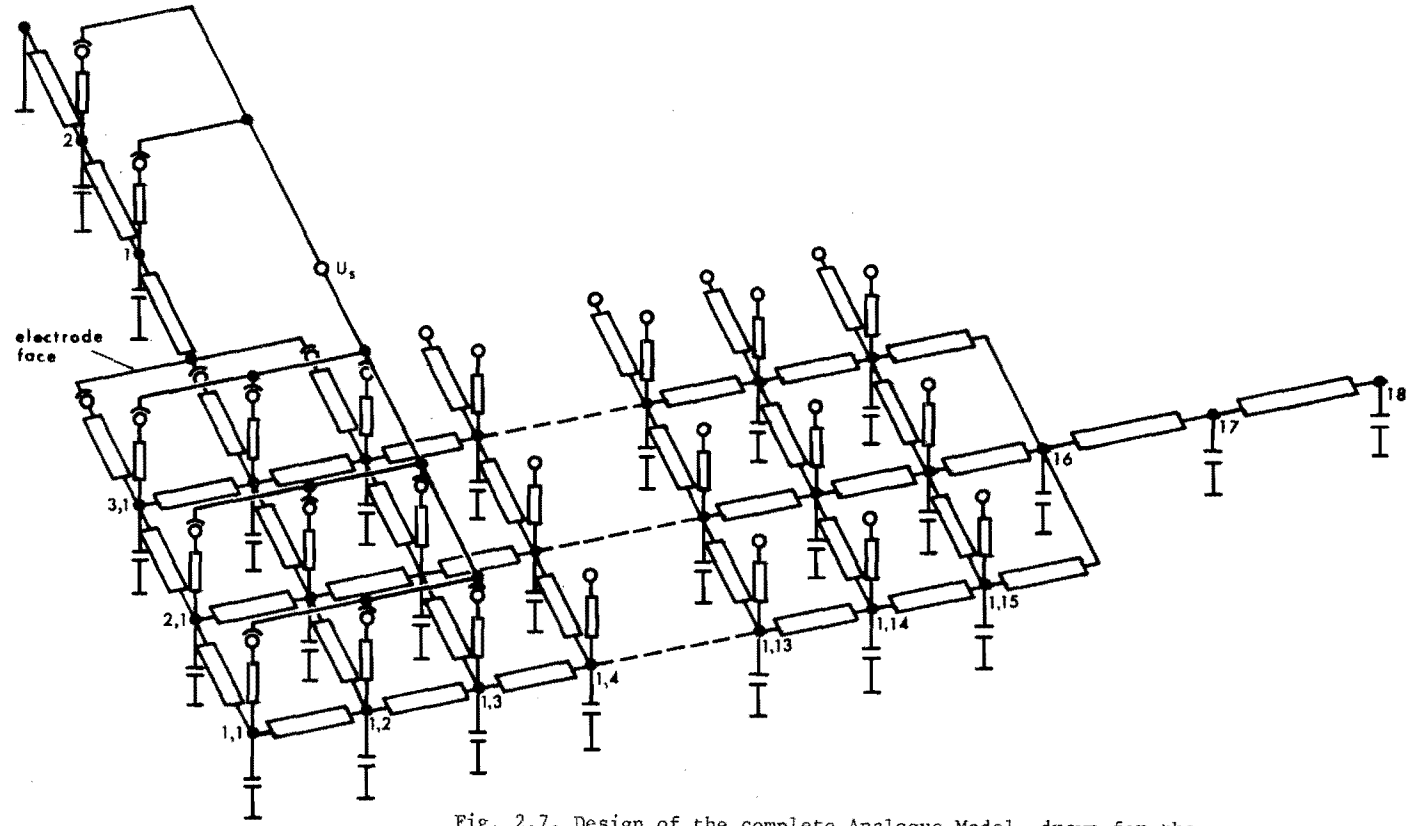
41

Fig. 2.7. Design of the complete Analogue Model, drawn for the case $O_D = 2$

$$Q_c \frac{\partial Q_\theta}{\partial Q_t} = Q_\lambda \frac{\partial^2 Q_\theta}{\partial Q_z^2} + Q_\rho \qquad\qquad (2.30)$$

in the same way as with (2.6).

If $C_o = C[m,1] = 10^{-6}$ F and $R_o = R_s[m,1] = 10^6 \Omega$,

and $t_m$ is expressed in seconds, it can be concluded from equation (2.22) that the numerical values of $Y_t$ and $t_m$ are equal.

---

[1]) Division of both members of equation (2.19) by a factor $(2n - 1)$ would simplify the set-up of the model. In doing so, $C[m,n]$ in equation (2.24) would acquire the same value for all nodal points. The same applies to $R_z[m,n]$ and $I[m,n]$. This fact became plain after the model network had been built. However, it does not change the results of the measurements.

## 2.3. Analogue Measurements

### 2.3.1. Design of the Measurements

With the aid of the analogue described in the foregoing sections the dependence of the potential $Q_\theta$ on $Q_t$ for a few selected points of the weld can be established. These points are the centre of the weld C $(Q_z = 0, Q_r = 0)$, where temperatures are generally maximum, the border of the weld nugget B $(Q_z = 0, Q_r = \frac{1}{2}Q_D)$, where the temperature just reaches the melting point, and the electrode face E $(Q_z = 1, Q_r < \frac{1}{2}Q_D)$, the temperature of which determines electrode life [31].
The six dimensionless products defined in (2.8) are to be considered independent parameters for these measurements. However, in order to limit the number of variables the shape and the geometric proportions of the electrode are not varied. Thus $Q_h$ is kept constant to 1.5. This value is relatively low compared with

standard practice [43], but as shown in [44] and [45] a thin wall
between electrode face and coolant channel substantially reduces
electrode wear. As indicated in section 1.3, a flat-faced
electrode is used with a 45 deg truncated cone in order to control
adequately the size of the electrode-workpiece contact area,
during welding.

As contact resistances are neglected in this stage of the
investigation, the influence of the product $Q_F$ is left out of
consideration.

From the Wiedemann-Franz-Lorenz law

$$\rho(\Theta) . \lambda(\Theta) = L.\Theta \tag{2.31}$$

where L is a constant which is practically independent of the
material choice and $\Theta$ the absolute temperature, it follows that

$$Q_\rho = Q_\lambda^{-1} \tag{2.32}$$

The three remaining parameters are varied numerically in such a way
that most of the usual machine settings or material properties are
covered, viz.

$Q_c$ = 1 and 2,

$Q_\lambda = Q_\rho^{-1}$ = 1, 3 and 9,

$Q_D = \frac{2}{3}$, 2, 4 and 8.

In this way continuous curves can be drawn showing the relation
$Q_\Theta(Q_t)$ for each combination of parameter values and for each of the
three points defined earlier in this section. Fundamentally, $Q_t$
varies from zero to infinity, although only the interval
$0.1 < Q_t < 10$ is of interest in practical cases.


## 2.3.2. Results of the Analogue Measurements

The measurements were carried out by applying the voltage $U_s$ to the
network for a well-defined time lapse and by recording the
potentials of the chosen points simultaneously on a multi-channel

44

recording oscillograph. Fig. 2.8 shows the analogue and the measuring devices. As a matter of course, any current shape can be simulated by means of the form of the function $U_s(t_m)$ instead of the direct welding current used in the present work.
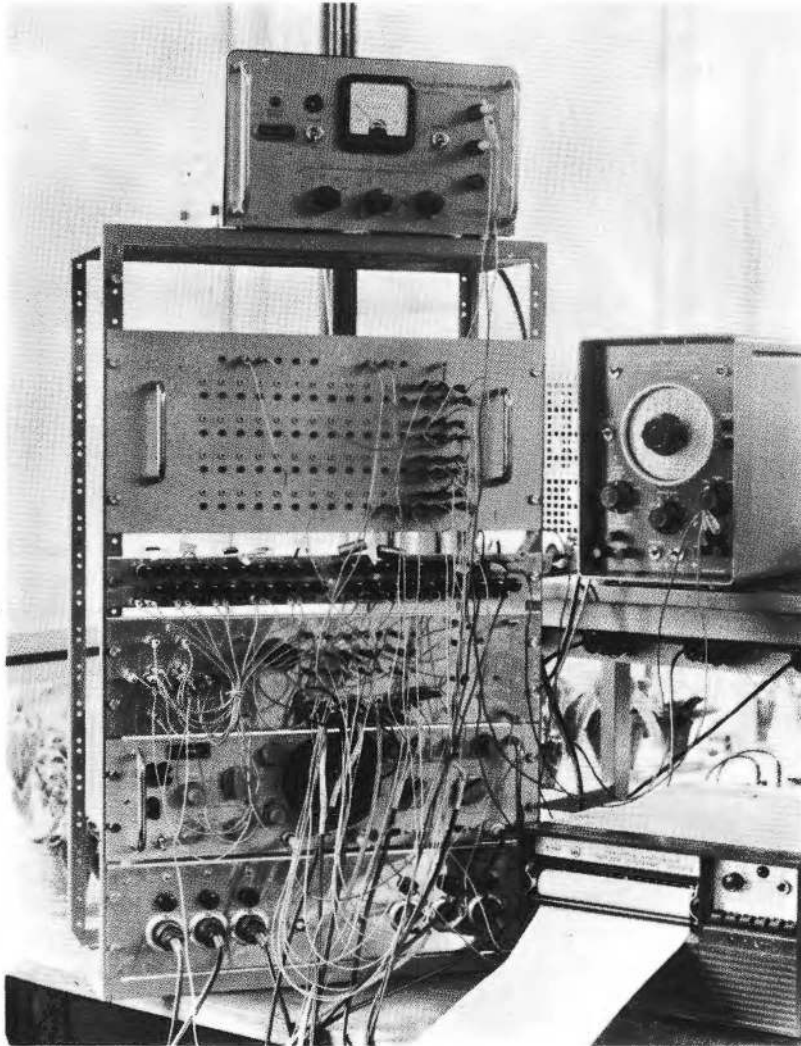


Fig. 2.8. View of the Analogue and the Measuring Devices. In the centre from top to bottom, Voltage Supply, Sheet Network, Electrode Network with interchangeable Components, Switch Panel, Oscilloscope and 6-channel Recorder Pre-amplifier. To the right, Time Switch and Galvanometer Recorder

As an example, some of the heating curves obtained in this way are
shown in fig. 2.9 for the centre of the weld. As can be concluded
from equation (2.6) the derivative $\partial Q_\theta / \partial Q_t$ approaches 1 for small
values of $Q_t$, since $\nabla^2 Q_\theta = 0$ initially. From the measurements it
appears that $Q_c$ has no perceptible influence on the course of the
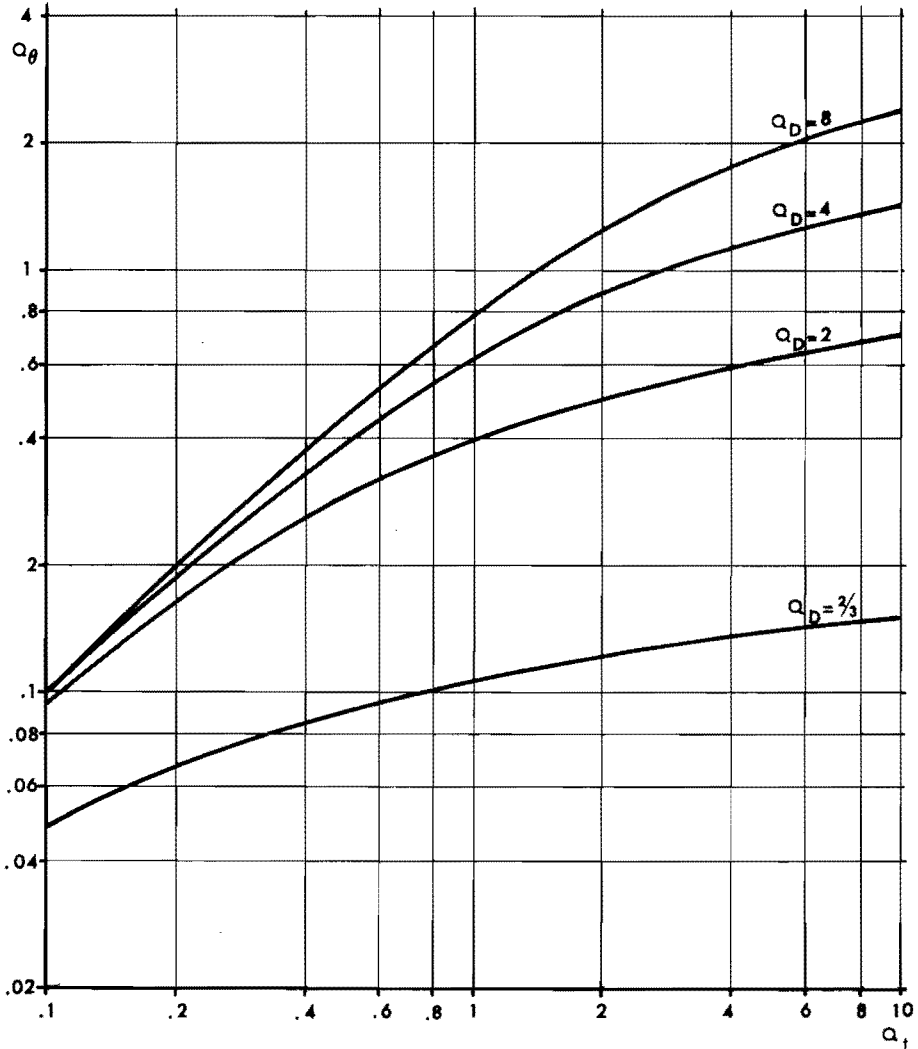


Fig. 2.9. $Q_\theta$ as a function of $Q_t$ for different values of $Q_D$
(Centre of the Weld, $Q_\lambda = 1$)

curves. On the other hand, the product $Q_\lambda$ considerably affects the
value of $Q_\theta$. Its influence is greater according as $Q_D$ and $Q_t$
increase, as is illustrated by fig. 2.10.
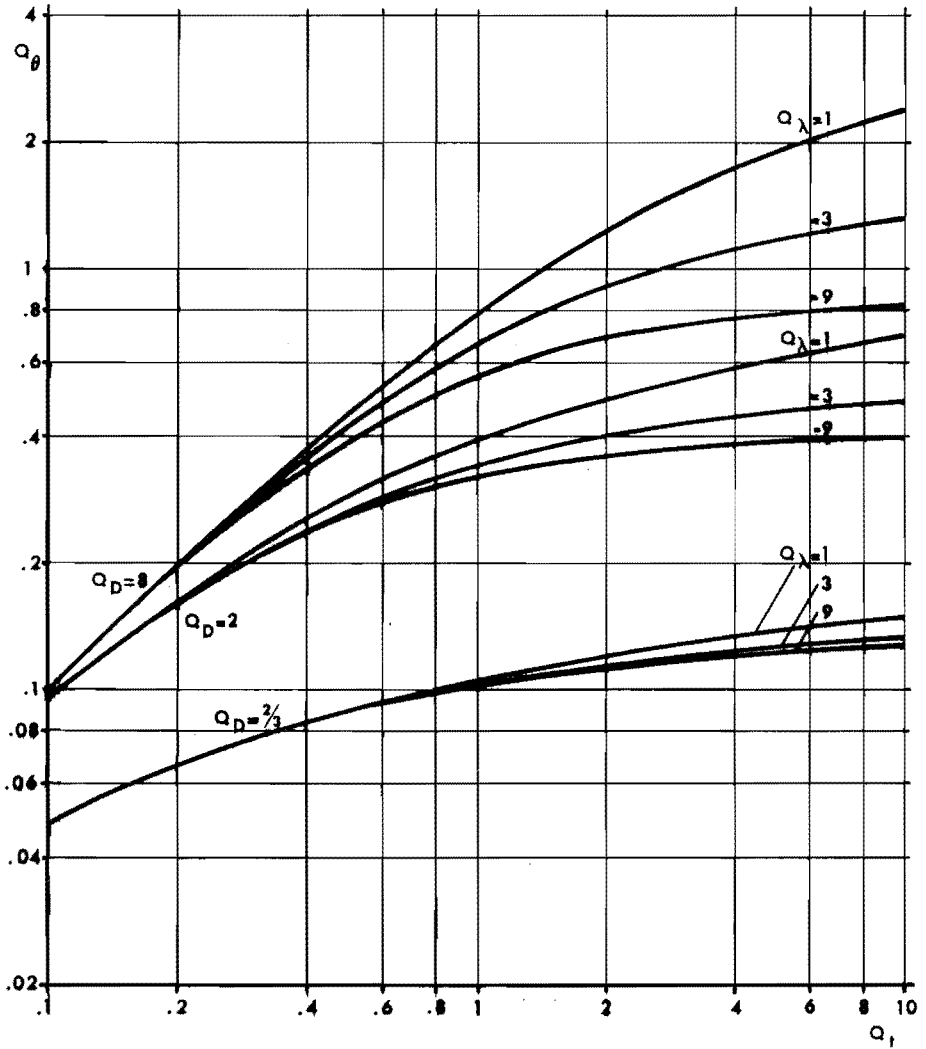


Fig. 2.10. The Influence of $Q_\lambda$ on the Function $Q_\theta(Q_t)$ for
some values of $Q_D$ (Centre of the Weld)

47
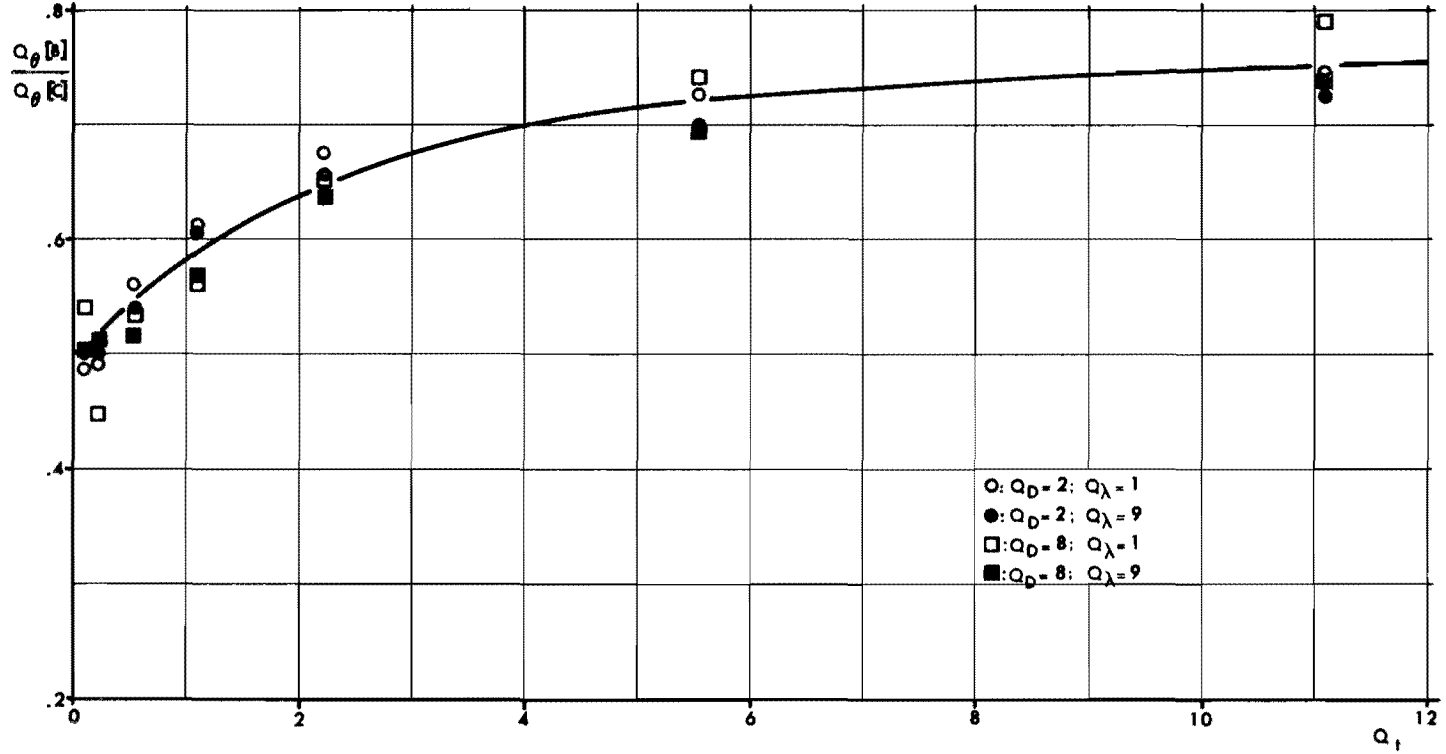
Fig. 2.11. The ratio of the $Q_\theta$ values at the Nugget Border B and
in the Centre of the Weld C in dependence on $Q_t$

The ratio of the $Q_\theta$ values at the nugget border B and in the centre of the weld C seems to be dependent on $Q_t$ only, as demonstrated in fig. 2.11. This ratio is $\frac{1}{2}$ for small $Q_t$ and approaches a constant value of $\frac{3}{4}$ for $Q_t > 5$. Since the relative deviations from the curve are generally less than five per cent., it is sufficiently accurate for technical applications.

If it is desired that the weld nugget diameter should become equal to that of the electrode, the temperature at the nugget border must reach the melting point of the welded material. In this case the electrode face temperature is determined by the ratios graphically shown in figs. 2.12 to 2.14 inclusive. From these graphs the importance of a high $Q_\lambda$ value, i.e. of thermally well conducting electrode material is evident. For example, when welding copper sheet, it can be seen from fig. 2.12 that the copper electrodes can only be prevented from being welded to the workpieces by choosing low $Q_D$ and high $Q_t$ values. On the other hand, the welding of stainless steel, where $Q_\lambda \approx 8$, will offer no problems as is known from practice.

Summarising it can be concluded that $Q_D$ is of major importance to the welding process, especially for $Q_t > 0,1$; $Q_\lambda$ is important for $Q_t > 1$, and $Q_c$ has no influence on the process.
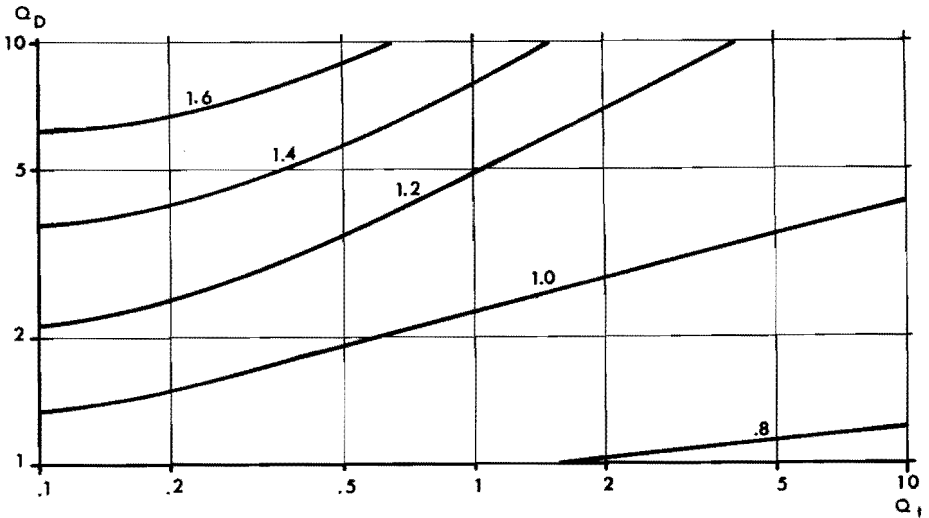


Fig. 2.13. The ratio of the $Q_\theta$ values at the Electrode Face and at the Nugget Border for $Q_\lambda = 3$
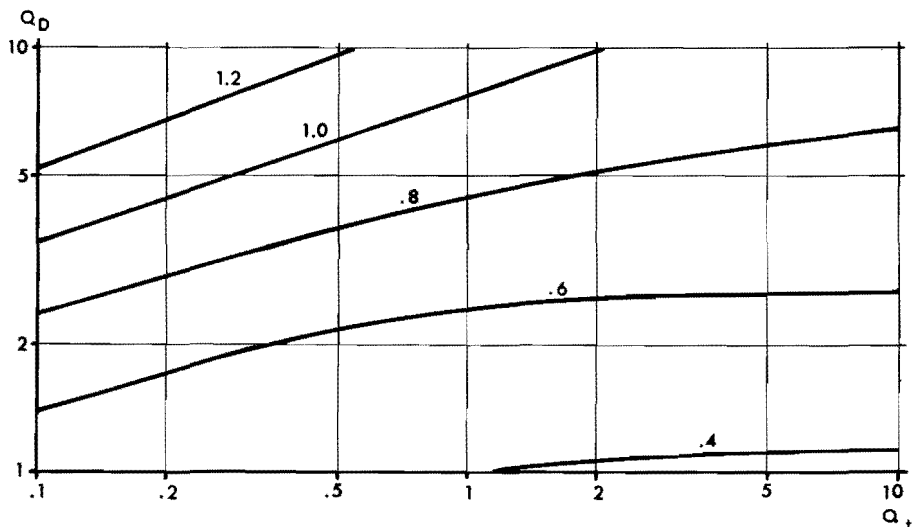
Fig. 2.14. The ratio of the $Q_\theta$ values at the Electrode Face and at the
Nugget Border for $Q_\lambda = 9$
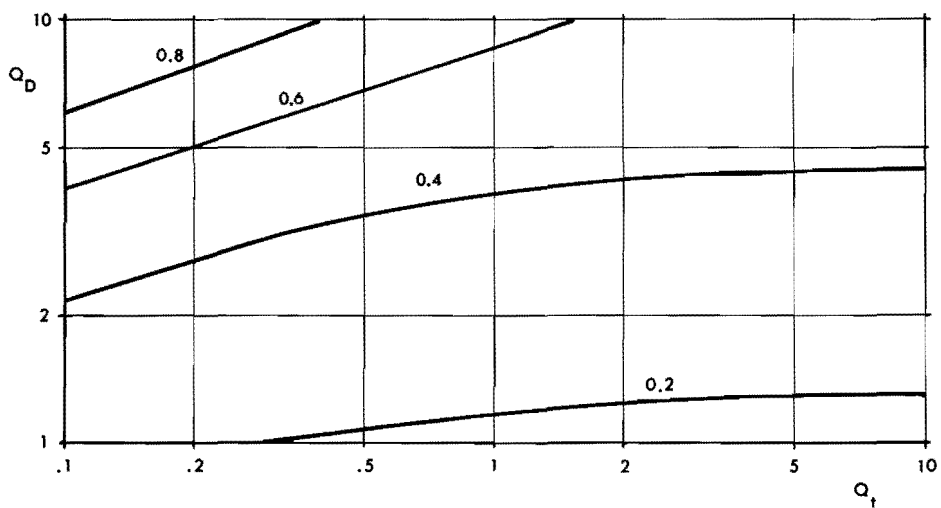


Fig. 2.12. The ratio of the $Q_\theta$ values at the Electrode Face and at the
Nugget Border for $Q_\lambda = 1$

3.1. Verification Method

As pointed out in section 1.2 the weld temperature can only be
determined accurately after welding in those places where it just
reached the melting point during the process, viz. at the
bounding surface between weld nugget and surrounding metal. This
boundary is easily perceptible after shearing the weld as is
illustrated for different materials in fig. 3.1.



(a)



(b)



(c)



(d)
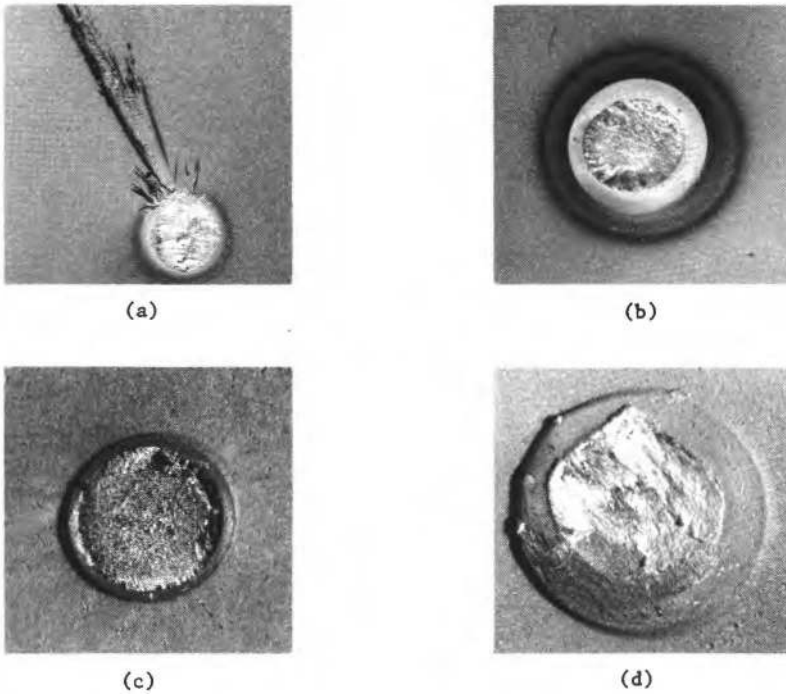
Fig. 3.1. Test Specimens after Shearing
    (a) stainless steel
    (b) low carbon steel
    (c) zinc
    (d) aluminium

The fundamental procedure in verifying the results of chapter 2
is as follows. First, for a given material and geometry a value
of the welding time t is chosen. By means of an adequate graph
of the type of fig. 2.9 valid for the border of the weld nugget
the value of the current i, required to make this border just
reach the melting point, is calculated. Then, a set of about five
welds is made with the same heating time t and with a number of
different current intensities, starting with the computed value.
In the following welds the current is adjusted either to higher
values if the first proved to be too low or to lower values in
the opposite case. The current setting is judged to be right if
the diameter of the nugget $D_N$, measured after shearing the weld,
does not deviate more than five per cent. from the electrode
diameter $D_E$. This is necessary in order that the assumption
$\theta = \theta_m$ at the nugget border holds. When the current intensity is
too high molten material frequently splashes from between the
workpieces before the heating time is over. In these cases, the
time at which splashing occurs is considered to be the right
welding time for the current setting used.
In this way a number of i,t combinations is found for constant
values of $Q_D$ and $Q_\lambda$, from which $Q_\theta$ and $Q_t$ values are computed
by putting $\theta = \theta_m$ in $Q_\theta$.

## 3.2. Design of the Experiments

### 3.2.1. Workpieces

In order to verify the analogue results for a wide range of
applications, workpiece materials with highly divergent physical
properties are chosen. Thus, for instance, low carbon steel with
a high melting point is compared with zinc having a very low
one, highly resistive stainless steel is compared with copper,
which has a very good thermal and electrical conductivity.
Aluminium is added to this set because of its well-known property
to form an insulating oxyde layer on its surface when exposed to
air.

The materials used are

SS, an austenitic chromium-nickel stainless steel, AISI
    number 316, composition ≤0.05% C; 17 - 18.5% Cr;
    10.5 - 11.5% Ni; 2.0 - 2.3% Mo,

St, a commercial low carbon steel, ≤0.06% C; 0.38% Mn;
    0.01% Si,

Zn, a commercial hot rolled zinc, ≤0.10% Pb,

Al, commercial pure aluminium, ASTM designation 1100-H18,
    ≤99.2% Al,

Cu, electrolytic copper, annealed, ≥99.92% Cu

The physical properties of these materials are given in table 3.1.

Table 3.1. Physical Properties of Workpiece Materials

| material | $\lambda$ $W.m^{-1}.deg^{-1}$ | $c$ $J.m^{-3}.deg^{-1}$ | $\rho$ $\Omega.m$ | $\theta_m$ deg | ref. | $H_V$ $N.m^{-2}$ | $\sigma_M$ $N.m^{-2}$ |
|---|---|---|---|---|---|---|---|
| SS | 23 | 4.90 | 108 | 1375 | [46] | 171 | 61.4 |
| St | 36.2 | 5.37 | 84.5 | 1480 | [46] | 119 | 38.8 |
| Zn | 104 | 2.78 | 11.1 | 393 | [47] | 58 | 14.1 |
| Al | 199 | 2.88 | 6.9 | 630 | [48] | 37 | 10.8 |
| Cu | 360 | 2.88 | 5.6 | 1056 | [48] | 89 | 25.8 |
| | | $\times 10^6$ | $\times 10^{-8}$ | | | $\times 10^7$ | $\times 10^7$ |

The mechanical properties $H_V$ and $\sigma_M$ were measured at room
temperature; the thermal and electrical properties were taken
from literature as functions of the temperature and averaged by
means of the relation

$$ k = \frac{1}{\theta_m} \int_0^{\theta_m} k(\theta)\ d\theta \qquad (3.1) $$

where $k(\theta)$ denotes any of the properties $c$, $\rho$ or $\lambda$, and $k$ its
mean value of table 3.1. Generally, this definition gives
satisfactory results when computing the dimensionless products Q.
However, from the results of the experiments described in section

53

3.4 and discussed in chapter 4 it appears that the choice of
slightly deviating values for the electric resistivity ρ improves
the agreement between theory and experiments. These values, given
in table 3.2, are further used throughout the present calculations.

Table 3.2. Comparison between Calculated and Empirical Values for
the Electrical Resistivity $\rho$ in $10^{-8}\Omega.m$

| material | calculated from equation (3.1) | empirical (best fitting) value |
|----------|--------------------------------|--------------------------------|
| SS | 108 | 74 |
| St | 84.5 | 61 |
| Zn | 11.1 | 9.5 |
| Al | 6.9 | 9.5 |
| Cu | 5.6 | 6.8 |

Rectangular workpiece specimens were used with width

$$w = 6 \ D_{Emax} \tag{3.2}$$

in accordance with section 2.2.2 and length

$$1 \geq 2.w$$
$$1 \geq 60 \ mm \tag{3.3}$$

where $D_{Emax}$ denotes the maximum electrode diameter to be used on
the specimen. The minimum length of 60 mm is maintained to
facilitate the pinching of the specimens in the tensile testing
machine. When welding, the specimens overlap each other over a
distance $w_L$ = w; the weld is made in the middle of the common
contact square, according to [4].
To minimize the influence of contact resistances, caused by the
presence of oxyde films, grease or dirt, the specimens are sand-

blasted and oiled afterwards. The oil is removed by means of an
adequate organic cleaning agent (trichlorineaethylane)
immediately before welding.

### 3.2.2. Electrodes

The electrode materials are chosen according to the specifications
given by the manufacturer of the welding machine [49]. These
specifications are based on the Resistance Welder Manufacturer's
Association standards [4]. For the welding of copper sheet
electrodes made of the same material were used. A description of
the electrode materials is given in table 3.3; the physical
properties at room temperature can be found in table 3.4.

Table 3.3. Description of the Electrode Materials

| manufacturer's designation | composition | RWMA class | used for the welding of |
|---|---|---|---|
| electrolytic copper | 99.97% Cu | – | Cu |
| Soudalox 100 | 1% Ag; bal. Cu | 1 | Al, Zn |
| Soudalox 200 | .5% Cr; .1% Be; bal. Cu | 2 | St |
| Soudalox 300 | 2.5% Co; .5% Be; bal. Cu | 3 | SS |

Table 3.4. Physical Properties of the Electrode Materials

| material | $\lambda_E$ $W.m^{-1}.deg^{-1}$ | $c_E$ $J.m^{-3}.deg^{-1}$ | $\rho_E$ $\Omega.m$ | $\theta_{max}$ [1]) $deg$ | $H_V$ $N.m^{-2}$ |
|---|---|---|---|---|---|
| el.copper | 402 | 2.5 | 1.75 | 200 | 94 |
| Soud. 100 | 320 | 2.5 | 2.1 | 320 | 99-124 |
| Soud. 200 | 290 | 2.5 | 2.45 | 470 | 153-181 |
| Soud. 300 | 180 | 2.5 | 3.6 | 520 | 208-245 |
| | | $\times 10^6$ | $\times 10^{-8}$ | | $\times 10^7$ |

[1]) $\theta_{max}$ = maximum operating temperature

The electrode dimensions are as defined in fig. 2.4, except that
the shaft diameter does not exceed 20 mm, whereas the coolant
channel has a diameter of 12 mm and a short conical end-surface
for all types (cf. fig. 1.1).

### 3.2.3. The Experimental Range

An inspection of standard welding practices [1] reveals that the
values of $Q_t$ generally lie in the range $0.1 < Q_t < 10$ as indicated
in section 2.3.1. This fact is quite comprehensible because for
very low values of $Q_t$ the large welding current required will soon
exceed the capacity of the welding equipment. For large $Q_t$ values,
on the other hand, an increase in the welding time would not yield
an appreciable increase in the weld temperature, as can be seen
from figs. 2.9 or 2.10. Consequently, the present experiments
are confined to the above-mentioned range of $Q_t$. Then, the
expected $Q_\theta$ values follow from the analogue measurements. They lie
in the range $0.01 < Q_\theta < 1$.
As for $Q_D$, most standards recommend a certain dependence of the
"optimum" electrode diameter on the sheet thickness to be welded.
In Europe, the relation

$$D_E = 5\sqrt{s} \qquad\qquad\qquad (3.4)$$

is used for steel, where $D_E$ and s are expressed in mm [7, 49],
whereas in the United States the formula

$$D_E = 2 \cdot s + 0.1 \qquad\qquad\qquad (3.5)$$

is applied, where $D_E$ and s are expressed in inches [4]. For
$0.3 < s < 5$ mm the resultant electrode diameter is about the same.
In both cases $Q_D$ has a value as low as 1.5 for sufficiently thick
sheets and as high as 20 or more for very thin sheets. Such a
choice of the electrode diameter does not necessarily have a
physical background. It might as well be made for practical
reasons, for instance in order to enlarge the working range of

56

the welding equipment. This range is limited both by the ratio of
maximum to minimum welding current and by the ratio of maximum to
minimum electrode force that can be applied. So a small range of
electrode diameters and hence of current intensities and electrode
forces is attractive.

Because of the availability of a welding machine with a large
range of current and force settings, the relation (3.4) and (3.5)
were disregarded and a number of $Q_D$ values was investigated for
each sheet gauge. The applied combinations of s and $D_E$ are
summarised in table 3.5. The underlined experiments have been
carried out twice.

In order to minimise the initial values of the contact resistance,
the electrode force is chosen so that the dimensionless product

$$Q_F = \frac{4F}{\pi D_E^2 \cdot H_V} = 0.2 \tag{3.6}$$

which means that the average contact pressure between workpiece
and electrode lies well above the yield stress of the material.
In this way the occurence of plastic deformations in the contact
areas and hence of small initial contact resistances is ensured
[36].

For each combination of $D_E$ and s from table 3.5 five welding times
were computed in such a way that $Q_t$ obtained values of 0.1, 0.3,
1, 3 and 10 approximately. For each welding time a set of five
measurements was carried out as described in section 3.1, as far
as the current and welding time settings could be realised with
the equipment used. After a set the electrodes were carefully
cleaned by grinding or polishing. In this way a number of 1070
welds was made.

As pointed out in section 1.2 it is a further aim of the present
work to consider the possibilities of quality control and adaptive
control. In order to determine the static strength of the weld
the tensile-shear force $F_s$ was recorded [4]. The appearance of
the weld was judged by means of the maximum electrode indentation

Table 3.5. Investigated Combination of Sheet Thickness and Electrode Diameter. Values of $Q_\lambda$ and $Q_D$

| | $Q_D$ = | 1 | 1.25 | 1.5 | 2 | 2.5 | 3 | 4 | 5 | 6 | 8 | 10 | 12 | 16 |
|---|---|---|---|---|---|---|---|---|---|---|---|---|---|---|
| | s and $D_E$ in mm | | | | | | | | | | | | | |
| SS | s = 4    $D_E$ = | 4 | 5 | 6 | | | | | | | | | | |
| | 2 | | | 3 | 4 | | 6 | | | | | | | |
| $Q_\lambda$ = 7.8 | 1 | | | | | 2.5 | 3 | 4 | | 6 | | | | |
| | 0.5 | | | | | | | | 2.5 | 3 | 4 | 5 | 6 | |
| St | s = 4    $D_E$ = | 4 | 5 | 6 | | | | | | | | | | |
| | 2 | | 2.5 | 3 | 4 | 5 | | 8 | | | | | | |
| $Q_\lambda$ = 8.0 | 1 | | | | | 2.5 | 3 | 4 | 5 | 6 | 8 | | | |
| | 0.5 | | | | | | | | | 3 | 4 | 5 | 6 | 8 |
| Zn | s = 1.5  $D_E$ = | | | | | 3.75 | 4.5 | | 7.5 | | | | | |
| $Q_\lambda$ = 3.1 | 0.8 | | | | | | | | 4 | 4.8 | 6.4 | 8 | | |
| Al | s = 4    $D_E$ = | | | 6 | 8 | 10 | | | | | | | | |
| | 2 | | | | | | 6 | 8 | 10 | | | | | |
| $Q_\lambda$ = 1.6 | 1 | | | | | | | | | 6 | 8 | | | |
| | 0.5 | | | | | | | | | | | | | 6 |
| Cu | s = 3 D  $D_E$ = | | | | 6 | | | | | | | | | |
| | 1 | | | | | | | 4 | 5 | | | | | |
| $Q_\lambda$ = 1.1 | 0.5 | | | | | | | | | | 4 | | | |

$d_i$ (cf. section 6.1). For the purpose of adaptive control the electrode potential drop U across the electrodes and the electrode displacement d during welding were recorded (cf. section 6.2). Besides, the potential drop U can be used to verify the resistance of the weld material, whereas the actual welding time can be derived from the variation of d.

## 3.3. Experimental Equipment

### 3.3.1. The Welding Machine

The welding machine is a single phase press welder SCIAKY type E 260, accomodated for spot welding by means of a special electrode die set mounted on the platens of the machine. It is equipped with a heavy transformer SCIAKY type TI 732 C having a rated power of 340 kVA at 50% and a maximum of 650 kVA at 9% duty cycle. The secondary e.m.f. can be set at 5.7 or 11.4 volts, the maximum secondary short-circuit current being 68 kA. In practice, with the electrode die set mounted, the secondary current intensity can be controlled up to 54 kA and by means of an electronic synchronous phase shift control down to a minimum value of about 2 kA. Continuous heating times can be realised from 0.02 up to 4 seconds in steps of 0.02 s, whereas a current modulator allows of numerous possibilities arise as regards pulsation welding. The moving head of the machine is operated by direct acting air pressure, governed by the electronic control unit. The maximum adjustable electrode force is 15 kN. A minimum value of about 1.5 kN is caused by the action of static packing friction in the air cylinder resulting in insufficient pressure during the weakening of the workpiece.
The welding machine, the electronic control unit and the measuring devices are shown in fig. 3.2. In fig. 3.3 a closer view is given of the electrode arrangement and some of the measuring transducers.

### 3.3.2. Measuring Devices

A number of devices were used to measure the values of the rele-
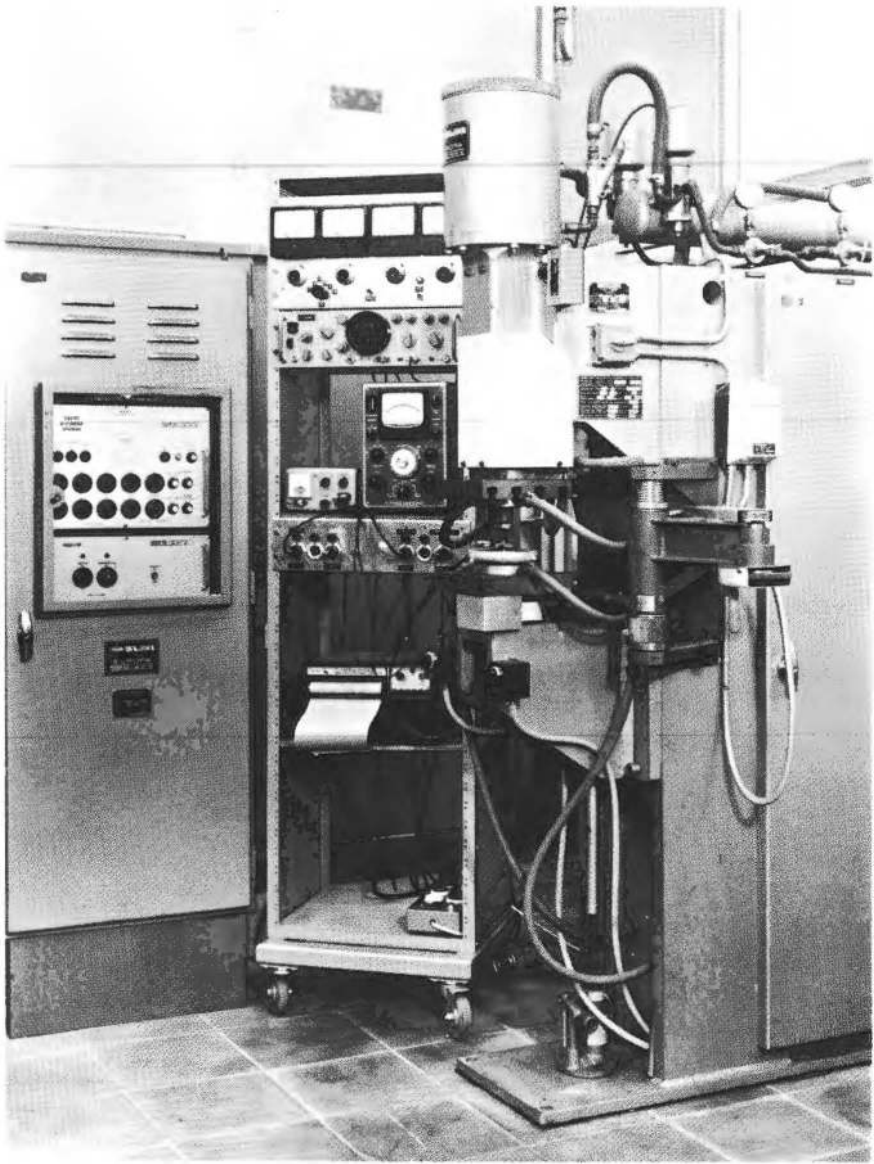
Fig. 3.2. The Experimental Equipment. From left to right, welding
control unit, instruments rack, press welder. In the rack
from top to bottom, r.m.s. ammeter unit, oscilloscope,
displacement transducer power source and strain indicator,
recorder pre-amplifier, recording oscillograph

60
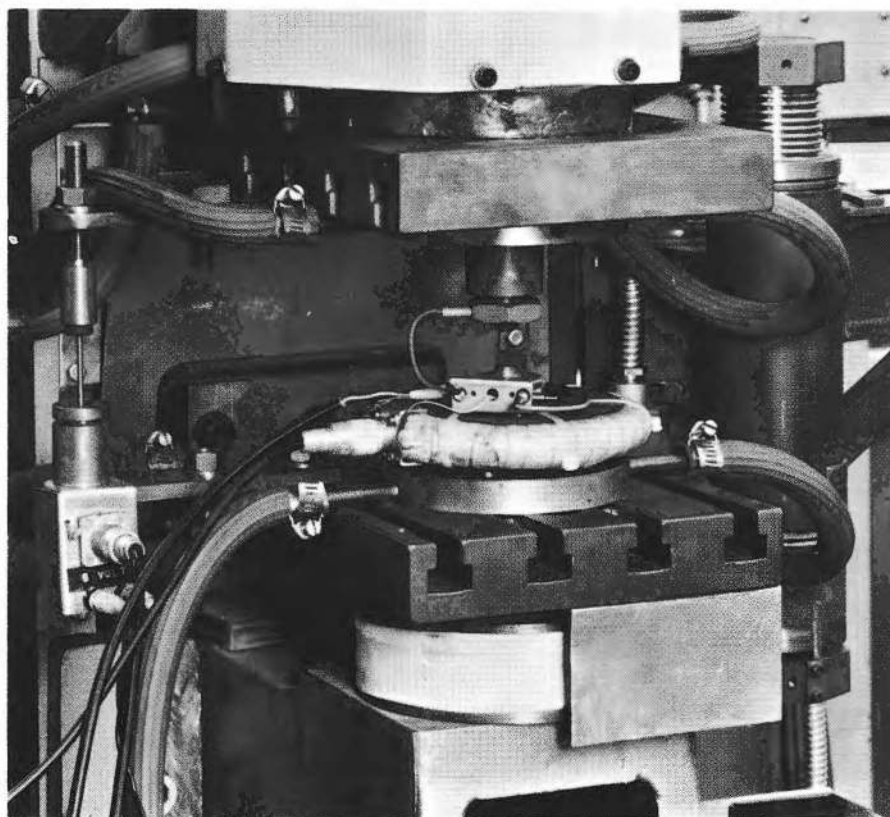
Fig. 3.3. Electrode Arrangement and Measuring Transducers.
Around the lower electrode, the current toroid; under the
lower platen, the strain gauge element; to the left,
displacement transducer.
The potential drop across the electrodes is taken from the
nuts near the electrode tips

vant parameters. Some of these parameters may vary considerably
during the heating period, hence they were recorded on a CEC
model 5-124 oscillograph at a paper speed of 80 $mm.s^{-1}$ for
analysis afterwards. This goes for the current intensity i, the
potential drop across the workpieces U, the electrode displace-
ment d and the electrode force F. The following variables were
measured.

(a) Intensity of the Welding Current. Owing to the application of

phase-shift to control the intensity of the welding current the
resultant secondary current wave form is far from sinusoidal [51].
In order to determine the r.m.s. value defined by

$$i_{rms} = \sqrt{\frac{1}{t'} \int_0^{t'} i^2(t)dt}$$  (3.7)

for a heating time t', the true r.m.s. ammeter, diagrammatically
shown in fig. 3.4, was developed. A toroidal measuring transformer
(Rogovskii belt) supplies a voltage proportional to the first
derivative di/dt of the welding current with respect to time.
After passing a calibrated attenuator (used to fix the measuring
range) and an integrator, the signal - then proportional to i -
is led to the recording oscillograph. Besides, in order to
facilitate the reading of the current value after welding, the
signal is squared and transferred to a second integrator after
being divided by the welding time t' by means of a pre-set poten-
tiometer. The second integrator is followed by a direct-reading
voltmeter, and designed to hold the pointer of that instrument in
its position for a few seconds after the current has ceased to
flow. In fact, there are four of these integrating branches, thus
permitting the subsequent reading of the currents during the pre-
weld, first and second weld and post-weld heating periods, if
required. The signal is guided to the right branch by means of the
reed relays 1 through 4, operated by synchronised pulses from the
welder control unit. The error of this instrument is estimated
to be smaller than 2 per cent. of the measured value.

(b) Voltage across the Workpieces. The knowledge of the electric
potential difference U across the workpieces permits the calcula-
tion of the workpiece resistance if the current is measured
simultaneously. This voltage is taken from two points of the
electrode tip bodies and recorded on the oscillograph. In order
to cancel the pick-up of an undesirable e.m.f. induced by the
magnetic field of the welding current in the voltage signal leads,
a compensation toroid may be added to the design [50]. However,
the compensation voltage is more easily taken from the current
toroid, as was done in the present investigation. In computing the
resistance of the welding work that part of the voltage that is

62

to recorder

$\frac{di}{dt}$

measuring toroid

calibrated attenuator

integrator

i

amplifier    multiplier

$i^2$

$\pi$

from welder control unit

reed relays 1.....4

$i^2$

ten turns potentiometer

$\frac{i^2}{t}$

integrator

$\frac{1}{t}\int i^2 dt$

voltmeter, visual display of $i_{rms}$ immediately after welding

$i_{rms}$

pre—weld    first weld    second weld    post—weld period
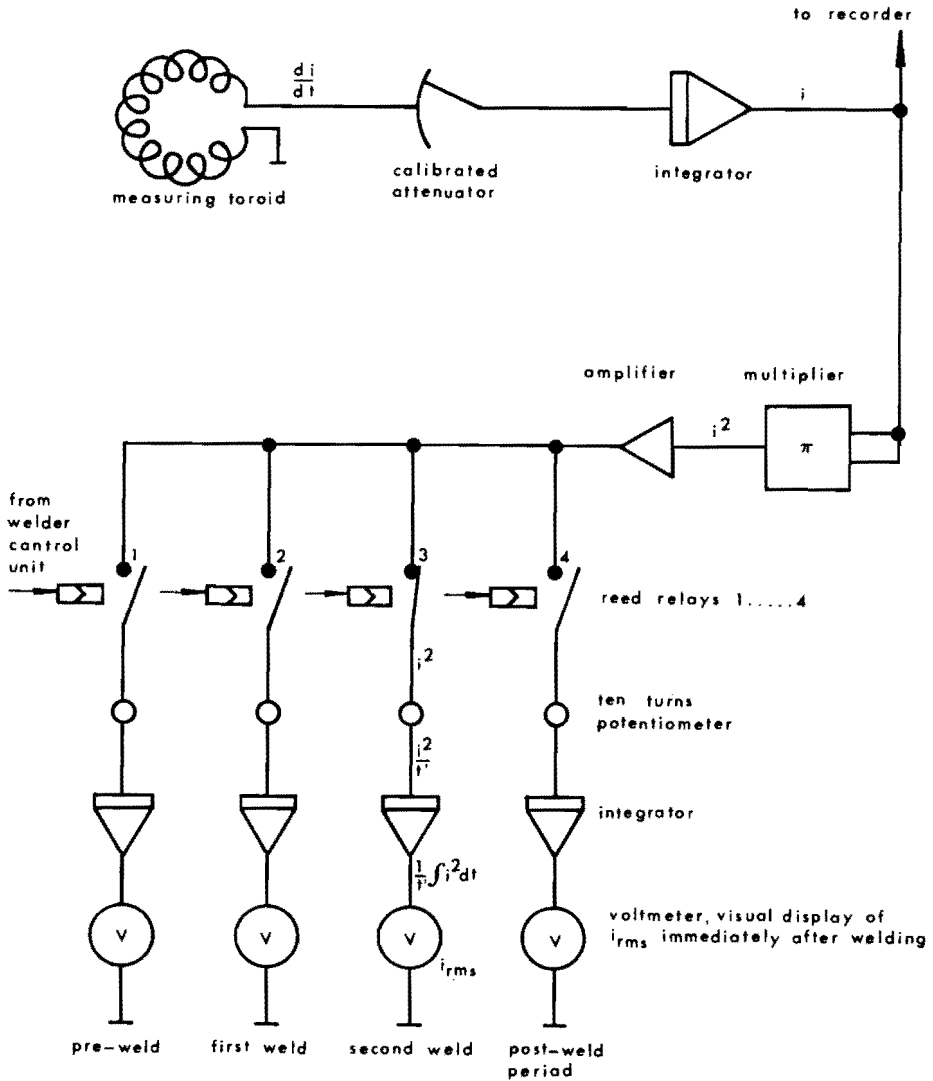
Fig. 3.4. Diagrammatic Representation of the True R.M.S. Current
          Measuring Device

caused by the potential drop across the electrode bodies is
arithmetically subtracted. The estimated error of the voltage
measurement is smaller than 5 per cent.

(c) Electrode Displacement. Owing to the expansion of the workpiece
materials during the heating cycle and the weakening of the weld

63

at higher temperatures, an electrode movement d occurs, which is useful as an indication of weld quality [50]. This movement is measured by means of a SANBORN model 7 DCDT 050 differential transformer displacement transducer, the output voltage of which is recorded on the oscillograph. The error is estimated to be smaller than 2 per cent.

(d) Electrode Force. The electrode force F is measured by means of resistance wire strain gauges, cemented on an elastic element, viz. a specially designed thin-walled cylinder, mounted under the lower platen of the welder (cf. fig. 3.3). The strain is read from a HOTTINGER type KWS II/50 universal strain indicator and recorded on the oscillograph.The readings are calibrated in newtons. The estimated error is smaller than 2 per cent. of the measured value.

(e) Tension-Shear Strength of the Welds. The tension-shear strength of the weld $F_s$ is measured by subjecting the welded specimen to a tensile pull in a standard WOLPERT model U6 testing machine until fracture occurs. The ultimate strength of the specimen and the manner of failure, whether by shear of the weld metal or by tear of the parent metal is recorded. The error of this measurement is estimated to be smaller than 5 per cent.

(f) Dimensions. The sheet thickness s and the workpiece indentation $d_i$ were measured by means of a standard dial indicator. The electrode diameter $D_E$ and the nugget diameter after shearing $D_N$ were determined with the aid of a measuring microscope. The error in these measurements does not exceed 0.01 mm.


3.4. Results


3.4.1. Types of Weld

A classification of spot welds can be made using various criteria. In order to facilitate the comprehension of the welding process an arrangement based on the behaviour of a few parameters that vary significantly during the process is of particular interest. The electrode movement d as well as the total resistance R of the weld material during the heating period have proved to be very useful in this respect.

In fig. 3.5 a general shape of the d(t) curve is shown. After the
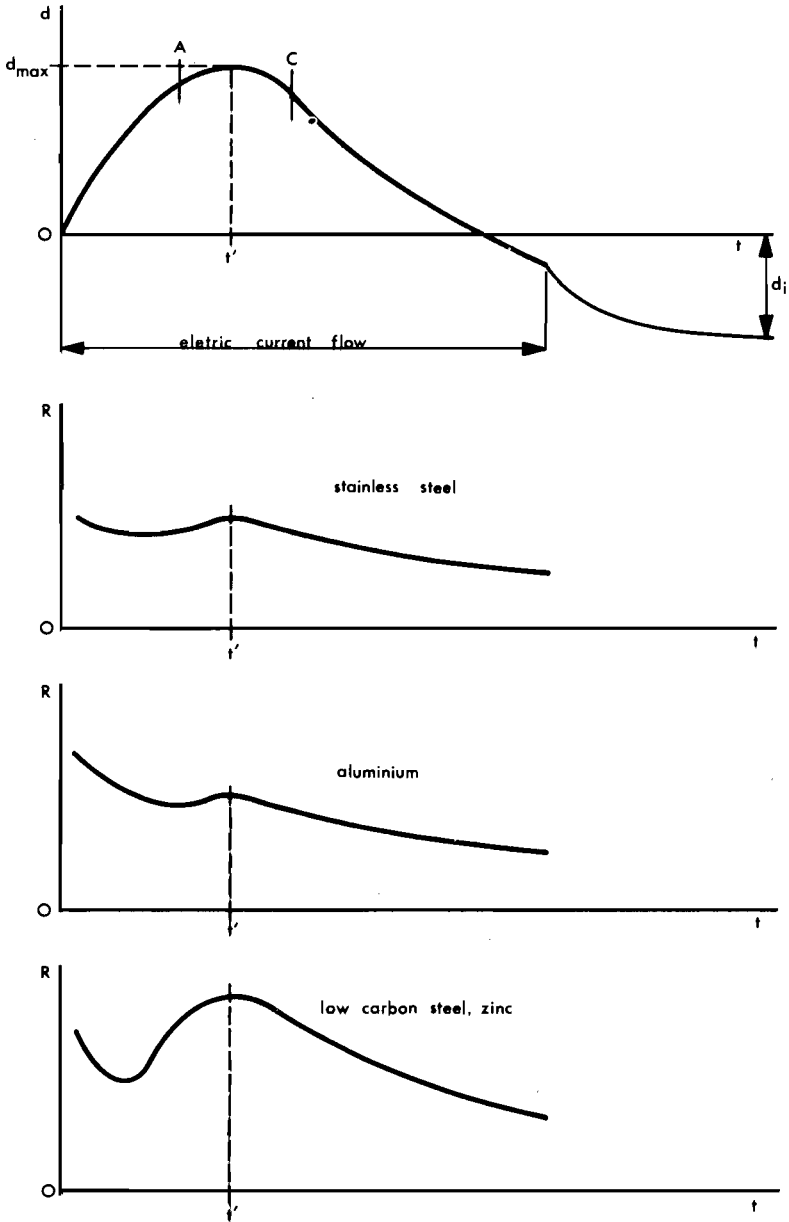electric current is switched on, the workpieces are rapidly heated,



Fig. 3.5. Typical Electrode Movement and Workpiece Resistance Curves

resulting in thermal expansion of the weld material. This
expansion mainly takes place along the electrode axis owing to the
constraint offered by the cold metal surrounding the heated spot
[50, 52]. As the material softens, plasticises and melts the
electrodes force their way towards each other in the weakened
metal so that the electrode movement changes its direction, resul-
ting in a marked indentation $d_i$ in the workpiece surfaces after
the weld has cooled.

The shape of the curves representing the total resistance R of the
workpieces as a function of time, depends on the material welded.
For stainless steel the resistance of the weld is practically
constant before the metal reaches the weakening point, where a
slight maximum appears. Afterwards, the value of the resistance
decreases substantially, owing to a decrease in the material
thickness and to the increase in the effective electrode contact
diameter, resulting from the penetration of the electrode into the
weld material. In extreme cases, $d_{max}$ may reach values of 30 per
cent. and $d_i$ of 60 per cent. of the sheet thickness. For aluminium,
the initial resistance is generally much higher than that at the
weakening point, whereas for low carbon steel and zinc the opposite
is true. A further analysis of the workpiece resistances will be
given in chapter 4.

While leaving the other welding parameters unchanged, the heating
time may be reduced to a value t > t' in fig. 3.5. For example,
the welding current is interrupted in point C. It then appears
that a satisfactory weld with a diameter $D_N \geq D_E$ is made in all
cases. If the welding time is greater than t', the growth speed
of the weld nugget is substantially reduced. This is due to the
reduction of the sheet thickness and to the apparent growth of the
electrode diameter, resulting in a lower current density in the
weld.

If the welding time is further reduced, so that t < t' (point A),
generally no weld is formed, unless the heat input is increased
to such an extent that the point t' is also shifted to the left.
Only when applying very high heat input values, the weakening of
the weld material in the surroundings of the nugget takes place
at a lower rate, and a weld can be formed with a type A electrode
displacement curve. From figs. 2.13 and 2.14 it can be seen that

this may be the case for low $Q_t$ values, where the ratio of the
temperatures at the electrode face to those at the nugget border
is comparatively low, premised that $Q_\lambda$ has a sufficiently high
value.

On the basis of the foregoing the time required to reach the
maximum electrode displacement $d_{max}$ is considered to be the
proper heating time for obtaining a weld nugget with a diameter
equal to that of the electrode tip.

Splashing of molten material between the workpieces, mentioned in
section 3.1, mainly takes place if $Q_D > 4$. Radial thermal expan-
sion, which is greater in the plane $z = 0$ than at the electrode
contact area as a result of the higher temperature in the first
plane, forces the workpiece sheets apart. This phenomenon, called
sheet separation, is a form of bending of the sheet, which occurs
more easily for comparatively thin workpieces. A wall of solid
material that carries the welding force, surrounds the molten pool
in the centre, but at high energy input rates that wall may burst
at its weakest point, permitting the molten metal to be splashed
away between the sheets. This results in an electrode displacement
curve as represented in fig. 3.6. As the illustration shows,
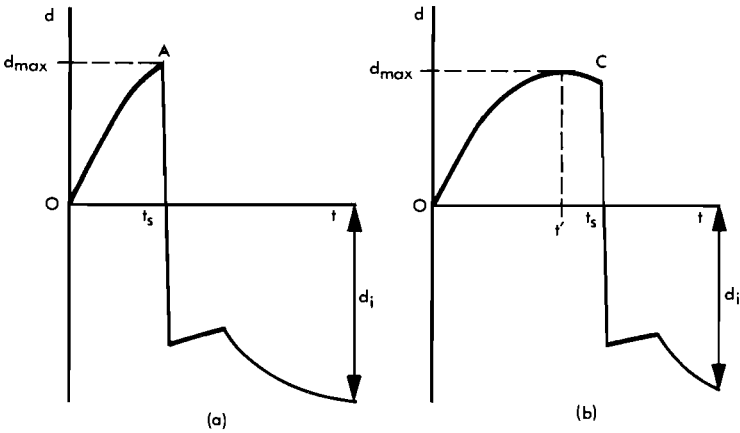


Fig. 3.6. Electrode Movement for Splashing Welds

      (a) type AS, splashing occurs at point A of fig. 3.5

      (b) type CS, splashing occurs at point C of fig. 3.5

splashing may occur at point A of fig. 3.5 or at point C not too
far beyond the point of maximum electrode displacement. The total

workpiece resistance R falls to a significantly lower level,
depending on the amount of metal splashed away and on the local
reduction in sheet thickness. Various investigators have observed
the phenomenon of splashing [50, 53, 54]. They agree that a sound
weld is formed whenever splashing occurs, although equally good
welds can be produced without it [55].



Fig. 3.7. Comparison of Experimental Results (Dots) and Analogue
Measurements (Drawn Curves) when Spot Welding Stainless
Steel
(a) $Q_\lambda$ = 7.8; $Q_D$ = 5.9; square dots; q = 1.72
(b) $Q_\lambda$ = 7.8; $Q_D$ = 1.07; circular dots; q = 0.43

68

From our experiments it appeared that the weld type C occurs for
$Q_t > 1$, type A and AS for $Q_t < 1$, while the transition type CS
chiefly occurs in the range of $0.5 < Q_t < 1.5$. The boundaries
mentioned, however, are not strict. In reference [54] the time $t_s$
is shown to depend on the electrode force F.
From the discussion in this section it seems justified to use the
time at which the maximum electrode displacement is realised as
the proper welding time for all the types of weld described.



Fig. 3.8. Comparison of Experimental Results (Dots) and Analogue
Measurements (Drawn Curves) when Spot Welding Low Carbon
Steel
(a) $Q_\lambda = 8.0$; $Q_D = 8.8$; square dots; q = 2.14
(b) $Q_\lambda = 8.0$; $Q_D = 2.65$; circular dots; q = 0.91

## 3.4.2. Discussion

The measurements were carried out as described in section 3.1.
The results of each series of experiments having constant $Q_\lambda$ and
$Q_D$ values are compared with the appropriate $Q_\theta(Q_t)$ curve for the
nugget border obtained from the analogue measurements. These
curves were interpolated for those values of $Q_\lambda$ and $Q_D$ that are
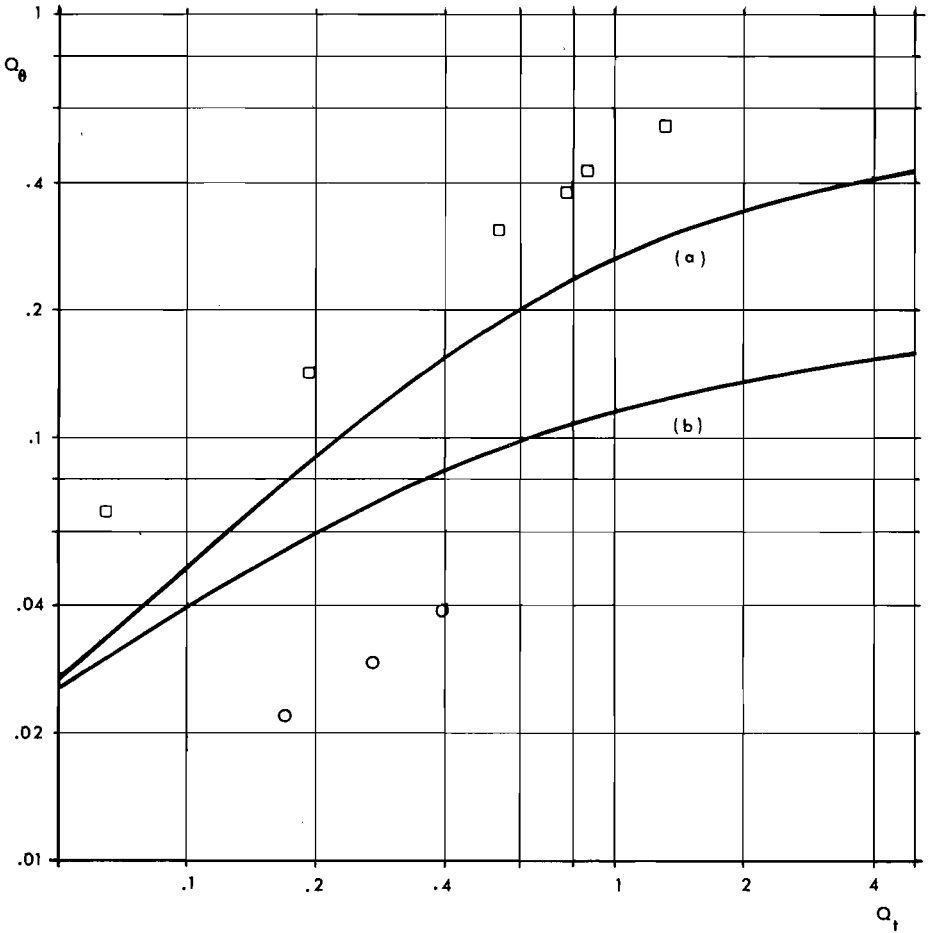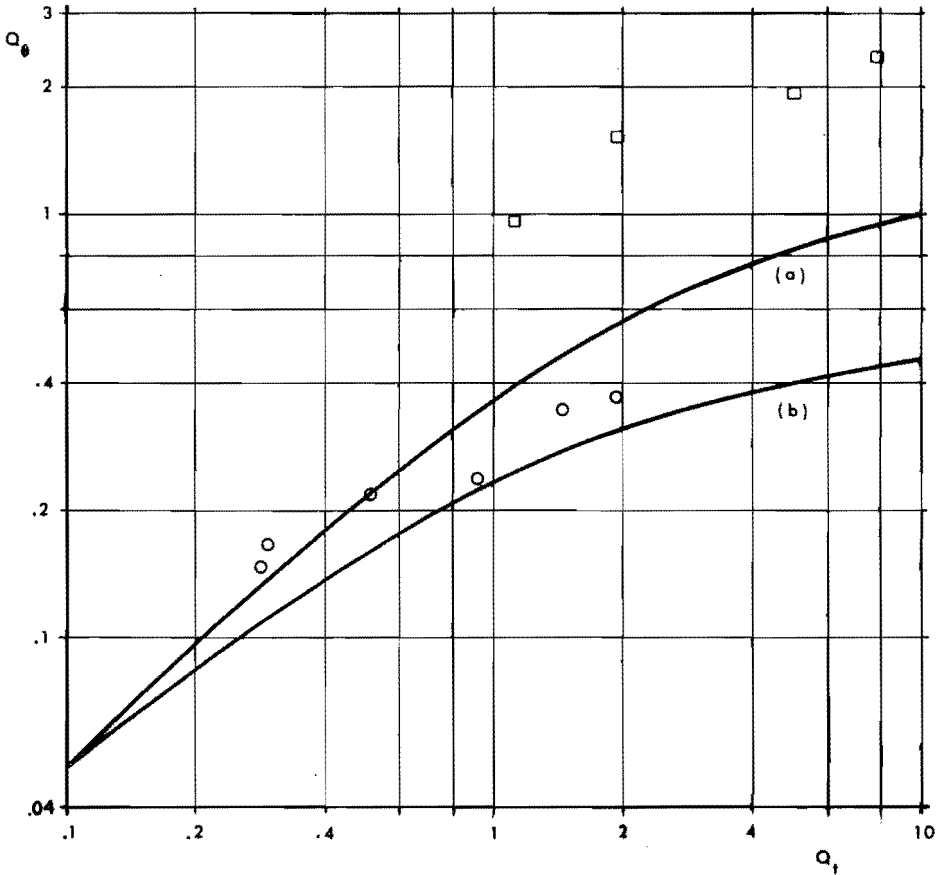


Fig. 3.9. Comparison of Experimental Results (Dots) and Analogue
Measurements (Drawn Curves) when Spot Welding Zinc
(a) $Q_\lambda$ = 3.1; $Q_D$ = 9.7; square dots; q = 2.48
(b) $Q_\lambda$ = 3.1; $Q_D$ = 2.67; circular dots; q = 1.09

not mentioned in section 2.3.1. It appeared to be impossible to
spot weld pure copper sheet with the aid of copper electrodes in
the normal way, as could be expected from long-standing workshop
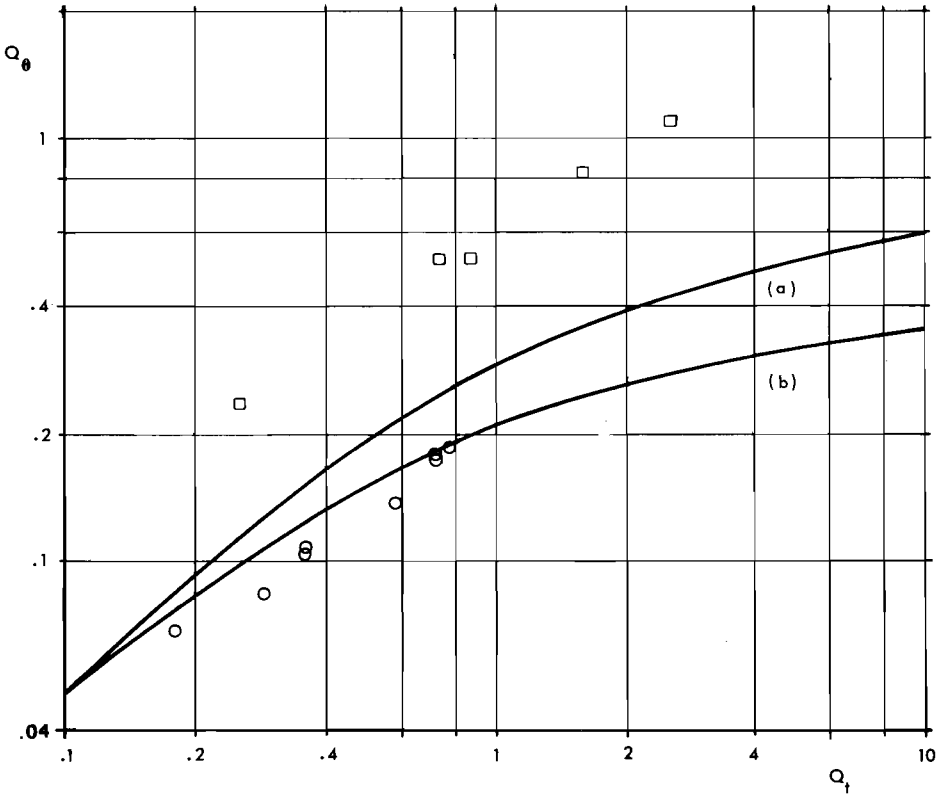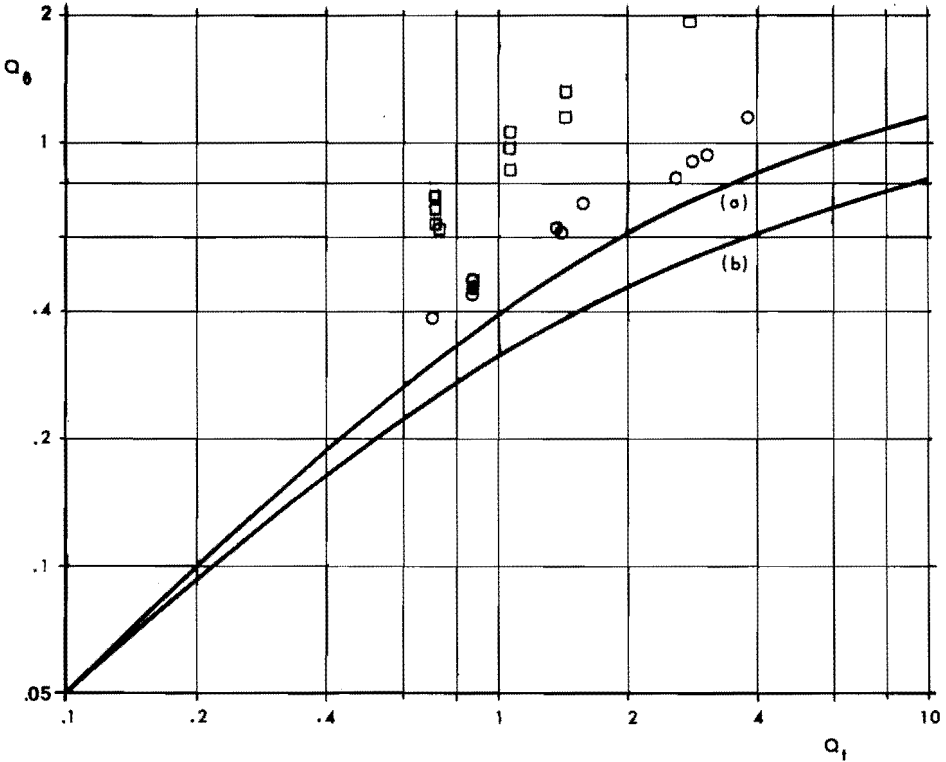


Fig. 3.10. Comparison of Experimental Results (Dots) and Analogue
        Measurements (Drawn Curves) when Spot Welding Aluminium
        (a) $Q_\lambda = 1.6$; $Q_D = 6.5$; square dots; $q = 2.24$
        (b) $Q_\lambda = 1.6$; $Q_D = 4.1$; circular dots; $q = 1.62$

experience [2]. A method of welding copper, based on the theore-
tical considerations of chapter 4 will be dealt with in section
5.2.
As an example, the results of two series for each of the other
workpiece materials investigated are shown in figs. 3.7 to 3.10
inclusive. From these graphs two important conclusions can be
drawn..

(a) The course of the curves which may be drawn through the experimental plottings of the dimensionless product $Q_\theta$ as a function of $Q_t$ is fundamentally the same as of those predicted by the analogue measurements.

(b) However, a very distinct deviation exists between the positions of the experimental and of the analogue curves.

This deviation can be expressed in a multiplying factor
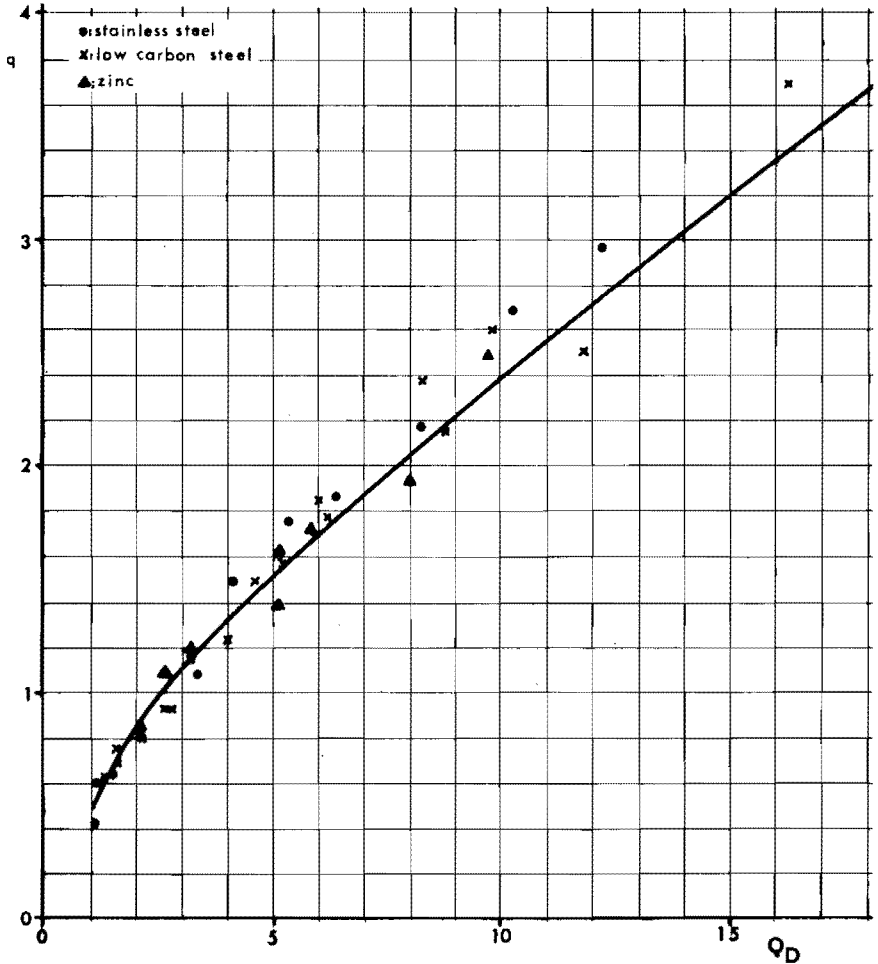


Fig. 3.11. The Ratio q as a Function of $Q_D$ for Stainless Steel, Low Carbon Steel and Zinc

$$q = \frac{Q_\theta \text{ observed}}{Q_\theta \text{ calculated}} \tag{3.8}$$

This factor appears to be a function of $Q_D$ only. As such it is
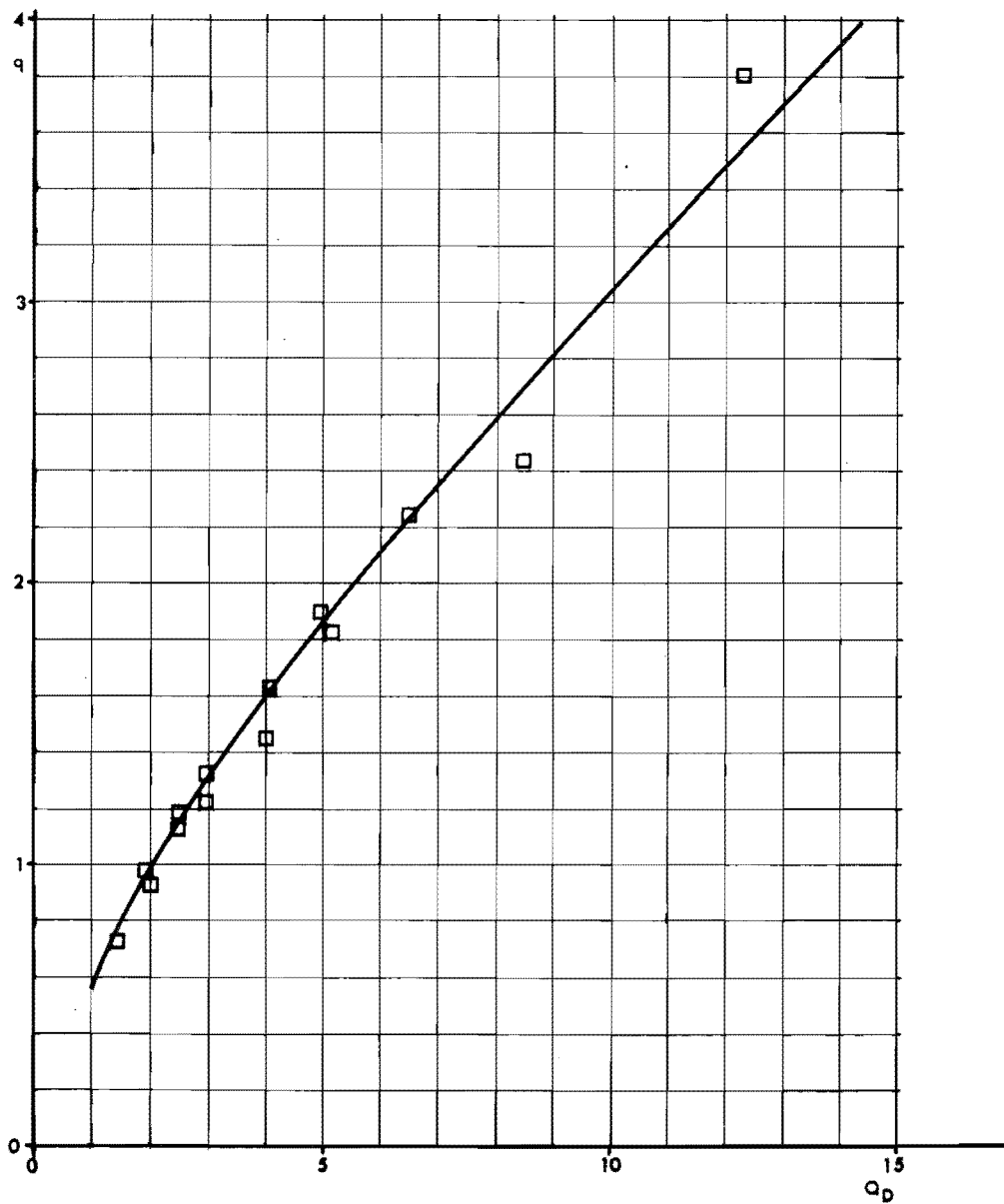


Fig. 3.12. The Ratio q as a Function of $Q_D$ for Aluminium

recorded in figs. 3.11 and 3.12.

In conclusion, it appears that an important and systematic deviation exists between the model described in chapter 2 and the results of the experiments presented in this chapter. The deviation seems to be chiefly dependent on the dimensionless product $Q_D$. In the next chapter an interpretation of the phenomena leading to this deviation will be offered.

## Chapter 4. IMPROVEMENT OF THE THEORY

### 4.1. Introduction

In chapter 3 a discrepancy between the experiments and the results of
the analogue measurements was observed. It is shown there that this
can be expressed in the form of a function $q(Q_D)$, as defined in
equation (3.8). Since the value of q varies between 0.4 and 4 in the
investigated range of $Q_D$, it can be concluded that for low $Q_D$ values
the mean current density $\bar{J}$, and thus the current intensity i required
to make a satisfactory weld, is greater than that expected on the
basis of the analogue model. On the other hand, the opposite is true
for high $Q_D$ values.
From this it might be concluded that the total resistance R of the
workpieces substantially differs from that assumed in the model of
chapter 2. There, only the resistance

$$R_o = \frac{8\rho s}{\pi D_E^{\,2}} \tag{4.1}$$

of a cylinder of diameter $D_E$ and height 2s is taken into account,
whilst a uniformly distributed current is assumed to flow through
this cylinder (cf. section 2.2.2). In that case, the heat development
in the workpieces is equal to

$$\phi_o = \int_0^{t'} i^2 R_o \, dt = i^2 R_o t', \tag{4.2}$$

since i is constant during the heating time t' and $R_o$ is regarded to
be so, because of the use of a mean value for the resistivity, as
defined in section 3.2.1.
However, if $R \neq R_o$ and, moreover, if R is not constant during the
heating period, the real heat production becomes

$$\phi = \int_0^{t'} i^2 R \, dt = i^2 \int_0^{t'} R \, dt, \tag{4.3}$$

75

assuming that i remains constant when the total resistance of the
workpieces varies. This is caused by the rather high impedance value
of 270μΩ of the secondary circuit of the welder.
It will be shown in the next sections that a correction of the
computed $Q_\theta$ value by means of a factor $\phi/\phi_o$ fully accounts for the
discrepancy observed in the foregoing chapter. This means that the
relation

$$q = \frac{\phi}{\phi_o} = \frac{1}{t'} \cdot \int_0^{t'} \frac{R}{R_o} dt \tag{4.4}$$

will be proved to be applicable.


## 4.2. The Influence of the Current Distribution

The assumption made in section 2.2.1 concerning a uniform
distribution of the electric current in the cylinder of the workpiece
metal between the electrode faces does not hold. Especially for low
$Q_D$ values the error introduced by this simplification becomes
inadmissable. As a matter of fact, the current entering the workpiece
sheet via the electrode-workpiece contact plane "bulges" in the sheet
metal outside the cylinder mentioned and crosses the interworkpiece
contact plane over a circular area, having a diameter considerably
greater than $D_E$ (cf. fig. 4.1).
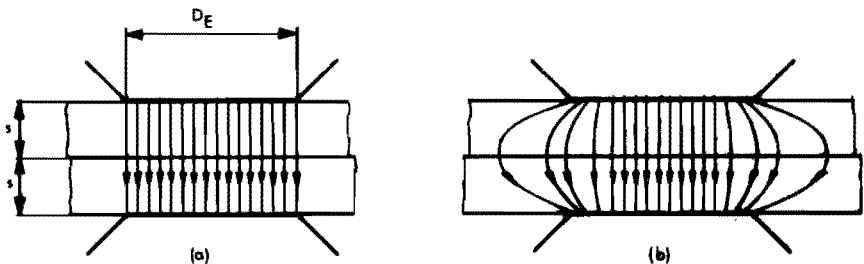


Fig. 4.1. Comparison of Assumed (a) and Actual (b) Current Distribution
in Spot Welding

This phenomenon, as well as its dependence on the value of $Q_D$, has been known for a long time [1, 4, 5]. It means a lower current density at the interworkpiece contact plane than at the electrode face, and a less favourable value of the ratio of the electrode face temperature and the nugget temperature.

Besides, it means a lower resistance of the workpieces. Consider the cylinder in fig. 4.2 with diameter $w_L$ and height 2s. At the top and
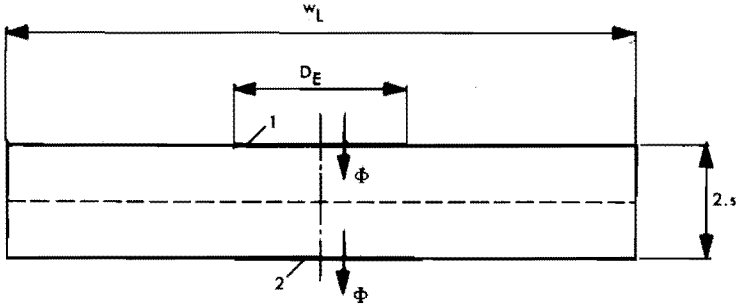


Fig. 4.2. Model of the Workpiece Sheets for the Computation of the
Electric Resistance between the Points 1 and 2

the bottom of the cylinder a constant flux $\phi$ is supplied and removed over concentric circular areas 1 and 2 respectively, each having a diameter $D_E$. Reference [42(p. 223)] gives an expression for the average temperature difference between these areas for the case that $\phi$ is a flux of heat. The solution is easily transformed in an expression for the average potential difference for the case that $\phi$ is an electric current, because of the homology of the potential equation for heat flow and of that for the flow of electric charge. It may be recalled to mind that this homology was used earlier as a basis of the analogue model. Using the above-mentioned expression, the actual resistance $R_o'$ of the workpieces, measured between the electrode faces, can be written

$$R_o' = R_o \cdot f(Q_D, \frac{w_L}{s})$$

(4.5)

with

$$f(Q_D, \frac{w_L}{s}) = 1 - \frac{16}{\pi^2} \sum_n \left\{ \frac{I_1(n\pi Q_D/4)}{n^2 I_1(n\pi w_L/4s)} \right. \cdot$$

$$\left. \cdot \left[ I_1(\frac{n\pi w_L}{4s}) \cdot K_1(\frac{n\pi Q_D}{4}) - K_1(\frac{n\pi w_L}{4s}) \cdot I_1(\frac{n\pi Q_D}{4}) \right] \right\} \qquad (4.6)$$

where the summation is over odd values of n, and where $I_1$ and $K_1$ denote the first order modified Bessel functions of the first and second kind respectively. When computing the values of this function f for different combinations of $Q_D$ and $w_L/s$ it appears that the latter has no influence on the result if

$$w_L > 4D_E \quad \text{for} \quad Q_D > 1 \quad \text{or}$$

$$(4.7)$$

$$w_L > 2D_E \quad \text{for} \quad Q_D > 2$$

Since these conditions are always fulfilled in practical cases, f may be regarded as a function of $Q_D$ only. It is graphically shown as such in fig. 4.3. Experimental values, given by TARASOV [24] are plotted in this figure additionally.
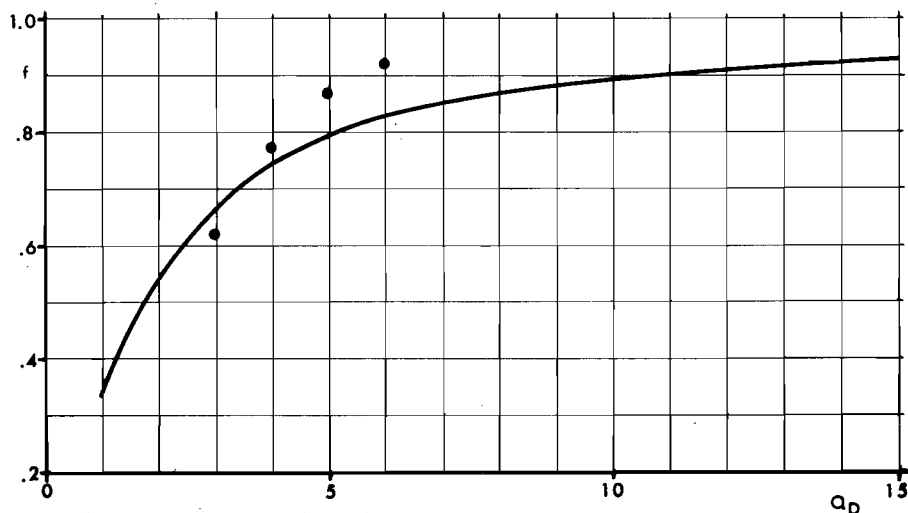


Fig. 4.3. The Function $f(Q_D)$.

The dots indicate experimental values from [24]

An affirmation of this approach is found in the results of the resistance measurements. The total resistance R between the electrode faces at the instant when the nugget reaches the melting point, i.e. at the time t' of fig. 3.5, reflects the course of $f(Q_D)$ for the lower range of $Q_D$. As an example, the ratio $R/R_o$ for low-carbon steel is plotted in fig. 4.4. It appears that
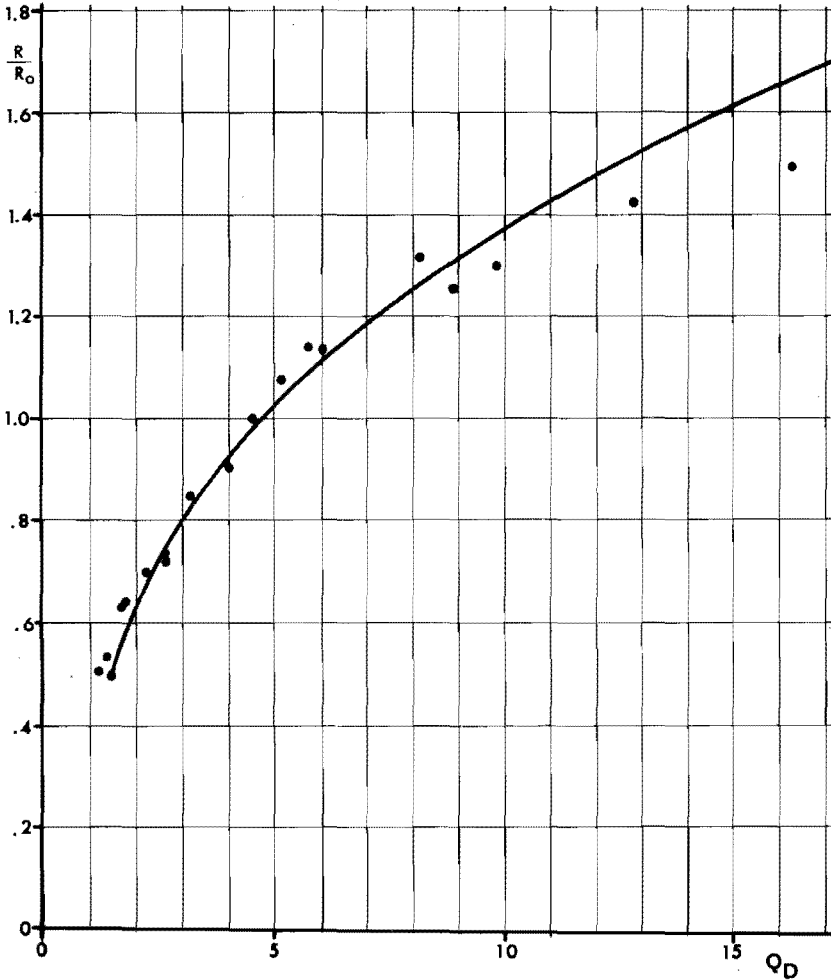


Fig. 4.4. The Ratio $R/R_o$ as a Function of $Q_D$ for Low Carbon Steel.
For the curve the relation $R/R_o = f + 0.047\ Q_D$ holds

$$\frac{R}{R_o} = f(Q_D) + \xi.Q_D \qquad\qquad (4.8)$$

The extra term $\xi.Q_D$ will be proved to result from the influence of the contact resistance. The curves for the other materials investigated show an analogous behaviour. The values of $\xi$ are presented in table 4.1.

Table 4.1. Values of $\xi$ in Relation (4.8)

| material welded | $\xi$ |
|-----------------|-------|
| stainless steel | 0.022 |
| low-carbon steel | 0.047 |
| zinc | 0.040 |
| aluminium | 0.169 |

Because of the deviation of the real current distribution from that assumed in the analogue model, the real heat production $\phi_o'$ is lower than the assumed value $\phi_o$. Since $R_o'$ and $R_o$ are considered independent of the time t, it follows from the equations (4.4) and (4.5) that

$$\frac{\phi_o'}{\phi_o} = \frac{R_o'}{R_o} = f(Q_D) \qquad\qquad (4.9)$$

4.3. The Influence of the Contact Resistance

4.3.1. Introduction

In section 2.1.6, mention was made of the divergence of the results obtained by various investigators with respect to the influence of the contact resistance $R_k$. The conclusion was that it appears to be impossible to predict the value of $R_k$ with universal validity.

80

Nevertheless, in the following sections an attempt will be made to obtain a useful estimation of the influence of the contact resistance on the spot welding process.

According to HOLM [36], only a small fraction of the apparent contact area is electrically conducting, owing to the unevenness of the contacting surfaces. Hence, the contact resistance $R_k$ always implies or is a constriction resistance $R_c$, which is the consequence of the current flow being constricted through small conducting spots. The extra resistance between the contact members, owing to the presence of one spot, which is assumed to be circular and to have a radius a, can be shown to be equal to

$$R_c = \frac{\rho}{2a} \tag{4.10}$$

if the contact is a pure metallic one.

If a number of n of these "a-spots", uniformly distributed over the apparent contact surface $A_r$ at an average distance of $2\ell$ between neighbouring centres, is present, the total constriction resistance [36] reduces to

$$R_c(n, a, \ell) = \frac{\rho}{\pi n a} \cdot \arctan \frac{\sqrt{\ell^2 - a^2}}{a} \tag{4.11}$$

where n and $\ell$ are related by means of

$$A_r = 4n\ell^2 \tag{4.12}$$

An alien film with resistivity $\rho_f$ and thickness $s_f$ in the contact may give rise to an additional film resistance

$$R_f = \frac{\rho_f s_f}{A_c} \tag{4.13}$$

where $A_c$ is the total conducting area. In practical cases the film resistance may be some orders of magnitude greater than the constriction resistance.

The influence of the contact force F on the value of the total contact resistance $R_k$ can empirically be expressed as follows

$$R_k = R_c + R_f = cF^{-m} \tag{4.14}$$

where the constant c depends on the contact materials and the
exponent m depends on the conditions of the contacting surfaces, on
the presence of films or oxyde layers and on the fact whether the
deformations of the surface asperities caused by the load F are of
an elastic nature or of a plastic one. Generally m lies between the
values 0.33 and 1.

From the summary of the properties of static contacts given above,
the conclusionsof section 2.1.6 are well comprehensible. From
equation (4.13) follow the conclusions(a), (c) and (d). Conclusion
(b) is explained by equation (4.14). The value of the static contact
resistance restricts the maximum permissible current intensity be-
cause of the increasing probability of excessive heat production in
the contact areas with increasing $R_k$. This also explains conclusion
(e) because of the higher welding current intensities required for
short welding times.

The application of mechanical or chemical cleaning methods improves
weld quality and reduces the fouling of the electrode tips [37], for
which reason the maximum surface resistances are bound to a
prescribed level in standard specifications for high-quality
resistance welding [10]. These cleaning methods may remove the oxyde
films and thus reduce the value of the static contact resistance by
a factor 100 [37], but of course do not reduce the influence of $R_c$.
Owing to the lack of information about the number, the distribution
and the dimensions of the microscopic contact spots no computation
of the constriction resistance can be made in the case of spot
welding.

### 4.3.2. The Dynamic Contact Resistance during Welding

Resistance measurements during welding have shown the contact
resistance to have an essentially dynamic character [6, 37, 38]. As
soon as the welding current starts to flow the resistance decreases
rapidly below the initial static value described in the foregoing
section. The resistance attains its minimum value at the moment the
current reaches its top, after which the static resistance does not
change appreciably any more. Consequently, when using a 50-cycle

82

alternating welding current, this minimum is reached after 5 ms.
ROBERTS [38] observed the following relation between the peak current
intensity $i_p$ and the ultimate value of the total workpiece resis-
tance after 1 half current cycle,

$$R = c_1 + \frac{c_2}{i_p^2} \qquad (4.15)$$

where $c_1$ and $c_2$ are constants for a given material and set of
conditions. He also observed the electrode force to play no role with
respect to the ultimate value of R as it did for the initial resis-
tance.

The dynamic character of the contact resistance is due to the heating
of the contact spots, resulting in a weakening of the surface
asperities, which causes the a-spots to grow rapidly in dimension as
well as in number.

A relation between the temperature $\theta_c$ of a single current constric-
tion and the contact voltage U is given by [36]

$$\int_{\theta_a}^{\theta_c} \rho\lambda d\theta = \frac{U^2}{8} \qquad (4.16)$$

where $\theta_a$ is the temperature of the bulk of the metal in the vicinity
of the contact spot.

In spot welding, the current intensity has such a high value that
the melting temperature $\theta_m$ is always reached before the current is
at its top in the first half cycle. When the melting point is reached,
the above mentioned weakening of the surface asperities and the
consequent growth of the a-spots result in a rapidly decreasing
contact resistance [36]. If it is assumed that for this reason $\theta_c$
does not exceed the melting point of the metal and if the weld
temperature $\theta$ is taken for $\theta_a$, equation (4.16) becomes

$$\int_{\theta}^{\theta_m} \rho\lambda d\theta = \frac{i_p^2 R_k^2}{8} \qquad (4.17)$$

after the current intensity has reached its top value for the first

time. By means of numerical evaluation it appears that the first
member of equation (4.17) can be written

$$\int_{\theta}^{\theta_m} \rho\lambda d\theta = (\rho\lambda)' \cdot (\theta_m - \theta) \tag{4.18}$$

where the quantity $(\rho\lambda)'$ varies from 0.8 to 1.2 times the mean value
given in table 4.2 for $0 < \theta < \theta_m$. The exposed values of $(\rho\lambda)'$, which
are further regarded – as an approximation – to be constant, differ
markedly from the product of $\lambda$ and $\rho$ from the tables 3.1 and 3.2
respectively, thus giving rise to a multiplying factor

$$\alpha^2 = \frac{(\rho\lambda)'}{\rho\lambda} \tag{4.19}$$

which is also represented in table 4.2.

Table 4.2. Values of $(\rho\lambda)'$ compared with $\rho\lambda$

| material | $(\rho\lambda)'$ | $\rho\lambda$ | $\alpha^2$ |
|----------|------------------|---------------|------------|
| SS | 3220 | 1700 | 1.89 |
| St | 3390 | 2210 | 1.54 |
| Zn | 1360 | 985 | 1.38 |
| Al | 1540 | 1890 | 0.815 |
| Cu | 2350 | 2450 | 0.96 |
| | $\times 10^{-8}$ | $\times 10^{-8}$ | |

Using the equations (4.17), (4.18) and (4.19), the contact resistance
can be expressed in known variables

$$R_k^2 = \alpha^2 \cdot \frac{8\rho\lambda}{i_p^2} (\theta_m - \theta) \tag{4.20}$$

in accordance with relation (4.15) if for $c_1$ the body resistance $R_0'$ is read. Both members of this equation are divided by the body resistance $R_0$, defined in relation (4.1), thus yielding

$$\frac{R_k}{R_o} = \alpha\sqrt{2}.(\frac{i}{i_p}).\sqrt{\frac{\pi^2}{16}\cdot\frac{\lambda\theta_m D_E^4}{\rho i^2 s^2}}\ .\ \sqrt{1-\frac{\theta}{\theta_m}} =$$

$$= k\sqrt{1-\frac{\theta}{\theta_m}} \qquad\qquad (4.21)$$

with

$$k = \alpha\sqrt{2}.(\frac{i}{i_p}).Q_{\theta m}^{0.5} \qquad\qquad (4.22)$$

in which formula $Q_{\theta m}$ denotes the ultimate value of this product, obtained by putting $\theta = \theta_m$ in equation (2.7) and by defining $\rho\bar{J}^2$ as in equation(2.9).

With the aid of (4.21) the form of the resistance curves of fig. 3.5 can be explained. The body resistance $R_o'$ of the workpieces increases during the heating period because of the increase in electric resistivity with weld temperature. The contact resistance $R_k$ falls rapidly from an initial high value to that predicted by (4.21) and decreases at a slower rate with increasing weld temperature. The total resistance R, being the sum of $R_o'$ and $R_k$ consequently descends or rises, depending on the fact which term prevails.

In the interworkpiece contact area the contact resistance will be zero when the welding temperature is reached. In the electrode-workpiece interfaces a small contact resistance may be left, because $\theta < \theta_m$ in those areas (cf. table 4.1).

From our experiments it appears that the relation between the peak value of the current intensity $i_p$ in amperes and the r.m.s. value i in amperes can be expressed as

$$i_p = 18.1\times i^{0.765} \qquad\qquad (4.23)$$

for a secondary e.m.f. of 11.4 V of the welder. As a matter of course, this relation is dependent on the electrical characteristics of the equipment used. With the use of this relation the expression for the factor k transforms into

$$k = \alpha \frac{i^{0.235}}{12.8} Q_{\theta m}^{0.5} \qquad (4.24)$$

The factor k was computed for a large number of cases with the aid of equation (4.24). As expected from the figures 3.11 and 3.12 and from relation (4.9) its mean value – at constant $Q_D$ – appeared to be dependent on the product $Q_D$ as follows

$$k = k_1 Q_D \qquad (4.25)$$

where the constant $k_1$ has the values of 0.074 for stainless steel, 0.077 for low-carbon steel, 0.140 for zinc and 0.143 for aluminium.

### 4.3.3. The Heat Development in the Contact Areas

As indicated in section 4.1 the ratio of the real heat production $\phi$ and that assumed in the analogue model, $\phi_o$, will be used to correct the $Q_\theta$ values found by means of the model. The heat production $\phi_k$ in the contact areas owing to the presence of contact resistances can be written

$$\frac{\phi_k}{\phi_o} = \frac{1}{t'} \cdot \int_0^{t'} \frac{R_k}{R_o} dt = \frac{k}{t'} \cdot \int_0^{t'} \sqrt{1 - \frac{\theta}{\theta_m}} \, dt \qquad (4.26)$$

analogous to equation (4.4) and using equation (4.21). In order to evaluate the integral an assumption must be made with respect to the relation $\theta(t)$. It seems to be a fair approximation to write

$$\theta = \theta_e \cdot (1 - e^{-\beta t}) \qquad (4.27)$$

86

where

$$\theta_e = \theta_e(Q_D, Q_\lambda) = \lim_{t \to \infty} \theta \qquad (4.28)$$

It follows from equation (4.27) that

$$\lim_{t \to 0} \left(\frac{d\theta}{dt}\right) = \beta\theta_e \qquad (4.29)$$

In order to facilitate the comparison of equation (4.29) with the experimental results, the former has to be expressed in the dimensionless products $Q_\theta$ and $Q_t$ by using the equalities

$$\frac{\theta}{\theta_m} = \frac{Q_\theta}{Q_{\theta m}} \qquad \text{and} \qquad \frac{t}{t'} = \frac{Q_t}{Q_{t'}},$$

which follow from the definition (2.7). This results in

$$\lim_{t \to 0} \left(\frac{d\theta}{dt}\right) \equiv \frac{\theta_m}{t'} \cdot \frac{Q_{t'}}{Q_{\theta m}} \cdot \lim_{Q_t \to 0} \left(\frac{dQ_\theta}{dQ_t}\right) \qquad (4.30)$$

where $Q_{t'}$ and $Q_{\theta m}$ denote the observed ultimate values of these products at the time $t = t'$. The experiments have shown that the relation

$$\lim_{Q_t \to 0} \left(\frac{dQ_\theta}{dQ_t}\right) = q \cdot \lim_{Q_t \to 0} \left(\frac{dQ_{\theta c}}{dQ_t}\right) = q \cdot \tfrac{1}{2} \qquad (4.31)$$

is valid. Here, the value of $\tfrac{1}{2}$ originates from the analogue measurements, in analogy with the value of 1, observed in section 2.3.2 for the centre of the weld. $q = Q_\theta/Q_{\theta c}$ is a consequence of the discrepancy to be explained in this chapter, $Q_{\theta c}$ denoting the value

87

of this product obtained from the analogue measurements (cf. equation (3.8)).

Combination of the equations (4.29), (4.30) and (4.31) yields

$$\beta t' = \frac{q}{2} \cdot \frac{\theta_m}{\theta_e} \cdot \frac{Q_{t'}}{Q_{\theta m}} \qquad (4.32)$$

The ratio $\theta_m/\theta_e$ is known from (4.27)

$$\frac{\theta_m}{\theta_e} = 1 - e^{-\beta t'}$$

Substitution in relation (4.32) results in an implicite equation from which $\beta t'$ may be solved,

$$\beta t' = \frac{q}{2} \cdot \frac{Q_{t'}}{Q_{\theta m}} \cdot (1 - e^{-\beta t'}) = \frac{1}{2} \cdot \frac{Q_{t'}}{Q_{\theta c}} \cdot (1 - e^{-\beta t'}) \qquad (4.33)$$

From equation (4.27) follows

$$1 - \frac{\theta}{\theta_m} = 1 - \frac{1 - e^{-\beta t}}{1 - e^{-\beta t'}} = \gamma^2 \cdot \left\{ e^{\beta(t' - t)} - 1 \right\} \qquad (4.34)$$

where

$$\gamma^2 = (e^{\beta t'} - 1)^{-1}$$

After the combination of the equations (4.34) and (4.26) the latter becomes

$$\frac{\phi_k}{\phi_o} = \frac{\gamma k}{t'} \cdot \int_0^{t'} \sqrt{e^{\beta(t' - t)} - 1} \, dt \qquad (4.35)$$

88

By substitution of the variable

$$v^2 = e^{\beta(t' - t)} - 1$$

the integral is transformed into

$$\frac{\phi_k}{\phi_o} = -\frac{2\gamma k}{\beta t'} \cdot \int_{\sqrt{e^{\beta t'} - 1}}^{0} \frac{v^2 dv}{1 + v^2} =$$

$$= \frac{2\gamma k}{\beta t'} \cdot \left\{ \sqrt{e^{\beta t'} - 1} - \arctan \sqrt{e^{\beta t'} - 1} \right\} =$$

$$= \frac{2k}{\beta t'} \cdot \left\{ 1 - \frac{\arctan \sqrt{e^{\beta t'} - 1}}{\sqrt{e^{\beta t'} - 1}} \right\} =$$

$$= k \cdot g_1(\beta t') \qquad\qquad (4.36)$$

The value of $\beta t'$ can be calculated from equation (4.33), since the ratio $Q_{t'}/Q_{\theta c}$ is known from the analogue measurements for given values of $Q_{t'}$ and the welding parameters $Q_D$ and $Q_\lambda$. As $g_1(\beta t')$ and $\beta t'(Q_{t'}/Q_{\theta c})$ are both single-valued functions the former can be replaced by

$$g_1 \left\{ \beta t'(\frac{Q_{t'}}{Q_{\theta c}}) \right\} = g(\frac{Q_{t'}}{Q_{\theta c}}) \qquad\qquad (4.37)$$

This function g is calculated numerically from the relations (4.33) and (4.36) and graphically represented in fig. 4.5.
Eventually, the expression for the heat production in the contact areas becomes
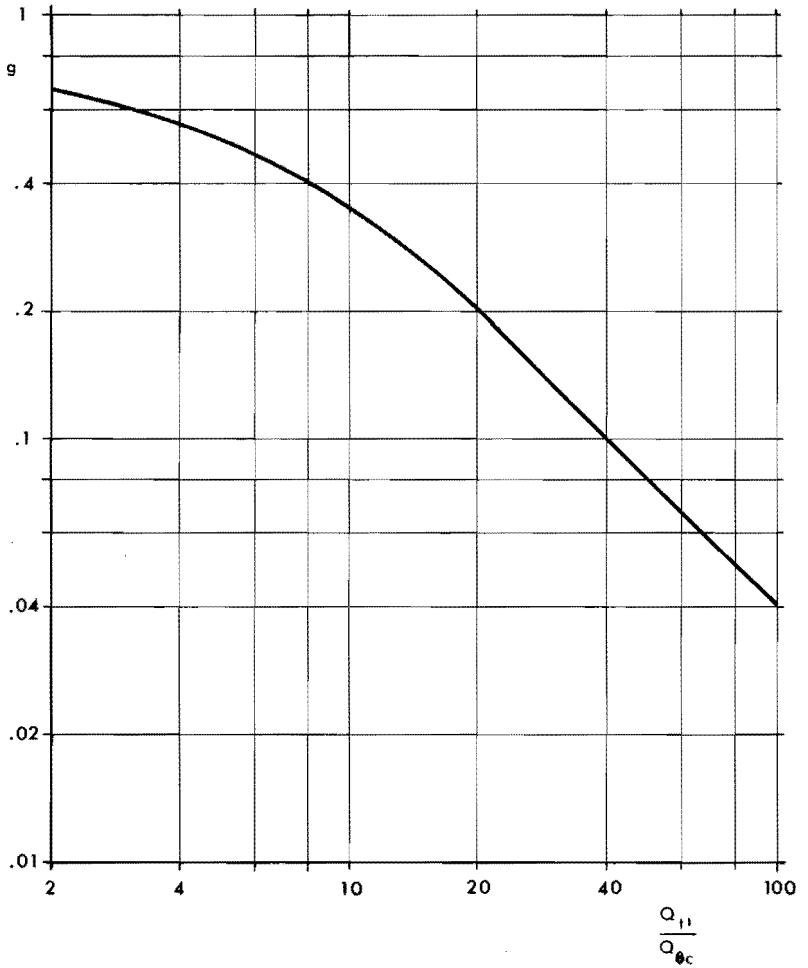
Fig. 4.5. The Function $g(Q_{t'}/Q_{\theta c})$

$$\frac{\phi_k}{\phi_o} = k.g(\frac{Q_{t'}}{Q_{\theta c}}) = \alpha . \frac{i^{0.235}}{12.8} . Q_{\theta m}^{0.5} . g(\frac{Q_{t'}}{Q_{\theta c}}) \qquad (4.38)$$

The values computed for the ratio $\phi_k/\phi_o$ are plotted in fig. 4.6 as
a function of $Q_D$. It appears that the formula
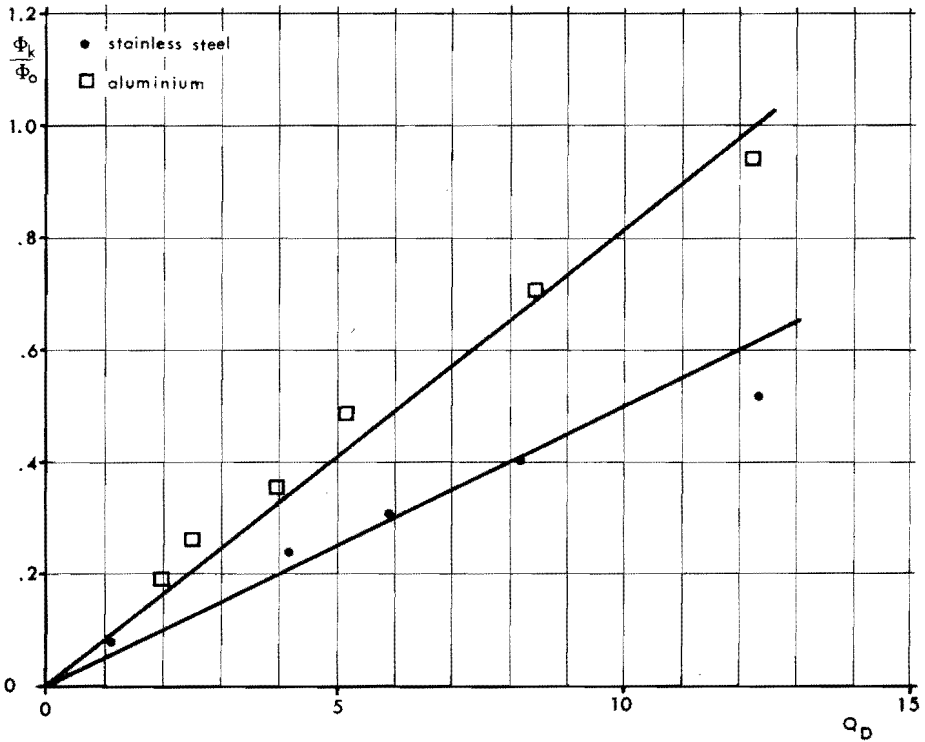
Fig. 4.6. The Ratio $\phi_k/\phi_o$ as a Function of $Q_D$ for Stainless Steel and
Aluminium

$$\frac{\phi_k}{\phi_o} = k \cdot g = k_2 \cdot Q_D \qquad (4.39)$$

describes the position of the calculated points to a fair degree of
correctness, although an extension of the range of $Q_D$ might prove
a second order approximation to yield more accurate results. In
(4.39) the constant $k_2$ has the values of 0.045 for stainless steel,
0.046 for low-carbon steel, 0.073 for zinc and 0.081 for aluminium.


## 4.4. The Total Heat Production


### 4.4.1. Correction of the Analogue Results

On the basis of the derived relations (4.9) and (4.39) the total heat

91

production in the weld material can now be written

$$\frac{\phi}{\phi_o} = \frac{\phi_o'}{\phi_o} + \frac{\phi_k}{\phi_o} = f(Q_D) + 3.k_2.Q_D = q \qquad (4.40)$$

where the factor 3 is added as an approximation, assuming the existence of three equally important contact areas. Comparison of this relation with the experimental result from section 3.4.2 shows that the latter is covered by curves of the form

$$q = f(Q_D) + \zeta.Q_D, \quad \text{for} \quad Q_D < 16 \qquad (4.41)$$

in such a way that no deviations occur of more than ten per cent. of the value of q. In table 4.3 the derived values of $3.k_2$ are compared with the experimental values of $\zeta$ for the workpiece materials investigated.

Table 4.3. Comparison of Theoretical and Experimental Results

| material | $3.k_2$ | $\zeta$ |
|----------|---------|---------|
| SS | 0.135 | 0.15 |
| St | 0.138 | 0.15 |
| Zn | 0.219 | 0.15 |
| Al | 0.243 | 0.22 |

As demonstrated, the computed values agree rather well with the experimental ones, except for the welding of zinc.


4.4.2. Discussion

By introducing the factor 3 in equation (4.40) the following assumptions were made.

(a) The heat production in the electrode contact surfaces in equal to

that in the interworkpiece contact area, i.e. equation (4.17) is
valid for the three contacts. This is only true if $\theta_m$ is smaller than
the melting temperature of the electrode materials, as is the case
for the welding of aluminium and zinc. For steel, however, the
weakening temperature of the contact spots will be equal to the
melting point of the electrode material. The solution of the integral
(4.17) will therefore yield a lower value.

(b) All the heat developed in both electrode-workpiece contact areas
flows to the workpieces and raises the temperature of the weld.
Although this is not very probable, the existence of a temperature
barrier in the contact spots during the formation of the weld
diminishes the passage of heat to the electrodes.

From the results it seems that the effects of these simplifications
balance each other to a considerable extent.
A final remark must be made with respect to the values used for the
electric resistivity $\rho$. As appears from table 3.2, the best fitting
values of $\rho$ are much lower than those defined by equation (3.1) for
the welding of steel, whereas for aluminium the opposite is true.
However, equation (3.1) is a rather arbitrary definition of the
average values of the physical material properties. The average
temperature in the sheet during the heating period, determined for
the region $0 < z < s$, is lower when welding steel than when welding
aluminium. This is because of the influence of $Q_\lambda$ (cf. fig. 2.12 and
2.14). It is therefore acceptable that the mean value of $\rho$ is
relatively low for the former and high for the latter metal.


## 4.5. Conclusions


### 4.5.1. The Validity of the Analogue Model


The discrepancy between the experimental results and the predictions
of the analogue model, noted in chapter 3, has been demonstrated to
be due to two important shortcomings of the mathematical model in
the present chapter. These shortcomings are the assumed current
distribution, which differs markedly from the true distribution for
low $Q_D$ values, and the neglect of the contact resistances, which may
cause deviations of a factor 4 or more from the computed temperatures

for high $Q_D$ values. It is shown that these deviations are accounted
for by means of a correction factor q, the value of which can be
derived with acceptable correctness. In this way the temperatures of
the weld are predicted satisfactorily as far as the border of the
weld is concerned. Presumably, this is also true for the centre of
the weld, in as far as the melting point of the weld metal is not
exceeded.

Because of the extra heat production in the electrode-workpiece
contact surfaces, however, the real temperature values in those
areas become uncertain. As a consequence, the curves of the figures
2.11 to 2.14 inclusive can only be used as indications of the
influence of the welding parameters on the mean electrode face
temperatures.

A possible future research on the spot welding process might include
the improvement of the RC-network with respect to both the electric
contact resistances and the distribution of heat generation
throughout the weld material.

In the present work it is shown that neither a solution of spot
weld temperatures based on the production of the welding heat in the
workpiece bodies only [6, 30, 31, 34], nor an approach based on the
exclusive heat production in one or more contact surfaces [27, 34],
will yield satisfactory results for a wide range of the electrode
diameter to sheet thickness ratio.


### 4.5.2. The Choice of the Electrode Diameter

The electrode diameter $D_E$ can be chosen from a wide range for a given
thickness s of the sheets to be welded. The choice should be based on
the weld diameter required to obtain a weld of sufficient strength
[56]. In workshop practice, the working range of the welding equip-
ment will play an important role in this choice, as has been demon-
strated in section 3.2.3.


### 4.5.3. The Influence of the Electrode Material

It appears from the analogue as well as from the experimental
results that the thermal and electrical conductivities of the

94

electrode material are of great importance to the temperature development in the weld, especially for long welding times and at the electrode tips. From a thermal point of view, these conductivities should be as high as possible. In practice, a compromise must be made between good conductivity on the one hand and satisfactory mechanical properties at high temperatures on the other.

From the analogue measurements it appeared that the volumetric heat capacity of the electrode $c_E$ has no influence on the process (cf. section 2.3.2).

## 4.5.4. The Influence of the Electrode Force

The evaluation of the contact resistance $R_k$ in section 4.3.2 is based on the assumption that the electrode force F has no influence on the value of $R_k$, in as far as F has a sufficiently high value to press the contact members towards each other when the contact spots are weakened by the passage of the electric current.

Nevertheless, references [54, 57] observe that for $Q_D > 4$ a decrease in electrode force

(a) not only decreases the maximum permissible welding current, but also reduces the current intensity required to obtain a weld of prescribed dimensions $(D_N < D_E)$;

(b) reduces the maximum nugget diameter that can be formed.

Observation (a) may be explained by the following considerations. If the electrode tips are not exactly flat and parallel, a decrease in electrode force will reduce the macroscopic area of contact between electrode and workpiece, thus yielding a smaller effective electrode diameter and consequently, a lower $Q_D$ value. For this reason, the body resistance $R_o'$ of the workpieces increases. The contact resistance will increase too, owing to the lower current intensity applied. In this way, the total heat production $i^2 R$ may vary little for small variations in the effective electrode diameter. Observation (b) may be explained by the same mechanism, viz. a decreasing effective electrode diameter for lower electrode forces. Here, $D_{Nmax}$, which may be much greater than $D_E$, is brought about by the weld temperature reaching the equilibrium value $\theta_e$.

In conclusion, a high value of the electrode force will cause smaller

deviations of the true contact diameter, which may equally originate from the presence of dirt particles between the contacting surfaces. Consequently, the variation in weld quality is lower for high electrode forces [4]. The often undesirable indentation of the electrodes into the workpieces when the weld weakens is reduced by the application of a programmed force. This force should have a high value at the beginning of the heating period and be substantially decreased before the end of that period.

Besides, the influence of the static packing friction in the air cylinder and of the inertia of the moving parts of the welding machine is also reduced by the application of high electrode forces.

## 4.5.5. Representation of the Results

A definitive version of the dependence of $Q_\theta$ on $Q_t$ for the nugget border is graphically represented in fig. 4.7. In order to obtain the curves demonstrated, the results of the analogue measurements for $Q_\lambda = 8$ are corrected by means of formula (4.41) with $\zeta = 0.15$ and $f(Q_D)$ taken from fig. 4.3.

An experimental affirmation for conditions outside the range of our experiments is found in [24] for very thin sheets. It concerns the spot welding of 0.15 mm mild steel with a 0.75 mm electrode tip diameter by means of a capacitor discharge welder. The author has determined the current intensities required for welding times of 0.8 and 4 ms to be 2.15 and 1.36 kA respectively. Calculation of $Q_t$ and $Q_\theta$ with the aid of the data from the tables 3.1 to 3.4 inclusive yields values of 0.24 and 1.2 respectively for the first product, and 0.164 and 0.41 respectively for the second. These results agree very well with the curve for $Q_D = 5$ of fig. 4.7.

From the universally usable curves of fig. 4.7 graphs can be derived which are easily to be interpreted in workshop practice. As an example, conditions are calculated for the spot welding of 1 mm low-carbon steel sheet, using electrode diameters of 3 up to 8 mm and a wide range of welding times and current intensities (see fig. 4.8). The electrode forces given are calculated from $Q_F = 0.2$, in accordance with equation (3.6).

It should be realised that the graphs given originate from a thermal
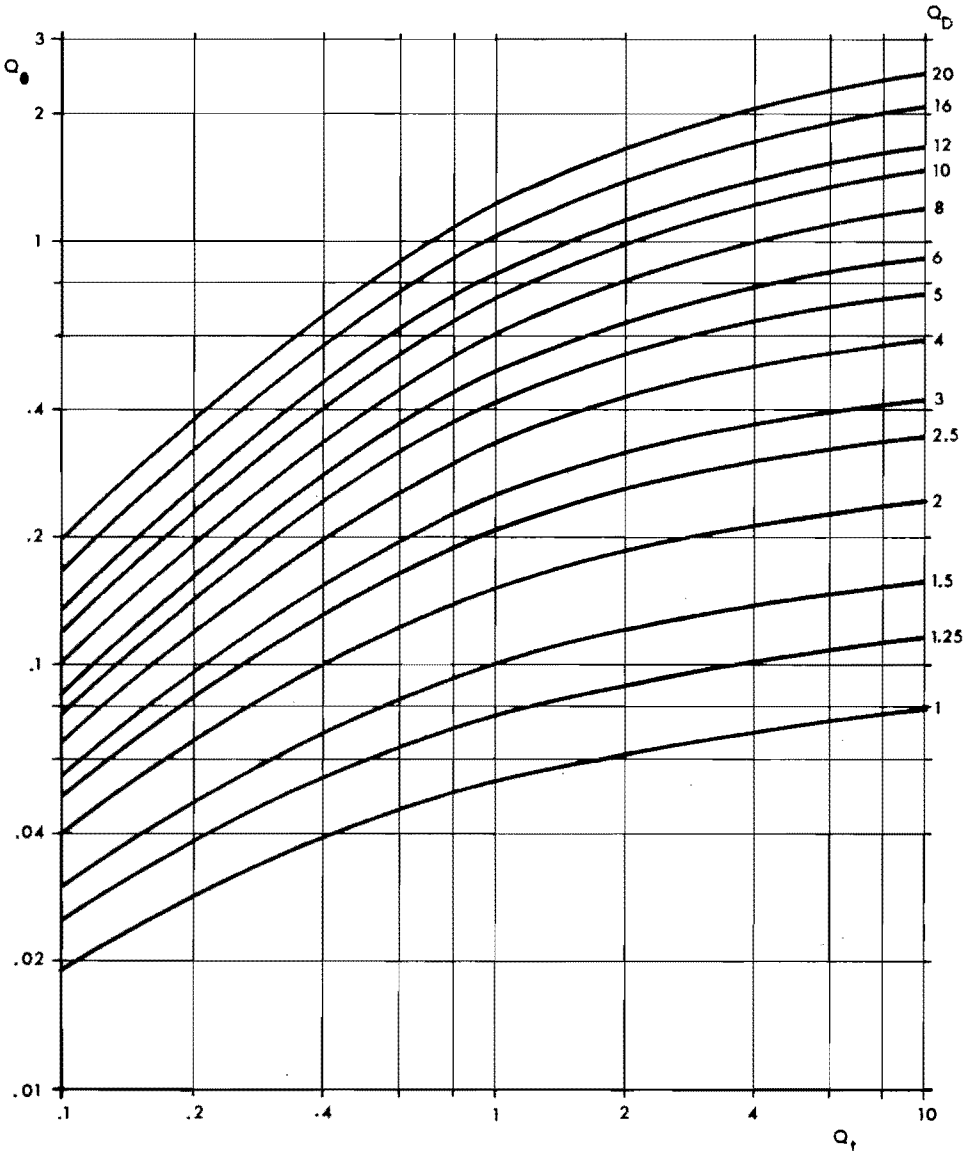
Fig. 4.7. Definitive Representation of $Q_\theta$ as a Function of $Q_t$ for
Different Values of $Q_D$.
The graphs are valid for low-carbon steel and stainless steel
$(Q_\lambda = 8)$

analysis only. In order to facilitate the choice of optimum welding
conditions, data should be available from which the quality of the
weld, made with any combination of welding parameters from these
graphs, can be predicted. In chapter 6, an attempt will be made to
link the thermal data to some quality criteria.
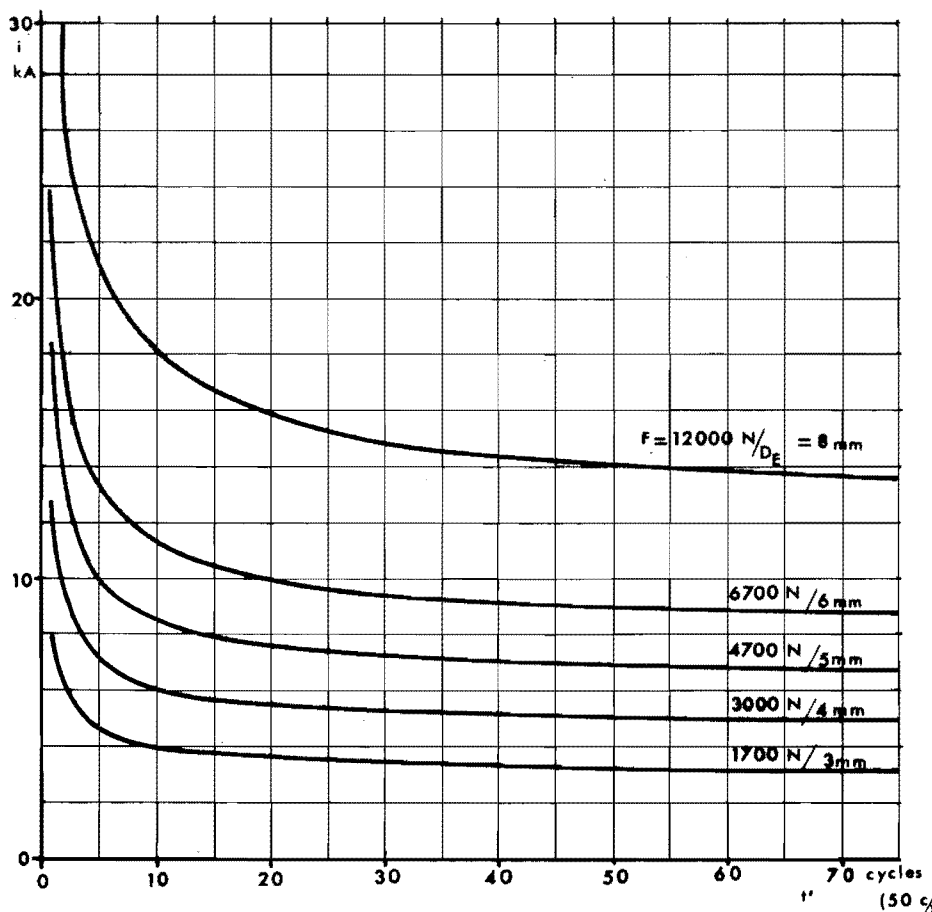


Fig. 4.8. Conditions for the Spot Welding of 1 mm Low Carbon Steel Sheet.
Electrode material is RWMA Class 2 [4]

Chapter 5. APPLICATIONS

## 5.1. Asymmetrical Geometry

### 5.1.1. Introduction

In this chapter, two cases are considered in which the geometrical
arrangement differs from that described in chapter 1. They can be
treated with the aid of the foregoing analysis, for which reason they
are looked upon as applications of the present theory.
The first case concerns the welding of sheets differing either in
thickness or in material, or in both. It is referred to as the case
of asymmetrical geometry since there is no longer symmetry with
respect to the plane $z = 0$.
In the foregoing analysis it was assumed that no heat would flow
across the plane $z = 0$ for symmetry reasons. Hence, only the system
consisting of one sheet and one electrode was considered. If, however,
two different "weld halves", in which the temperature gradients in the
direction of the z-axis are zero, are placed together and if certain
conditions of continuity are fulfilled, this abstraction can still
be applied.
The continuity conditions to be fulfilled are

(a) the welding current in both "halves" should have the same
intensity and distribution in $z = 0$,

(b) the welding times should have the same values,

(c) the temperature distributions in the plane $z = 0$ should be
congruent at any instant.

As a matter of course, these requirements are exactly met only in the
case of symmetry. However, if some of this exactness is relinquished
a suitable set of requirements is left. This means that (a) is
reduced to the requirement of equal current intensities and that (c)
is simplified to the requirement of equal temperatures at the nugget
border.
If the "weld halves" are labelled 1 and 2 the following conditions
thus remain

99

$$i_1 = i_2 = i$$

$$t_1' = t_2' = t'$$

$$\theta_1[B] = \theta_2[B] = \theta[B]$$

(5.1)

In the case of dissimilar sheet thicknesses only the following inequalities may exist

$$s_1 \neq s_2$$

$$D_{E1} \neq D_{E2}$$

(5.2)

and

$$\lambda_{E1} \neq \lambda_{E2}$$

(5.3)

while in the case of dissimilar workpiece materials the inequalities

$$\lambda_1 \neq \lambda_2$$

$$\rho_1 \neq \rho_2$$

$$c_1 \neq c_2$$

(5.4)

may, in addition, be valid.

Since it is assumed that in the first case $s_1$ and $s_2$ are given, and in the second case the material properties, the conditions (5.1) can be fulfilled only by an adequate choice of the electrode tip diameters and/or of the electrode materials.


## 5.1.2. Choice of the Welding Conditions

The application of the results of the present investigations to the welding of workpieces having dissimilar thicknesses or physical properties is illustrated in this section by means of a few examples. First, however, the graphical representation of the experimental

100

results of chapter 3 has to be adapted to the purpose. In order to remove the electrode diameter $D_E$ from the product $Q_\theta$ the latter is transformed into

$$Q_v = Q_\theta^{0.5} \cdot Q_D^{-2} = \frac{\pi}{4} \sqrt{\frac{\lambda \theta_m}{\rho}} \cdot \frac{s}{i} = b\frac{s}{i} \tag{5.5}$$

The definition (2.7) for $Q_t$ is maintained,

$$Q_t = a\frac{t'}{s^2} \tag{5.6}$$

where  a and b are  averaged material constants.

The dimensionless product $Q_v$, as derived from the data of fig. 4.7, is graphically shown in fig. 5.1. These curves are valid for the spot welding of low-carbon steel and stainless steel, which metals are used in the present section for the examples to follow. The values of a and b are derived from the tables 3.1 and 3.2 and rearranged in table 5.1.

Table 5.1. Material Constants and Electrodes Used

| material | a<br>$m^2.s^{-1}$ | b<br>$A.m^{-1}$ | $H_V$<br>$N.m^{-2}$ | electrode material |
|---|---|---|---|---|
| SS | $4.7\times10^{-6}$ | $0.162\times10^6$ | $171\times10^7$ | Class 3 |
| St | $6.74\times10^{-6}$ | $0.233\times10^6$ | $119\times10^7$ | Class 2 |

It was supposed that the materials to be welded to each other, their thickness and the required diameter of the weld nugget were given. Since $Q_{t1}$ and $Q_{t2}$ will generally have different values, which should neither be extremely high nor extremely low, in order to avoid too slow heating or excessive currents, it appears to be good practice to choose the welding time in such a way that their geometric mean has a value of about 1.

Thus,

$$\sqrt{Q_{t1} \cdot Q_{t2}} \approx 1 \tag{5.7}$$
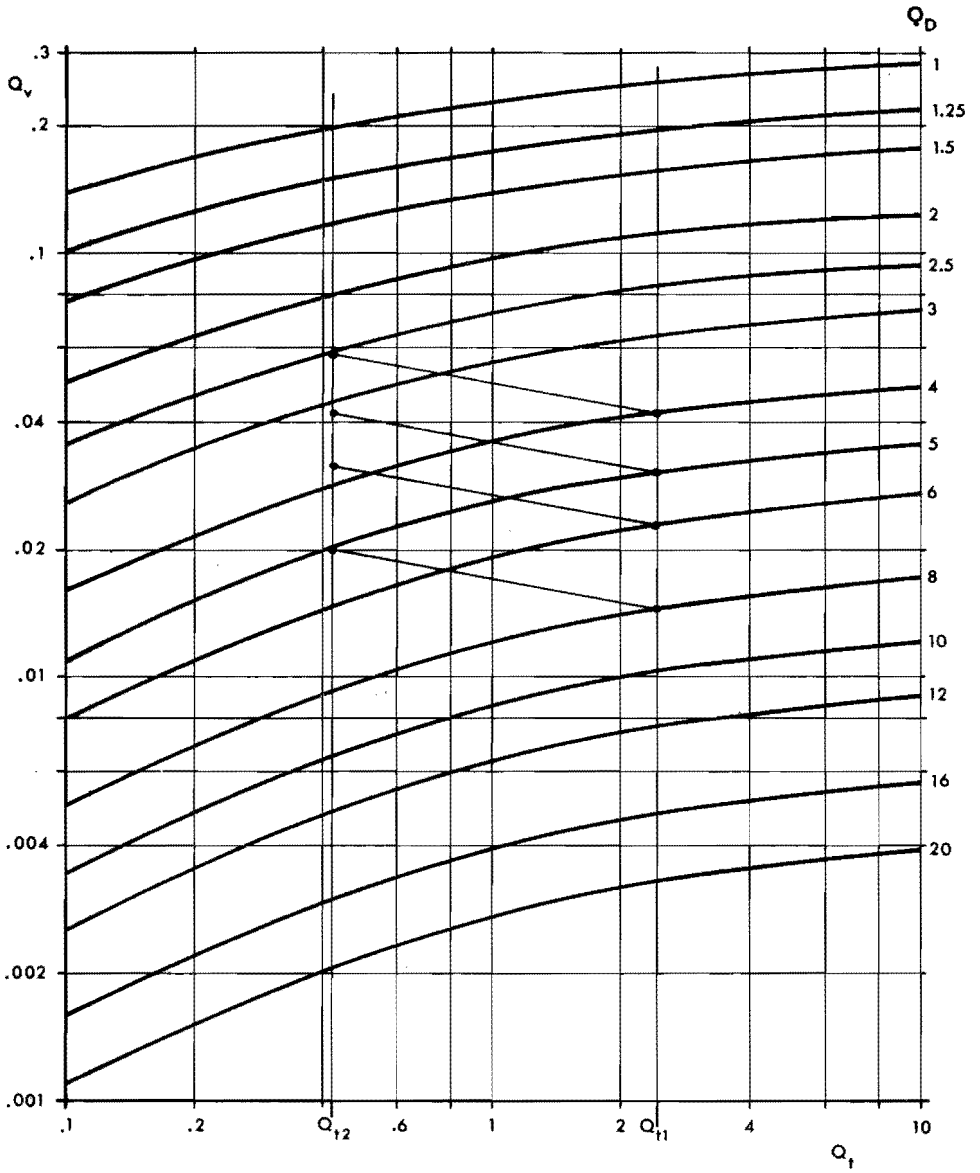
Fig. 5.1. Representation of the Dimensionless Product $Q_v = Q_\theta^{0.5} \cdot Q_D^{-2}$ as a Function of $Q_t$ for Different Values of $Q_D$, as derived from Fig. 4.7.

which means that the welding time t' becomes

$$t' \approx \frac{s_1 s_2}{\sqrt{a_1 a_2}} \qquad (5.8)$$

For the welding of 1 mm low-carbon steel sheet to a 2 mm stainless steel sheet, subscripted 1 and 2 respectively, t' attains the value of 0.36 s (18 current cycles). Then, $Q_{t1}$ = 2.43 and $Q_{t2}$ = 0.423. For $D_{E1}$ = 8 mm, and hence $Q_{D1}$ = 8, the value of $Q_{v1}$ can be read to be 0.0145 from fig. 5.1.
Since

$$Q_{v2} = \frac{b_2 s_2}{b_1 s_1} \cdot Q_{v1} \qquad (5.9)$$

and $Q_{t2}$ is already known, the value of $Q_{D2}$ is easily interpolated from the graph, thus yielding $D_{E2}$. The current intensity is calculated from

$$i = \frac{b_1 s_1}{Q_{v1}} = \frac{b_2 s_2}{Q_{v2}} \qquad (5.10)$$

The same calculations can be carried out for different values of $D_{E1}$. The results are shown in table 5.2. The electrode forces are obtained by applying equation (3.6) to both weld halves and by chosing the lower value.

The calculation method demonstrated above was successively applied to the following combinations of sheets

    I   $s_1$ = 0.5 mm SS; $s_2$ = 1 mm SS; $D_{E1}$ = 3, 4, 5 and 6 mm;

   II   $s_1$ = 0.5 mm SS; $s_2$ = 2 mm SS; $D_{E1}$ = 3, 4, 5 and 6 mm;

  III   $s_1$ = 1 mm SS; $s_2$ = 2 mm St; $D_{E1}$ = 4, 5, 6 and 8 mm;

   IV   $s_1$ = 1 mm St; $s_2$ = 2 mm SS; $D_{E1}$ = 4, 5, 6 and 8 mm.

The welding conditions thus determined were experimentally verified afterwards.

Table 5.2. Calculation of the Conditions for the Welding of 1 mm St
to 2 mm SS Sheet with the Aid of Fig. 5.1

| $s_1$ = 1 mm St; $s_2$ = 2 mm SS; $t'$ = 0.36 s | | | | | | | |
|---|---|---|---|---|---|---|---|
| $D_{E1}$ | $Q_{D1}$ | $Q_{v1}$ | $Q_{v2}$ | $Q_{D2}$ | $D_{E2}$ | $i$ | $F$ |
| mm | | | | | mm | kA | kN |
| 4 | 4 | 0.042 | 0.058 | 2.5 | 5 | 5.5 | 2.9 |
| 5 | 5 | 0.030 | 0.042 | 3.1 | 6.2 | 7.6 | 4.5 |
| 6 | 6 | 0.023 | 0.032 | 3.7 | 7.4 | 10.1 | 6.4 |
| 8 | 8 | 0.0145 | 0.020 | 5.0 | 10 | 16.0 | 11.5 |

5.1.3. Verification

The verification of the welding conditions determined in the fore-
going section for the spot welding of dissimilar workpieces, showed
the applied calculation method to be very successful. Yet, it seemed
to be necessary to increase the computed current intensities by 0 to
8 per cent., especially for low $Q_D$ values. Apparently, the weld
nugget tends to form in the area half-way the distance between the
electrode faces when the influence of the contact resistance is small,
which is the case for low $Q_D$ values [39]. Besides, the errors both of
the predicted values and of the measurements should not be expected
to be smaller than five per cent.
The values of the current intensity required to obtain a weld nugget
of prescribed dimension appeared to be very critical. However, this
is true for any spot welding condition, owing to the fact that for a
given welding time the temperature reached in an arbitrary point of
the workpiece is proportional to the square of the current intensity.
Principally, the described method is applicable to any combination
of metals to be welded, premised that the melting temperatures do not
differ too much, and that the metals concerned tend to alloy with
each other to some degree [1].

## 5.2. The Spot Welding of Pure Copper

### 5.2.1. Method

Since the weldability of a metal varies inversely with its electrical
and thermal conductivities [2], the spot welding of pure copper (more
than 99.9% Cu) is extremely difficult. This is demonstrated in fig.
2.12 where copper electrodes are used. According to this figure, only
relatively long welding times and extremely small ratios of electrode
tip diameter to sheet thickness would prevent the electrodes from
welding to the workpieces, producing as a consequence small weld
nugget diameters. The presence of contact resistances makes the situ-
ation still worse. The value of the electrode-to-workpiece resistance
is fundamentally the same as that of the workpiece-to-workpiece
resistance. Since the heat production in the first is confined to a
smaller area than in the second, owing to the "bulging" of the
current in the workpieces, this heat tends to increase the electrode
temperature in particular. A solution for this problem is found in
using an electrode material with a very high melting point, such as
tungsten [58].

Another method was used in the present investigations, based on the
theoretical considerations of section 4.2. This method is elucidated
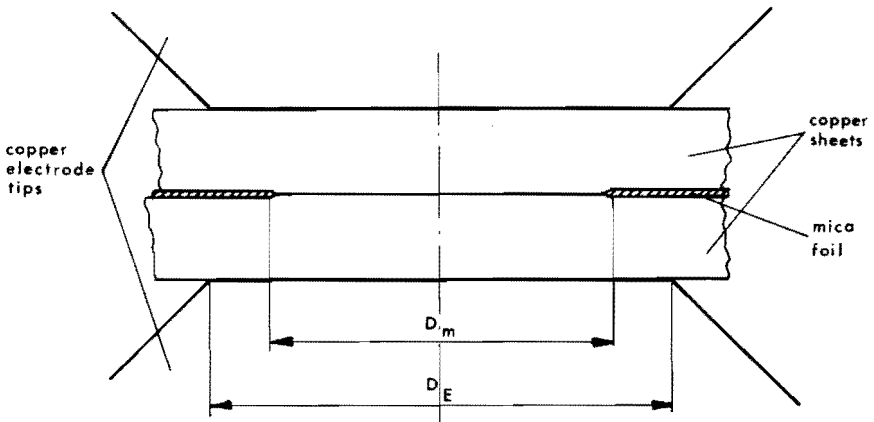in fig. 5.2. It consists in inserting a very thin foil of an



Fig. 5.2. The Spot Welding of Copper by Means of an Artificial Current
Constriction

electrically non-conducting material between the sheets to be welded.
A hole, having a diameter $D_m$, equal to that of the weld nugget
required, is punched in the foil. The electrode tips have diameters
which are substantially greater than $D_m$. They are positioned
centrally with respect to the hole. The electrodes press the copper
sheets upon each other, with such a force that in the area of the
hole there is metallic contact between them before the welding
current starts to flow.
High demands are made on the material of the foil. In fact, it must
be able to withstand very high pressures and temperatures. The foil
must be extremely thin to facilitate the metallic contact. A mica
foil of about 0.02 mm proved to give satisfactory results.
The objective of such a geometry is to obtain a high current density,
and thus a high specific heat production in the area where the weld
has to form, without affecting the heat flow to the electrodes. In
this way the bulging of the electric current near the workpiece
interface is effectively prevented.


## 5.2.2. Experimental Results

The spot welding of electrolytic copper sheets was carried out for
the welding conditions given in table 3.5. Except for the geometrical
arrangement of fig. 5.2 the general method was the same as that
described in section 3.1. A somewhat deviating definition of the
dimensionless products $Q_D$ and $Q_\theta$ was applied by using the hole
diameter $D_m$ instead of the electrode tip diameter $D_E$ in the equations
(2.7) and (2.8), thus

$$Q_D = \frac{D_m}{s} \tag{5.11}$$

$$Q_\theta = \frac{\lambda \theta_m}{\rho \bar{J}^2 s^2} = \frac{\pi^2 \lambda \theta_m D_m^4}{16 \rho i^2 s^2} \tag{5.12}$$

The electrode diameter $D_E$ was maintained at a value of about 8.5 mm
in all cases.
The resultant joints were sound welds with high strength and nugget

diameters of the same dimension as $D_m$. The welding time t' proved to be more critical than for the welding of the previous metals, since the tendency of the workpieces to weld to the electrodes was considerably greater.

On the basis of the considerations of chapter 4 it might be expected that the ratio q, defined in equation (3.8), would depend on $Q_D$ in the same way as in relation (4.40). This, indeed, appeared to be true if the definitions (5.11) and (5.12) were applied, viz.

$$q = \frac{\phi}{\phi_o} = f'(\frac{D_m}{D_E}) + \zeta Q_D \qquad (5.13)$$

However, the significance of the function $f'(D_m/D_E)$ differs from that of the previous $f(Q_D)$ because of the deviating geometry of fig. 5.2 (cf. section 4.2). Here, the body resistance $R_o'$ of the welding work is written

$$R_o' = \frac{8\rho s}{\pi D_m D_E} \qquad (5.14)$$

as an approximation. $R_o'$ represents twice the resistance of the truncated cone of fig. 5.3. The result (5.14) is easily obtained by
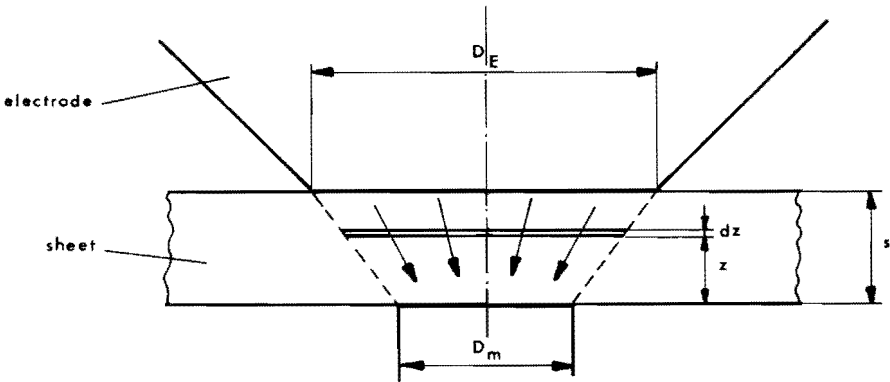


Fig. 5.3. Assumed Path of Current Flow for the Case that $D_E > D_m$

integrating the resistance of an infinitely thin cylindrical slice with radius

$$r(z) = \frac{D_m}{2} + \frac{D_E - D_m}{2s} \cdot z$$

and thickness dz over the range $0 < z < s$.

If in the expression for $R_o$ (4.1) the electrode diameter is replaced by $D_m$ as well, the function $f'$ becomes

$$f'(\frac{D_m}{D_E}) = \frac{R'_o}{R_o} = \frac{D_m}{D_E} \tag{5.15}$$

Thus, $f'$ represents the ratio of the true body resistance between the electrode tips and the resistance of the cylinder with height $2s$ and diameter $D_m$, which resistance was exclusively considered in the analogue model. Because of the considerations of section 4.2, the function $f'$ also represents the ratio between the true and the assumed heat development in the workpiece bodies, as in equation (5.13). The constant $\zeta$ in that equation appeared to have the value of 0.12 for the spot welding of pure copper.

In fig. 5.4 the correspondence of the relation (5.13) with the experimental results is demonstrated.
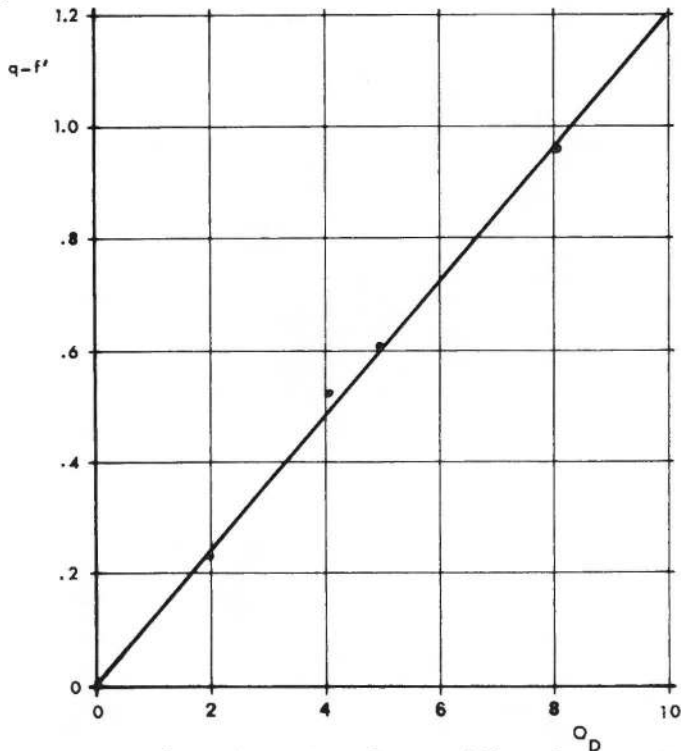


Fig. 5.4. Experimental Results of the Welding of Copper Sheet

5.2.3. Conclusions

By inserting a non-conductive foil of a few hundredths of a mm
thickness between the sheets, the weldability of electrolytic copper
is considerably improved with respect to the following points.

(a) The welding current required to make a weld of prescribed
dimensions is lowered.

(b) The tendency of the workpieces to weld to the electrode tips
is reduced.

(c) The appearance of the weld is improved by the use of larger
electrode tip diameters, resulting in smaller indentations in the
surfaces of the workpieces.

The method described looks very much like the projection welding
process, to which the same advantages are adjudged [1]. Relative to
the plain spot welding geometry, both methods have the disadvantage
of a more laborious preparation of the welding work.
In the scope of the present work, however, the most important aim in
using the described method was not the development of a new method of
spot welding but a further verification of the assumptions made in
the last paragraph of section 4.1.
In conclusion, the errors, introduced in the mathematical model of
chapter 2 by the use of too unrealistic simplifications regarding
current distribution and contact resistances, are fully removed by
correcting the heat development assumed in the model. This correction
has to depend on the ratio $R/R_o$ of the true total resistance of the
workpieces to that assumed in the mathematical model, in the way
described in relation (4.4).

Chapter 6. QUALITY CONTROL

## 6.1. Quality of Spot Welds

### 6.1.1. Introduction

In the foregoing chapters an analysis of the thermal aspects of the
spot welding process was presented. With the aid of the derived
relations between the welding parameters it appeared to be possible
to determine adequate welding conditions if the materials to be
welded, their dimensions and the required size of the weld were
given. A graphical representation of these conditions was suggested
in fig. 4.8. From this figure it appears that either the welding
current or the welding time may be chosen freely for the obtainance
of a weld of prescribed dimensions.
In order to facilitate the choice of optimum welding conditions,
attention must be paid to the quality of the welds thus made.
However, a fundamental difficulty lies in the concept of weld
quality, since this concept cannot be defined without referring to
the demands made on the application for which the joint under
consideration is intended. As a consequence, a great number of
quality criteria is in use in industry. A review of commonly
applied testing methods of spot welds is found in literature
[4, 59, 60]. Each of these methods implies the use of its intrinsic
quality criterion.
The variety of criteria may be reduced to the investigation of a
few important weld characteristics, viz.
    (a) the external appearance of the joint made,
    (b) the mechanical strength of the weld under various
        conditions.
Other criteria used, such as the structure and the homogeneity of
the weld metal and the presence of residual stresses owing to the
thermal cycle, generally are a means of investigating
characteristic (b).
A third important characteristic concerns the technology of the
welding process rather than the quality of the weld made, viz. the
life of the electrode tips. This factor is considered in literature
[31, 45]; it was not investigated explicitely in the experiments

under review, although general conclusions may be drawn from
section 2.3.2 as to the height of the electrode tip temperatures,
which strongly influence electrode tip life [31], in dependence on
$Q_D$ and $Q_\lambda$.
The characteristics (a) and (b) will be discussed in the following
sections.


## 6.1.2. The Appearance of Spot Welds


The appearance of the spot weld, involving the phenomena of sheet
separation and of surface indentation (cf. fig. 6.1), in addition
to external defects such as pits, tip pickup and external cracks,
is of importance for a number of applications. These applications
concern especially those cases, where aerodynamic considerations
play an important role, where demands are made on the tightness of
the joint or where a good appearance is necessary, as in the
manufacture of motor-car bodies or household appliances.



$d_i$ = surface indentation
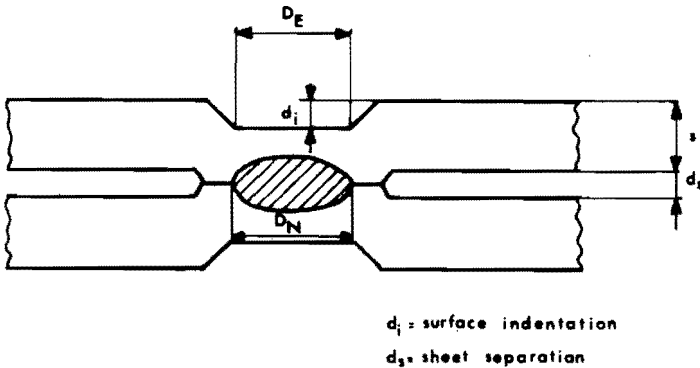$d_s$ = sheet separation

Fig. 6.1. Appearance of a Spot Welded Joint

$d_i$ = surface indentation

$d_s$ = sheet separation


The American Military Specifications [10] consider both the sheet
separation $d_s$ and the surface indentation $d_i$ unacceptable for
high-quality welds if values of 10 per cent. of the sheet thick-

ness are surpassed. The corresponding German Recommendation [14] gives a same value for $d_i$, but does not mention sheet separation. A phenomenological description of the deformations occurring in the environment of the weld as a consequence of the thermal cycle was given in section 3.4.1. From our experiments it appeared that the greater part of the total sheet deformation takes place after the weld nugget has formed. The following two cases are to be distinguished.

(a) Weld type AS or CS (cf. fig. 3.6). If the weld metal splashes away between the sheets when the weld nugget reaches its required size, a markable indentation $d_i$ results, the value of which is unpredictable since it depends on the accidental weakness of the wall surrounding the molten pool (cf. section 3.4.1).

(b) Other weld types (cf. fig. 3.5). Our statistical analysis of the influence of a number of welding parameters, among which were the products $Q_D$ and $Q_\theta$ and the ratio $t_h/t'$ of the applied heating time to the required welding time, revealed that

$$\frac{d_i}{s} \sim Q_D^{\ n} \cdot (\frac{t_h}{t'} - 1)^{0.5} \qquad (6.1)$$

The effect of the ratio $t_h/t'$ is far more pronounced than that of the product $Q_D$, the exponent n of which seemed to have a value of about 0.25, whilst the influence of $Q_\theta$ appeared to be insignificant.

In other words, the ultimate deformations are very sensitive for the precise value of the heating time. They are very small if the heating time is just long enough to permit the formation of a full-sized weld ($t_h = t'$). A similar relation is valid for the relative sheet separation $d_s/s$,

$$\frac{d_s}{s} \sim Q_D^{\ m} \cdot (\frac{t_h}{t'} - 1)^{0.5} \qquad (6.2)$$

although the statistical significance of the influence of $Q_D$ is smaller than in (6.1).

The observations regarding the disadvantageous effects of too long heating times are in agreement with workshop experience [10, 14].

The other external defects of spot welds mentioned above, appear
to be dependent on the electrode face temperature. Especially the
tendency of the electrodes towards sticking to the sheets, and
hence the occurrence of electrode pickup on the outer contact
surfaces of the workpieces, increases with higher electrode face
temperatures [31]. Our observations indicate that these phenomena
become more serious if the heating time is too long ($t_h > t'$),
i.e. if the electrodes indent considerably into the sheets, thus
resulting in both a higher effective $Q_D$ value and increasing
electrode face temperatures.

6.1.3. The Strength of Spot Welds

The most widely used quality criteria for resistance welds are
those regarding the strength of the weld made. Direct tests having
a destructive character, are generally used to check the strength
of the joint under circumstances identical to those of the actual
application. Commonly applied examples of these tests determine the
shear strength, the fatigue strength or the impact strength. Since
the first is comparatively easy to be determined, it is frequently
used as a quality criterion [4, 10, 14].
However, several investigators observe that the static shear
strength $F_s$ of a spot weld exclusively depends on the diameter $D_N$
of the weld nugget formed [56, 57]. Since this diameter can be
influenced at will by adjusting the welding parameters current and
heating time, and by choosing an adequate electrode diameter, the
authors consider neither the shear strength nor the nugget diameter
a yardstick for weld quality. They reject the prescription of one
special electrode and weld nugget diameter for a given sheet
thickness to be welded, i.e. the use of equations (3.4) and (3.5).
An affirmation of these points of view is found in the present work.
Two different modes of fracture are observed for welds having a
nugget diameter $D_N \approx D_E$, depending on the dimensionless product $Q_D$,
viz.

$$F_s = \sigma_s D_N (s - \frac{d_i}{2}) \quad \text{for} \quad Q_D > 4, \text{ approximately} \qquad (6.3)$$

and

$$F_s = \tau_s \frac{\pi}{4} D_N^2 \quad \text{for} \quad Q_D < 4, \text{ approximately} \tag{6.4}$$

The average values of the constants $\sigma_s$ and $\tau_s$ are given in table 6.1, compared with the ultimate tensile strength $\sigma_M$ of the materials investigated (cf. table 3.1).

Table 6.1. The Constants $\sigma_s$ and $\tau_s$ from the Relations (6.3) and (6.4)

| material | $\sigma_s$ | $\tau_s$ | $\sigma_M$ | $\sigma_s/\sigma_M$ | $\tau_s/\sigma_M$ |
|----------|-----------|----------|-----------|---------------------|-------------------|
| SS | 159 | 54.2 | 61.4 | 2.6 | 0.88 |
| St | 150 | 57.3 | 38.8 | 3.9 | 1.48 |
| Zn | 34.6 | 10.0 | 14.1 | 2.5 | 0.71 |
| Al | 22.1 | 5.6 | 10.8 | 2.1 | 0.52 |
| Cu | 57.5 | 15.3 | 25.8 | 2.2 | 0.59 |
|  | $\times 10^7$ N.m$^{-2}$ | $\times 10^7$ N.m$^{-2}$ | $\times 10^7$ N.$\overline{\text{m}}^{-2}$ |  |  |

As pointed out, equation (6.3) is valid for $Q_D > 4$. The fracture occurs in the circumference of the weld nugget, resulting in the nugget being entirely torn out of one of the sheets. In fact, the joint does not yield in the weld nugget, but beside it. The other type of fracture, for which relation (6.4) holds, occurs by shearing of the original sheet interface.

Though it is not the author's intention to present a thorough analysis of the strength of spot welds, the high values for the constants $\sigma_s$ and $\tau_s$, given in table 6.1 for low-carbon steel need some comment.

It was observed that instead of a sound weld nugget, in which the metal has been liquefied and well stirred, a different type of bond develops between the workpieces when the welding current or the

heating time have insufficient values. In contrast with the sound
weld, with its rough-looking fracture face after shearing, the
appearance of the fracture face, which always coincides with the
original plane $z = 0$, is very smooth in the other type. Although
the dimension of the area of coherence cannot be easily determined,
since it gradually shades off into the surrounding non-bonded
sheet surface, the maximum value of the constant $\tau_s$ can be
estimated to be equal to about $23 \times 10^7$ N.m$^{-2}$ both for stainless
and for low-carbon steel. This type of bond was observed in
particular in welding steels and copper. Since an area of this type
always surrounds any well-developed weld nugget in these materials,
part of the shearing force will be carried by it, which results in
high values of $\sigma_s$ and $\tau_s$.
The existence of the described area of partial coherence may be
explained by the presence of a large number of grown-out current
constrictions, the temperatures of which equal the melting point
as described in section 4.3.2 (cf. fig. 3.1).

So far, no experimental results are available with regard to the
influence of the welding parameters $i$ and $t'$ on the fatigue
strength or the impact strength of spot welds. It appears that a
more extensive welding cycle, comprising pre-heating and especially
a post-weld heat treatment or forging period, or both, is required
in order to obtain welds with optimum fatigue strength [61, 62, 63].


6.1.4. Conclusions

In the foregoing section the static shear strength appeared to be no
useful  criterion in determining the quality of spot welds. Instead,
GLAGE [56] suggests to judge weld quality on the basis of the
following criteria.
   (a) Deformation of the workpiece surfaces (cf. section 6.1.2);
   (b) the size of the heat-affected zone outside the weld nugget;
   (c) the corrosion resistance of the weld;
   (d) sheet separation (cf. section 6.1.2);
   (e) the statistical standard deviation of the strength
       properties (cf. [64]);
   (f) position, shape and metallurgical structure of the weld
       nugget;
   (g) the presence of cracks in the welded material.

Such a definition of weld quality only has practical value if there is a relation between this quality and the behaviour of welds in actual constructions. It seems that particularly the criteria (b), (f) and (g) are of importance to the fatigue strength of the joint [62], especially in so far as they influence the presence of residual stresses after welding [61, 63]. At any rate, the criteria (a) to (g) should be defined unambiguously and numerically in order to facilitate a uniform interpretation by any investigator. Further research must decide whether GLAGE's suggestions contain useful quality criteria compared with the results of fatigue tests. Using these criteria when comparing welds made in 1 mm low-carbon steel with different combinations of $D_E$, i and t', GLAGE made a division into five quality classes I, A, B, C and D in order of quality. When the nugget diameter is chosen on the basis of the shear strength required, and the electrode diameter $D_E$ is taken equal to $D_N$, the welding time t' and the current intensity i follow from

$$t' = v_1 D_E \qquad\qquad (6.5)$$

$$i = v_2' t' = v_2 D_E \qquad\qquad (6.6)$$

where the constants $v_1$ and $v_2$ depend on the weld quality as in table 6.2.

Table 6.2. The Constants $v_1$ and $v_2$ from Relations (6.5) and (6.6)

| quality class | $v_1$ | $v_2$ |
|---|---|---|
| I | 14 | 2.5 |
| A | 30 | 1.63 |
| B | 70 | 1.5 |
| C | 134 | 1.38 |
| D | 226 | 1.2 |
| | $ms.mm^{-1}$ | $kA.mm^{-1}$ |

The values of i and t' computed from table 6.2 with the aid of the
relations (6.5) and (6.6) agree very well with the data of fig. 4.8,
which are likewise valid for the welding of 1 mm low-carbon steel,
in as far as the highest quality class I is considered. For lower
quality and large diameters, however, the computed current
intensities are up to 20% too low, compared with those of fig. 4.8.
This is undoubtedly due to the low electrode force, which was
chosen in dependence on i only. So when welding with $D_E$ = 8 mm and
i = 11 kA (class C) the electrode force F had a value of 2.5 kN
instead of the value of 12 kN given in fig. 4.8. The influence of
a too small electrode force was explained in section 4.5.4.
In conclusion, a shorter welding time and consequently a higher
current intensity appears to result in welds with a better quality
if the criteria (a) to (g) are used. The application of high
current values, on the other hand, increases the probability of
molten metal splashing from between the workpieces during the
heating period (cf. section 3.4.1), possibly resulting in
excessive surface indentations and sheet separation.
If the external appearance of the welds is not of primary
importance, high welding currents and short heating times may be
applied. If splashing is undesirable, the welding time should not
be taken too small. In that case, it seems to be a good compromise
to choose t' in such a way that $Q_t \approx 1$. Another possibility of
controlling the weld appearance lies in the application of a
programmed force, being high at the beginning of the heating period
and low when the weld metal is molten (cf. section 4.5.4).
In all cases, both the surface preparation (cf. section 4.3.1) and
the accurate adjustment of the welding variables current and time
are extremely important.


## 6.2. Adaptive Control of the Spot Welding Process

### 6.2.1. The Necessity of Adaptive Control

Resistance spot welding has two distinctive features. First, welds
can be made very quickly (speeds of 100 spots/min are often used);
second, most of the parameters can be preset on the control unit.

This in turn explains why the process is favoured for mass produc-
tion and automation. Unfortunately, the speed with which welds are
made implies that, when the process functions incorrectly, a large
number of defective welds could be made before they are detected.
Where spot welding is completely automated, there is a particular
demand for a reliable test of weld quality. In addition, where
every spot weld must be of high quality, there is a demand for
effective quality assurance for each weld [53].

It was concluded in the foregoing sections that the accurate ad-
justment of the main welding variables current and time is of
predominant importance for weld quality. Owing to the influence of
relatively small variations in the welding conditions this adjust-
ment should have a variable character. Examples of such variations
are deviations of the nominal supply voltage or of the sheet
thickness, increase in electrode tip diameter owing to electrode
wear, variations in the surface quality of the sheet welded and
shunting effects of the welding current [26].

Since the conditions for each individual weld may thus vary, it is
necessary that the welding variables are adjusted while the weld is
made. Because of the short duration of the process such an adjust-
ment should be effectuated automatically, governed by a process
variable, the behaviour of which is a useful indication of the
quality of the weld being made. Consequently, for the purpose of
such an "adaptive control" an adequate control variable must be
available.

### 6.2.2. The Selection of a Control Variable

The object is to find a process variable that gives an indication
of the quality of the developing weld during the initial phase
of the heating cycle. This control variable must allow an
interpretation of the direction in which the welding parameters
are to be changed during the heating period if the weld is
likely to become inferior.

If the size of the weld nugget being formed, or the ultimate values
of the temperatures developing in the weld are taken as a
satisfactory criterion for weld quality, a number of such control
variables is available. The most important of them were mentioned

118

in section 3.4.1, viz. the electrode movement d and the total
electric resistance R of the weldment.

Adaptive control mechanismsusing the variation of the total
resistance or of the voltage across the workpieces as a control
variable are described in references [26] and [65]. Although this
type of control mechanism is very useful in a number of cases, a
more generally applicable system is that using the electrode
movement as the control variable [50, 66], since the latter is a
direct measure for the mean value of the temperatures developing
during the heating cycle, as will be shown in the next section.

### 6.2.3. The Electrode Displacement

A detailed analysis of the magnitude of the electrode displacement,
which is a consequence of the thermal expansion of the workpiece
materials during the heating cycle, is considered to be outside the
scope of the present work. However, a few interesting observations
were made with respect to the electrode movement, which will more
easily be understood if the general physical background is
considered.

The linear expansion d of a slab with thickness 2s and an average
temperatue $\bar{\theta}$ may be written

$$d = 2\mu s\bar{\theta} \tag{6.7}$$

where $\mu$ is the coefficient of linear thermal expansion. The average
value $\bar{\theta}$ is assumed to be dependent on the temperature $\theta$ of the
point $B(z = 0, r = D/2)$, defined in section 2.3.1, as

$$\bar{\theta} = c_1\theta \tag{6.8}$$

with $c_1$ being a specific function of $Q_D$ and $Q_t$ (cf. figs. 2.11 to
2.14). The derivative of d with respect to time at the beginning of
the heating period can then be written, neglecting the dependence
of $c_1$ on $Q_t$,

$$\lim_{t\to0} (\frac{dd}{dt}) = 2\mu_o c_1 s \lim_{t\to0} (\frac{d\theta}{dt}) \tag{6.9}$$

119

where $\mu_o$ denotes the value of $\mu$ at room temperature. Using the equations (3.8), (4.30) and (4.31) this formula can be rewritten

$$\lim_{t \to 0} \left(\frac{dd}{dt}\right) = \mu_o c_1 sq \frac{\theta_m}{t'} \frac{Q_{t'}}{Q_{\theta m}} = \frac{\mu_o c_1 \theta_m a}{s Q_{\theta c}} \qquad (6.10)$$

By introducing the dimensionless quantity

$$\delta = \frac{s}{a} \lim_{t \to 0} \left(\frac{dd}{dt}\right) \qquad (6.11)$$

relation (6.10) is simplified to

$$\delta = c_2 Q_{\theta c}^{-1} \qquad (6.12)$$

in which relation $c_2 = \mu_o c_1 \theta_m$ depends on the metal welded and on the distribution of the temperatures throughout the heated zone. Some other important factors influencing the value of the rate of electrode displacement at the beginning of the heating period are neglected in the above derivation.

(a) The expansion of the workpiece metal in the radial direction is partly impeded by the presence of the cold metal surrounding the heated area. As a result of this, the expansion in the direction of the electrode axis will exceed the value given by relation (6.7).

(b) The electrode force F counteracts the thermal expansion. Since the electrode pressure is kept constant according to relation (3.6) in the present investigations, no serious deviations from (6.12) are expected. Only where the value of F is of the same order as that of the static friction force in the air cylinder $F_f$, the resultant electrode force, lying somewhere between the limits F and $F + F_f$ during the expansion of the workpiece metal, becomes too high.

The initial values of dd/dt were graphically determined from the oscillograph registrations and converted to values of $\delta$ in order to

check relation (6.12). It appeared that the true relation differs slightly from that formula, viz.

$$\delta = cQ_{\theta c}^{-4/3} \qquad (6.13)$$

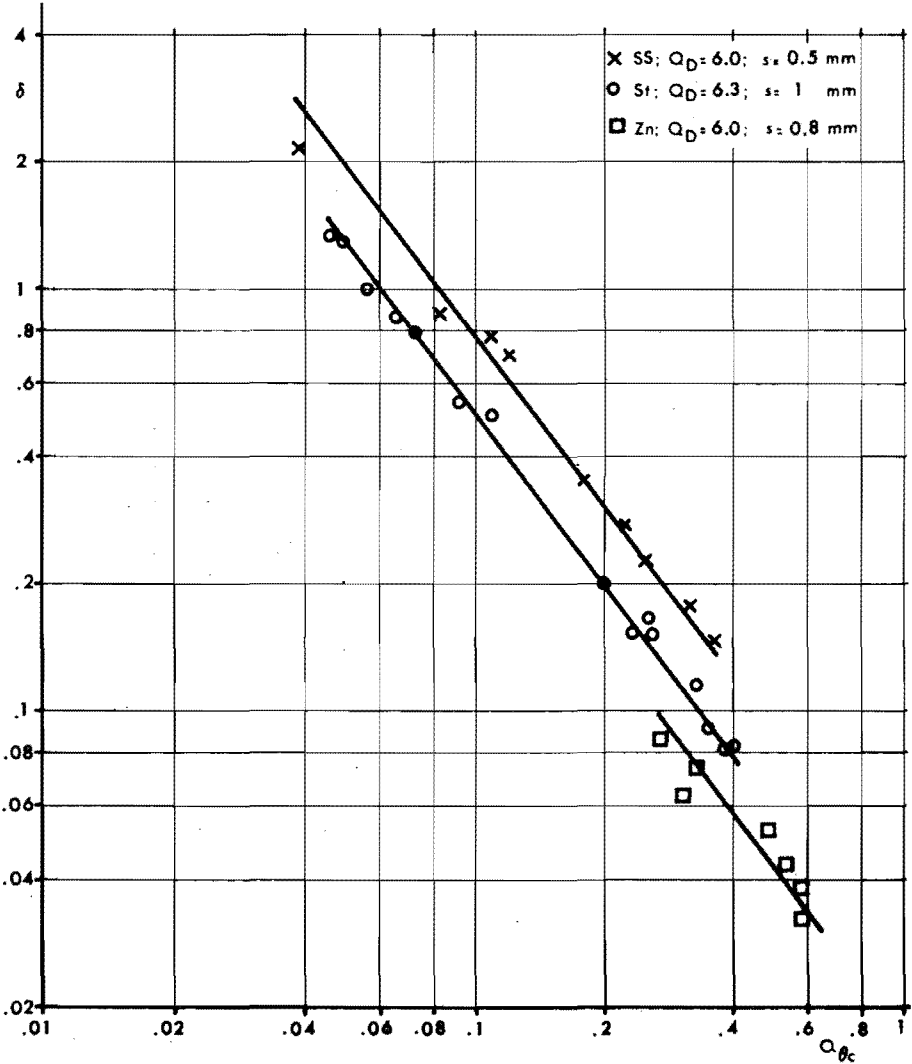for F > 3 kN. For smaller electrode forces the influence of $F_f$



Fig. 6.2. The Initial Expansion Rate $\delta$ as a Function of $Q_{\theta c}$ for the Welding of Different Materials

prohibits a clear interpretation of the results. The appearance of the exponent of 4/3 instead of 1 in (6.13) may be explained by the influence of the rate of heat production on the temperature distribution in the heated area. A high heat production rate, i.e. a low $Q_t$ value, results in high ratios of both $\theta[C]/\theta[B]$ and $\theta[E]/\theta[B]$, which means high average temperatures, and thus a high value of $c_1$ in equation (6.8). This was illustrated earlier in figures 2.11 to 2.14. According to the first figure, $dc_1/dQ_t$ and $dc_1/dQ_\theta$ are negative, resulting in an exponent $<-1$ in (6.13). Figs. 2.12 to 2.14 explain the influence of the product $Q_D$. High $Q_D$ values result in high $\bar{\theta}$ so that the constant c has a high value. Fig. 6.2. shows the dependence of $\delta$ on $Q_{\theta c}$ for a few illustrative cases, and fig. 6.3 demonstrates the dependence of c on $Q_D$ for the welding of stainless steel. The latter figure suggests a generalisation of equation (6.13), viz.

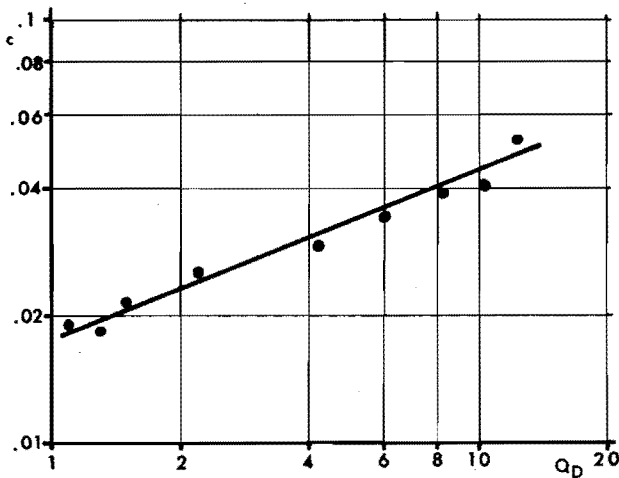$$\delta = c_o Q_D^{\,n} Q_{\theta c}^{\,-4/3} \qquad\qquad (6.14)$$



Fig. 6.3. The Dependence of the Constant c from Relation (6.13) on $Q_D$ for the Welding of Stainless Steel

Another important characteristic of the electrode movement is the maximum displacement $d_{max}$ reached during the welding cycle. The relative maximum displacement

$$\Delta = \frac{d_{max}}{s} \tag{6.15}$$

is expected to be dependent on $\bar{\theta}$, analogously to $\delta$. This proved to be true in our experiments, although the influence of the static friction force $F_f$ again camouflages the true relation between the welding variables under review. Generally, $\Delta$ increases with higher values of $Q_D$, although the relation is not simply one of linear proportionality, as is shown in fig. 6.4. It even seems that there is a maximum value of $\Delta$ at $Q_D \approx 7$ for aluminium. It is improbable that a thorough analysis of the electrode movement can be given
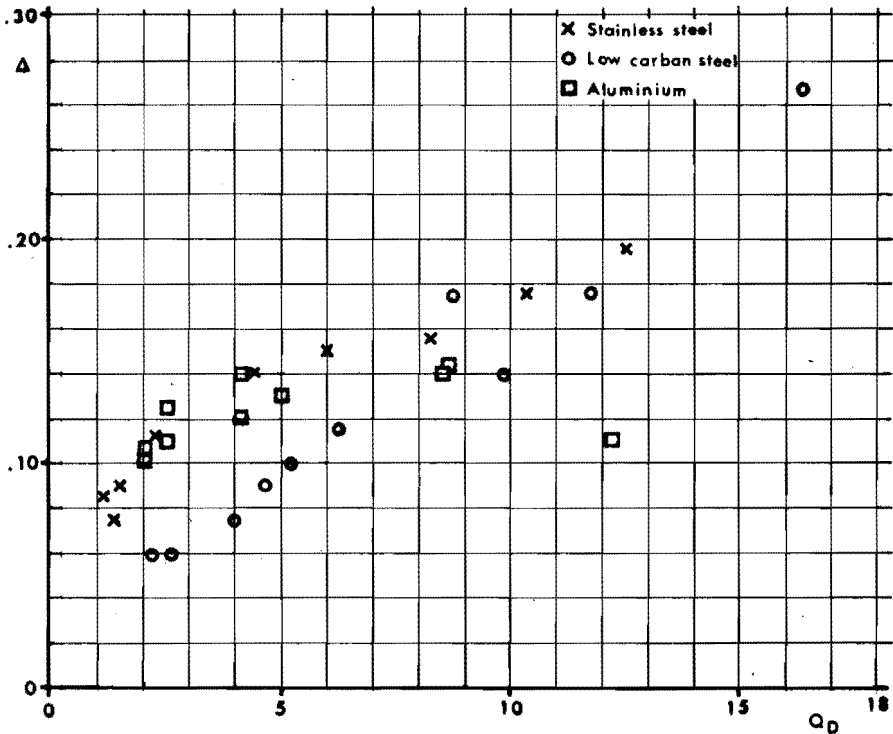


Fig. 6.4. The Dependence of $\Delta$ on the Value of $Q_D$ for Different Materials

without taking the mechanical stress distribution and the creep properties of the welded metal at high temperatures into consideration. Further research on this subject will be necessary. Nevertheless, an experimental determination of the maximum

electrode displacement offers an excellent possibility of
controlling the proper welding time, as was concluded earlier in
section 3.4.1.

6.2.4. Conclusions

From the observations described in the foregoing sections the
following important conclusions may be drawn with respect to the
control of resistance weld quality.

(a) The initial rate of electrode displacement $\delta$ is an adequate
measure for the quantity $Q_{\theta c}$ calculated with the aid of the
analogue model, or, since the factor q is known from chapter 4,
for the actual value $Q_{\theta m}$.

(b) Since the quality of the weld seems to depend to a
considerable extent on the rate of energy production (cf. section
6.1.4) and thus on the value of $Q_\theta$, the quantity $\delta$ can be
considered a measure for the quality of the developing weld.

(c) The proper adjustment of the heating time is of predominant
importance for the quality of the weld made, especially in so far
as the appearance of the weld is considered (cf. section 6.1.4).

(d) At the time when the maximum electrode displacement is
reached, the weld nugget has obtained a diameter equal to that of
the electrode tip (cf. section 3.4.1). Hence, the ultimate value of
the electrode displacement is a means of controlling the proper
weld time.

Obviously, the design of an adaptive control mechanism should be
realised on the basis of the foregoing conclusions. An electric
voltage signal u, proportional to the electrode displacement d is
easily obtained from a displacement transducer. Then, the first
derivative of this signal with respect to time is proportional to
$\delta$, and thus a univalued function of $Q_\theta$ and i. When this signal
du/dt is obtained after the first few cycles of the welding
current, it might be utilised to adjust the proper current
intensity if for any of the reasons mentioned in section 6.1.1 the
energy production were too small or too high. Such a system can
only perform well if the welding time has not a too small value.
Besides, a predetermined value $u_{max}$, proportional to $d_{max}$, of the
voltage signal may be used to limit the heating time to the
required value through interruption of the ignitron injection

voltage at the given level of $u_{max}$. Considerable research will be required for the effectuation of the control system described. The undesired influence of the static friction force acting on the moving part of the welding machine must be eliminated as much as possible in order to avoid unacceptable spreadings of the displacement values.

## CONCLUSIONS

As to the investigated geometrical arrangement exclusively concerning spot welding by means of flat-faced electrode tips, the following conclusions may be drawn.

(a) The relationship between the main welding parameters for the obtainance of a weld of prescribed strength and dimensions in any workpiece metal can be established with the aid of an improved version of the applied mathematical model.

(b) It was shown that both the electric current distribution and the electric contact resistances are of great importance in the spot welding process, although each of these factors has its typical range of influence.

(c) The improved model, though developed for symmetrical arrangements, can be applied to the welding of dissimilar metals or thicknesses as well.

(d) The electrode force should be given a sufficiently high value, especially at the beginning of the heating period, in order to minimise electric contact resistances and to enhance weld quality. The friction force, acting on the moving head of the welding machine, must be minimised.

(e) The static shearing force of the weld exclusively depends on the thickness of the welded material and on the dimensions of the weld nugget formed.

(f) The accurate adjustment of welding current and welding time is of predominant importance for the quality control of the weld made.

## REFERENCES

1  Welding Handbook (5th edition), Section 2,
   New York, American Welding Society, 1964.

2  Welding Handbook  (5th edition), Section 4,
   New York, American Welding Society, 1966.

3  Welding Handbook (5th edition), Section 5,
   New York, American Welding Society, 1967.

4  Resistance Welding Manual (3rd edition), Volumes 1 and 2,
   Philadelphia (Pa), Resistance Welder Manufacturers' Association,
   1956-1961.

5  LHEUREUX, G. and E. BELOTTE
   Le soudage par résistance
   Paris, Dunod, 1965.

6  BRUNST, W.
   Das Elektrische Widerstandsschweissen
   Berlin, Springer Verlag, 1952.

7  BRUNST, W. and W. FAHRENBACH
   Widerstandsschweissen, 3. Auflage,
   Werkstattbücher Heft 73 a/b
   Berlin, Springer Verlag, 1962.

8  EWAN, D.
   A Review of Sheet-Metal Welding Methods with Particular Reference
   to Resistance Welding
   Sheet Metal Industries $\underline{39}$(1962)9,p.609-623.

9  BIERETT, G. and O. STEINHARDT
   Untersuchungen zur Anwendung der elektrischen
   Widerstands-Punktschweissung im allgemeinen Stahlbau
   Köln, Stahlbau-Verlag, 1960.

10  Military Specification MIL-W-6858C
    United States Government, 1964.

11  Widerstandsschweissen II. Vorträge der 5. Stuttgarter Sondertagung
    Widerstands-Schweisstechnik 1962
    Düsseldorf, Deutscher Verlag für Schweisstechnik, 1963.

12  Widerstandsschweissen III. Vorträge der 6. Stuttgarter Sondertagung
    Widerstands-Schweisstechnik 1965
    Düsseldorf, Deutscher Verlag für Schweisstechnik, 1965.

13  PIERSIG, G.
    Die Anwendung der Schweisstechnik im Lokomotivbau
    Schweissen und Schneiden 12(1960)5,p.217-219.

14  Widerstandpunktschweissen von Aluminium und dessen Legierungen im
    Schienenfahrzeugbau. Merkblatt D.V.S. 1604
    Düsseldorf, Deutscher Verband für Schweisstechnik, 1966.

15  SANTINI, R.
    Schweissen im Karosseriebau in den U.S.A.
    Vitry (Seine), Sciaky.

16  KRIMIANIS, T.
    Structural Spot Welding in Heavy Steel Construction
    Vitry (Seine), Sciaky.

17  SANTINI, R.
    Anwendung der Elektrischen Widerstandsschweissung bei der
    Herstellung von Strahltriebwerken
    Vitry (Seine), Sciaky, 1958.

18  ZAREMBA, P.
    Die Bedeutung des Widerstandsschweissens für den deutschen
    Flugzeugtriebwerkbau unter Berücksichtigung der im
    internationalen Triebwerkbau verwendeten hochwarmfesten Legierungen
    Schweissen und Schneiden 16(1964)11,p.507-513.

19  STILLER, A.
    Praktische Erfahrungen mit dem Widerstandsschweissen im Flugzeugbau
    Schweissen und Schneiden 14(1962)10,p.428-434.

20  VERNON, C.
    Micro Welding Development
    Welding and Metal Fabrication 32(1964)9,p.326-334.

21  HEINDL, J., J. ALBERTS and B. BROCK
    Resistance Welding of Electronic Components
    Metal Progress 81(1962)6,p.97-101.

22  BENTLEY, K., J. GREENWOOD, P. McK.KNOWLSON and R.BAKER
    Temperature Distributions in Spot Welds
    British Welding Journal 10(1963)12,p.613-619.

23  FRANKEL, H., K.C. WU and R. LEWIS
    Universal Data for Resistance Welding
    Welding Journal 42(1963),p.151s-159s.

24  TARASOV, N.M.
    Spot Welding Conditions for Thin Metal Calculated and Analysed by
    the Similarity Method
    Welding Production 7(1961)11,p.23-32.

25  SCHMIEDGEN, D.
    Schweisslinsenbildung beim Widerstandspunktschweissen
    Schweisstechnik (Berlin) 16(1966)12,p.536-540.

26  ARCHER, G.
    A New System for Automatic Feedback Control of Resistance Spot
    Welding
    Welding Journal 38(1959)11,p.987-993.

27  ARCHER, G.
    Calculations for Temperature Response in Spot Welds
    Welding Journal 39(1960)8,p.327s-330s.

28  MYERS, P., O.A. UYEHARA and G. BORMAN
    Fundamentals of Heat Flow in Welding
    Welding Research Council Bulletin No. 123, July 1967.


29  ROBERTS, D., J. ROBERTS and A. WELLS
    Fundamental Resistance Welding Investigations
    British Welding Journal 5(1958)3,p.117-126.


30  GREENWOOD, J.
    Temperatures in Spot Welding
    British Welding Journal 8(1961)6,p.316-322.


31  RUGE, J. and P. HILDEBRANDT
    Einfluss von Temperaturverteilung und Werkstoffeigenschaften auf
    das Haften der Elektroden beim Widerstandspunktschweissen von
    Aluminium und Aluminiumlegierungen
    Schweissen und Schneiden 16(1964)4,p.115-124.


32  RICE, W. and E. FUNK
    An Analytical Investigation of the Temperature Distributions During
    Resistance Welding
    Welding Journal 46(1967)4,p.175s-186s.


33  BEUKEN, C.
    Wärmeverluste bei periodisch betriebenen elektrischen Öfen; eine
    neue Methode zur Vorausbestimmung nicht-stationärer Wärme-
    strömungen
    Thesis Bergakademie Freiburg, 1936.


34  RIEGER, E. and J. RUGE
    Temperaturverteilung beim Punktschweissen von Aluminium und Kupfer
    Fachbuchreihe Schweisstechnik, Band 40.
    Düsseldorf, Deutscher Verband für Schweisstechnik, 1965.


35  Internationales Kolloquium über neueste Entwicklungen bei der
    Anwendung des Beukenmodells
    Maastricht, PLEM, 1967.

36 HOLM, R.
   Electric Contacts, 4th edition,
   Berlin, Springer Verlag, 1967.


37 WYANT, R.
   Measurement  and Effect of Contact Resistance in Spot Welding
   Electrical Engineering Transactions 65(1946)1,p.26-33.


38 ROBERTS, W.
   Resistance Variations During Spot Welding
   Welding Journal 30(1951)11,p.1004-1019.


39 DIX, A.
   Metallurgical study of resistance weld nugget formation and stuck
   welds
   British Welding Journal 15(1968)1,p.7-15.


40 LANGHAAR, H.
   Dimensional Analysis and Theory of Models
   New York, Wiley & Sons, 1960.


41 FENECH, H. and W. ROHSENOW
   Prediction of Thermal Conductance of Metallic Surfaces in Contact
   Journal of Heat Transfer 85(1963)1,p.15-24.


42 CARSLAW, H. and J. JAEGER
   Conduction of Heat in Solids, 2nd edition
   Oxford, Clarendon Press, 1959.


43 German Standard DIN 44750, Gerade Punktelektroden
   Deutscher Normenausschuss, 1965.


44 MATTING, A. and U. KRÜGER
   Standzeituntersuchungen mit Molybdän- und Wolfram-Elektroden
   beim Punktschweissen verzinkter Feinbleche
   Bänder, Bleche, Rohre 8(1967)5,p.277-283 and 8(1967)6,p.371-380.

45  SIMMONS, W.
    Spot Welding Electrode Life
    Welding Journal 46(1967)11,p.915-920.

46  R. and E. KOHLHAAS
    Physikalischen Eigenschaften der Eisenwerkstoffe,
    Landolt-Börnstein, Band IV, Teil 2, Bandteil a, p. 185-239,
    Berlin, Springer Verlag, 1963.

47  Zink-Taschenbuch
    Berlin, Metall-Verlag, 1959.

48  Handbook of Thermal Properties of Solid Materials
    Oxford, Pergamon Press, 1962.

49  Electrodes pour machines à souder par résistance
    Publication Sciaky no. 984,
    Vitry (Seine), Sciaky.

50  HAYWARD, B.
    Scientific Instrumentation as an Aid to the Control of Resistance
    Weld Quality
    British Welding Journal 14(1967)11,p.582-591.

51  GENGENBACH, O.
    Messtechnische Probleme beim Widerstandsschweissen
    Schweissen und Schneiden 10(1958)1,p.1-12.

52  DE VOS, M.
    Measurement of Electrode Movement as a means of Spot Weld
    Quality Control
    Lastechniek 32(1966)4,p.65-75.

53  WALLER, D. and P. KNOWLSON
    Electrode Separation Applied to Quality Control in Resistance
    Welding
    Welding Journal 44(1965)4,p.168s-174s.

54  WELLINGER, K. and E. BIRKEL
    Untersuchungen der Einflussgrössen beim Punktschweissen von
    Stahlblech durch Beobachten der Elektrodenbewegung
    Schweissen und Schneiden 16(1964)7,p.263-271.

55  MEYER, A.
    Beitrag zur Analyse der Elektrodenbewegung beim Widerstands-
    punktschweissen
    Technische Mitteilungen 58(1965)9,p.501-503.

56  GLAGE, W.
    Einflussgrössen, Güte und Festigkeiten beim Widerstandspunkt-
    schweissen
    Schweissen und Schneiden 13(1961)4,p.135-139.

57  BECKEN, O. and K. HAVERS
    Beim Punktschweissen von Kohlenstoffstahl erreichbare Scherzug-
    kräfte bei Blechdicken bis 6 mm
    Schweissen und Schneiden 13(1961)4,p.127-135.

58  ZLOBIN, G.
    The Spot Welding of Copper
    Automatic Welding (1962)10, p. 52-54.

59  Welding Handbook (5th edition), Section 1,
    New York, American Welding Society, 1963.

60  HARTMANN, E.
    Mechanical Tests of Spot Welds
    Welding Journal 37(1958)11, p. 520s-523s.

61  JOUMAT, P.
    A Unique Method of Spot Weld Quality Control
    Los Angeles, Sciaky, 1949.

62  KLÖPPEL, K.
    Untersuchung der Dauerfestigkeit bei ein- und zweischnittigen
    punktgeschweissten Stahlverbindungen
    Der Stahlbau 31(1962)5, p. 161-171.

133

63  CHOQUET, J.
    Improvement of the Fatigue Life of Spot Welds
    Welding Research Council Bulletin no. 112, 1966.

64  BECKEN, O. and K. HAVERS
    Uber die Streuung der Scherzugkraft beim Punktschweissen von
    Kohlenstoffstahl
    Schweissen und Schneiden 13(1961)12, p. 585-588.

65  MILCKE, H.
    Steuerung der Schweisszeit in Abhängigkeit vom Widerstandsverlauf
    zwischen den Elektroden
    Schweissen und Schneiden 19(1967)4, p. 152-156.

66  ORLOV, B. et al.
    Selection of a Control Variable for Spot Welding Aluminium Alloys
    Welding Production 12(1966)8, p. 4-7.

# SAMENVATTING

Het belangrijkste onderwerp van dit proefschrift is de analyse van de
tijdens het puntlassen optredende temperaturen in het materiaal van het
werkstuk. Voor dit doel werd een vereenvoudigd analoog model ontworpen
teneinde een kwantitatief inzicht te verkrijgen in de grootte van de
optredende temperaturen. Met behulp van dit model kon de invloed van
een aantal belangrijke lasparameters, alsmede van de materiaaleigen-
schappen van werkstukken en electroden en van enkele facetten van de
lasgeometrie worden nagegaan. De juistheid van het model werd experimen-
teel gecontroleerd voor een aantal representatieve werkstukmaterialen.
Geconstateerd wordt, dat er een systematische afwijking bestaat tussen
de uitkomsten van het mathematisch model en de resultaten van de
experimenten. Deze afwijking kan kwantitatief verklaard worden als een
gevolg van de discrepantie tussen dit model en de experimentele
situatie met betrekking tot de electrische stroomverdeling tussen de
electroden en de invloed van de kontaktweerstanden.
Vervolgens worden de verkregen inzichten op bevredigende wijze toegepast
op het lassen van onderling verschillende werkstukken en op het lassen
van electrolytisch koper met behulp van een kunstmatige stroomvernauwing.
Tenslotte wordt een beschouwing gegeven over de invloed van de las-
parameters op de kwaliteit van de las en wordt een methode aangegeven
voor het automatisch regelen van het proces en het beheersen van de las-
kwaliteit.

## CURRICULUM VITAE

De schrijver van dit proefschrift werd in 1938 te Utrecht geboren. Hij
bezocht daar de Sint Gerardus Majella school, waar hij in 1954 het
diploma MULO-B behaalde. Daarna volgde hij onderwijs aan de
Gemeentelijke Hogere Technische School voor de Mechanische Technologie
te Utrecht, alwaar hij in 1958 het eindexamen met goed gevolg aflegde.
Van 1958 tot 1960 vervulde hij zijn militaire dienstplicht.
In 1960 begon hij zijn studie aan de Technische Hogeschool te Eindhoven;
in 1965 verwierf hij daar met lof het diploma van werktuigkundig
ingenieur. Van augustus 1965 tot en met december 1968 was hij als mede-
werker verbonden aan het Laboratorium voor Mechanische Technologie en
Werkplaatstechniek van eerder genoemde hogeschool, in welke functie hij
de gelegenheid vond dit proefschrift te bewerken.
Sinds januari 1969 is hij als wetenschappelijk medewerker verbonden aan
het Natuurkundig Laboratorium van de N.V. Philips Gloeilampenfabrieken
te Eindhoven.

I

Indien de betekenis van de wetenschap moet worden afgemeten naar de moge-
lijkheden die zij de mens biedt voor zijn zelfontplooiing, dienen
futurologische beschouwingen zich niet te beperken tot het aangeven van
te verwachten wetenschappelijke en technische  mogelijkheden op basis van
extrapolatie van de actuele stand van onderzoek en ontwikkeling.
Deze beschouwingen behoren tevens een basis te vormen voor het toekennen
van prioriteiten binnen de wetenschappelijk-technische ontwikkeling. Daar-
bij moeten als criteria gehanteerd worden:
   1. het lenigen van elementaire menselijke noden,
   2. de mate waarin de mens inderdaad mogelijkheden tot zelfontplooiing
      geboden worden.

> A.G.M. van Melsen, De Betekenis van de
> Wetenschap.
> Voordracht gehouden tijdens het congres
> "Leven met de Wetenschap".
> Utrecht, Oosthoek, 1968.

II

De kwantitatieve statistische analyse van de resultaten van metingen
verricht aan een te verklaren proces moet niet gekoppeld worden aan een
willekeurig gekozen wiskundig model, teneinde verder fundamenteel
onderzoek niet bij voorbaat te bemoeilijken.

III

Een thermische analyse van het puntlasproces leidt in het algemeen niet
tot bevredigende resultaten indien óf alleen van de warmte-ontwikkeling
in de kontaktplaatsen óf alleen van de warmte-ontwikkeling in het werk-
stukmateriaal wordt uitgegaan.

IV

Het is ongewenst de diameter van een te maken puntlas groter te kiezen
dan noodzakelijk is voor het verkrijgen van een mechanisch voldoend
sterke verbinding.


V

De geringe mate van creativiteit die de kandidaatsstudie in de afdeling
der werktuigbouwkunde van deze hogeschool vraagt van de studerenden kan
wellicht wezenlijk vergroot worden door het invoeren van een weldoor-
dacht systeem van project-onderwijs.


VI

De relatie, die het Welding Handbook geeft voor de grootte van de beno-
digde energie als functie van de materiaaldikte en de hardheid bij het
ultrasoon lassen van plaatmateriaal, is in zijn algemeenheid onjuist. Met
name voor metalen met een vlakken-gecenterd kristalrooster en voor edele
metalen treden grote afwijkingen op.

> Welding Handbook (5th edition),
> Section 3, p. 49.5
> New York, American Welding Society, 1965.


VII

De kwalificatie "ideaal-plastisch" voor een metaal dat bij plastische
deformatie niet verstevigt, is voor technologische toepassingen mis-
leidend omdat hij suggereert dat het betreffende metaal zeer goed plas-
tisch te bewerken zou zijn.


VIII

Bij het draaiproces kan voor gegeven beitelgeometrie, werkstukmateriaal
en snedediepte het verloop van de spaankontaktlengte in de tijd beschre-
ven worden door middel van een dimensieloze grootheid, gevormd door de
verhouding van de draaitijd en de levensduur van de beitelpunt.

> A.P.A.J. Hulst, De spaankontaktlengte
> bij draaien.
> Eindhoven, Laboratorium-rapport WT 129, 1965.

IX

Het verdient aanbeveling om de verplichte stellingen bij een proef-
schrift niet af te schaffen, omdat deze de promovendus een unieke gele-
genheid bieden zijn gemoed te luchten, c.q. zijn geweten te ontlasten.

Eindhoven, 15 april 1969                          A.P.A.J. Hulst